OXALATE-DEGRADING ENZYMES OF *Oxalobacter formigenes* AND *Escherichia coli*

By

CORY G. TOYOTA

A DISSERTATION PRESENTED TO THE GRADUATE SCHOOL
OF THE UNIVERSITY OF FLORIDA IN PARTIAL FULFILLMENT
OF THE REQUIREMENTS FOR THE DEGREE OF
DOCTOR OF PHILOSOPHY

UNIVERSITY OF FLORIDA

2008

© 2008 Cory G. Toyota

To Stefán Jónsson
(1972-2007)

ACKNOWLEDGMENTS

There are far too many people to thank for their support and help these past five years: Lori; my parents and family; Bubba; the Richards Group past and present, especially Patricia, Sue, Jemy, and Larissa; Mark Settles; John and Tracy; Jessica Light; Beth-Anne; Reid Bishop; Ylva Lindqvist; and my Committee, especially Drs. Lyons and Horenstein for their advice, so I would just like to kindly thank

Catrine Berthold, St. Jude, and Nigel Richards, in that order.

TABLE OF CONTENTS

LIST OF TABLES

LIST OF FIGURES

LIST OF ABBREVIATIONS

ACP	Acyl-carrier protein
ADP	Adenosine diphosphate
ANS	8-Anilino-1-naphthalenesulfonic acid
AR	Acid resistance
atoDA	Acetate CoA-transferase
ATP	Adenosine triphosphate
BaiF	Putative bile acid induced CoA transferase
BbsEF	Succinyl-CoA:(R)-benzylsuccinate CoA-transferase
Bis-Tris Propane	1,3-bis(tris(hydroxymethyl)methylamino)propane
CaiB	γ-butryobetaine-CoA:carnitine CoA transferase
CD	Circular dichroism
CoA	Coenzyme A
DTNB	Ellman's reagent; 5,5-dithio-bis(2-nitrobenzoic acid)
DTT	1,4-dithio-DL-threitol
dzThDP	3'-deaza thiamine diphosphate
F-CoA	Formyl-CoA
FldA	Cinnamoyl-CoA: phenyllactate CoA-transferase
FPLC	Fast protein liquid chromatography
FRC	Formyl-CoA transferase from *Oxalobacter formigenes*
FRET	Förster resonance energy transfer
GCT	Glutaconyl-CoA:glutarate CoA transferase
HAc	Acetic Acid
HadA	2-Hydroxyisocaproate CoA transferase
HEPES	4-(2-hydroxyethyl)piperazine-1-ethanesulfonic acid

IAEDANS	5-((((2-iodoacetyl)amino)ethyl)amino) naphthalene-1-sulfonic acid
MES	2-(N-morpholino)ethanesulfonic acid
MFS	Major facilitator superfamily
MW	Molecular weight
NMR	Nuclear Magnetic Resonance
OXC	Oxalyl-CoA transferase from *Oxalobacter formigenes*
Ox-CoA	Oxalyl-CoA
OxlT	Oxalate:formate antiporter from *Oxalobacter formigenes*
PEG	Polyethylene glycol
RP-HPLC	Reverse phase high-performance liquid chromatography
SCOT	Succinyl-CoA:3-ketoacid CoA transferase
SmtAB	Succinyl-CoA:citramalate CoA-transferase
Suc-CoA	Succinyl-CoA
ThDP	Thiamine diphosphate
ThTDP	Thiamine-2-thiazolone diphosphate
YfdU	OXC homolog encoded by *yfdU* gene in *Escherichia coli*
YfdW	FRC homolog encoded by *yfdW* gene in *Escherichia coli*

Abstract of Dissertation Presented to the Graduate School
of the University of Florida in Partial Fulfillment of the
Requirements for the Degree of Doctor of Philosophy

OXALATE-DEGRADING ENYZMES OF
Oxalobacter formigenes AND *Escherichia coli*

By

Cory G. Toyota

August 2008

Chair: Nigel G. J. Richards
Major: Chemistry

Oxalate is a toxic organic diacid found in a variety of foods; build up of oxalate in the gut is linked to the formation of calcium oxalate kidney stones. Humans have no innate mechanism for metabolizing oxalate, so enzymes that catalyze the degradation of oxalate may represent a form of therapy. *Oxalobacter formigenes* and *Escherichia coli* may influence oxalate homeostasis in man. The focus of this work is on understanding the kinetic mechanisms and metabolic roles of the proteins involved in oxalate metabolism in these organisms. Two enzymes are essential to *O. formigenes* metabolism: formyl-CoA transferase (FRC) and oxalyl-CoA decarboxylase (OXC). FRC catalyzes the transfer of CoA from formyl-CoA to oxalate to yield one molecule each of formate and oxalyl-CoA. The thioester product is subsequently decarboxylated by OXC in a proton-consuming reaction that is essential in energy generation for the organism. In addition to recombinant wild-type and His-tagged fusion proteins, a series of active site and truncation mutants were prepared for steady state kinetic analysis. Hydroxylamine and borohydride trapping experiments in conjunction with high resolution X-ray crystallographic freeze trapping experiments have outlined the complete kinetic mechanisms for both OXC and FRC. This work has demonstrated that despite differing in kinetic mechanism both Family I and Family III CoA transferase reactions proceed through an enzyme-CoA

thioester intermediate. In addition, flexible loops in both enzymes, the C-terminal peptide loop of OXC and the tetraglycine loop (^{258}GGGGQ^{262}) of FRC, have been identified as critical to catalysis and substrate specificity.

Structural genomics studies have shown that YfdW, encoded by the gene *yfdW* from an operon that appears to enhance the ability of *Escherichia coli* MG1655 to survive under acidic conditions, is structurally homologous to FRC. This work confirms that YfdW is a formyl-CoA transferase that appears to be more stringent than FRC in employing formyl-CoA and oxalate as substrates. Replacing Trp-48 in the FRC active site with the glutamine residue that occupies an equivalent position in the *E. coli* protein shows that Trp-48 precludes oxalate binding to a site that mediates substrate inhibition for YfdW. In addition, the replacement of Trp-48 by Gln-48 yields an FRC variant for which oxalate-dependent substrate inhibition is modified to resemble that seen for YfdW. Finally, in addition to demonstrating the value of utilizing structural homology in assigning protein function, this work suggests that the *yfdW* and *yfdU* genes in *E. coli* may be be involved in conferring oxalate-dependent acid resistance to the bacterium.

CHAPTER 1
INTRODUCTION

Oxalic Acid

Oxalic acid is the simplest organic diacid. It is both a relatively strong organic acid, pK_a^1 of 1.23 and pK_a^2 of 4.19, and a strong chelator of divalent cations forming mostly insoluble oxalates (110). Rapid heating can cause degradation into CO_2, CO, and H_2O and oxalic acid can be oxidized by permanganate to CO_2 and water. Oxalic acid is used in household cleaners, as a mordant for dyeing, wood stripper, and as a miticide. It is synthesized industrially by heating NaOH and CO under pressure. Oxalate biosynthesis in plants is linked primarily to cleavage of ascorbate and oxidation of byproducts of photorespiration, glycolate and glyoxalate, by glycolate oxidase (198, 215). Plants are proposed to utilize oxalate in calcium regulation, heavy metal detoxification, and, in the form of calcium oxalate, as protection. Calcium oxalate is thought to be a source of hydrogen peroxide for cereal defense and a thick layer of calcium oxalte armours spruce from insect infestation (85). Oxalate in mammals comes partly from dietary sources, like rhubarb and spinach, and partly from metabolic processes in the body, e.g. a byproduct of amino acid degradation (112). Man has no endogenous oxalate metabolism.

Oxalobacter formigenes

Sheep grazing in the western United States are susceptible to oxalate poisoning through consumption of oxalate-containing plants like Halogeton (120). Efforts to understand oxalate resistance in ruminants led to researcher awareness of ruminal microbes with oxalate degrading activity. In a study of two crossbred sheep and one 600 kg fistulated Holstein cow it was reported that degradation activity was increased if the animals were adapted to increased levels of dietary oxalate (2). Isolation of the bacterium responsible proved difficult; the same study reported that of the 99 pure bacterial isolates collected from adapted sheep none degraded

oxalate. It was not until 1980 that Dawson and coworkers isolated an anaerobic, gram negative rod with oxalate-catabolic activity (57). Similar isolates from sheep rumena, pig ceca, and human feces compose a unique group and have been designated with the new genus and species *Oxalobacter formigenes* (1).

Medical Relevance in Humans

Oxalic acid is both an organic acid and a strong chelating agent for divalent cations such as Ca^{+2} (110). In addition to the potential lethal toxicity in humans and animals at high concentrations, hyperoxaluria leads to the formation of calcium oxalate stones, the most prevalent form of kidney stone (105). Several oxalate-degrading bacteria, including *Bifidobacterium infantis* (38), *Eubacterium lentum* (117), *Enterococcus faecalis* (111), *Clostridium oxalicum* (58), *Lactobacillus* spp. (38, 247), *Oxalobacter formigenes* (1, 56), *Oxalobacter vibrioformis* (58), and *Streptococcus thermophilus* (38), have been identified and are possible candidates for probiotic treatment of hyperoxaluria in man. *O. formigenes* is by far the best studied and its presence has been linked to normal urinary oxalate excretion and its absence coincides with an increased incidence of hyperoxaluric patients (66, 224). Treatment of patients suffering from primary hyperoxularia with oral doses of *O. formigenes* (frozen paste or enteric-coated capsules) has been successful at lowering urinary excretion levels, but has had mixed long term results—intestinal colonization appears to be mainly of a transient nature (69, 113, 114). In addition to intraluminal oxalate-degrading activity, some product of, or *O. formigenes* itself, interacts with colonic mucosa to stimulate oxalate secretion, effectively lowering urinary oxalate levels (99).

Metabolism of *Oxalobacter formigenes*

In their 1985 study, Allison *et al*. reported that oxalate is the sole growth substrate for *O. formigenes*, but that a small amount of acetate (0.5 mM) is also required (1). Further, for every

mole of oxalate degraded, 1 mol of protons was also consumed with the concomitant production of about equimolar CO_2 and 0.9 mol of formate. Carbon assimilation is mediated by conversion of oxalyl-CoA into 3-phosphoglycerate by way of glycerate (51).

Formate appears to be an end product of oxalate catabolism in *O. formigenes* rather than a substrate for NAD-linked formate dehydrogenase and source of cellular reducing equivalents (1). Careful studies with native membrane vesicles in reconstituted proteoliposomes have demonstrated that energy generation in *O. formigenes* is the result of both electrostatic and proton gradients created by the $oxalate^{-2}$:$formate^{-1}$ membrane-bound antiporter Oxlt (3).

Key Metabolic Proteins of *Oxalobacter formigenes*

O. formigenes depends on three identified proteins for the generation of metabolic energy from oxalate: an $oxalate^{-2}$:$formate^{-1}$ antiporter (OxlT), formyl-CoA transferase (FRC), and oxalyl-CoA decarboxylase (OXC). In the metabolic cycle, OxlT transports one molecule of divalent extracellular oxalate into the cell with the concomitant transfer of one molecule of monovalent formate out of the cytosol (3). Oxalate is activated by transfer to coenzyme A from formyl-CoA in a reaction catalyzed by FRC. The thioester product is subsequently decarboxylated by OXC producing CO_2, regenerating formyl-CoA for subsequent cycles, and consuming one equivalent of cytosolic protons (3, 9). Anion exchange promotes a polarization of the membrane. The net extrusion of protons has the effect of increasing cytosolic pH and drives an F_1F_0ATP synthase with a proposed stoichiometry of $3H^+$/ATP. Decarboxylation of oxalate and the assumption that CO_2 diffuses irreversibly from the cell ensures a near stoichiometric link between oxalate and the combination proton-motive and chemiosmotic gradient. The importance of these three proteins is evident: together FRC and OXC make up 20% of the total cytosolic protein (9) and OxlT constitutes a major fraction (~10%) of the inner membrane proteins in *O. formigenes* (205).

Oxalate^{-2}:formate^{-1} antiporter (OxlT)

OxlT, an oxalate:formate exchange protein, is an inner-membrane bound protein with 12 transmembrane helices (205). OxlT transfers one divalent oxalate ion across the membrane for every monovalent formate ion shuttled in with an estimated turnover number of about 1000 s^{-1} (205), a value that is about an order of magnitude higher than other secondary carriers. OxlT, a member of the major facilitator superfamily (MFS) of transporters (182), has been the focus of extensive study: substrate analysis (255), topology analysis by fluorescence labelling (267), homology modelling (265), and kinetic studies of the protein in reconstituted liposomes (3, 205).

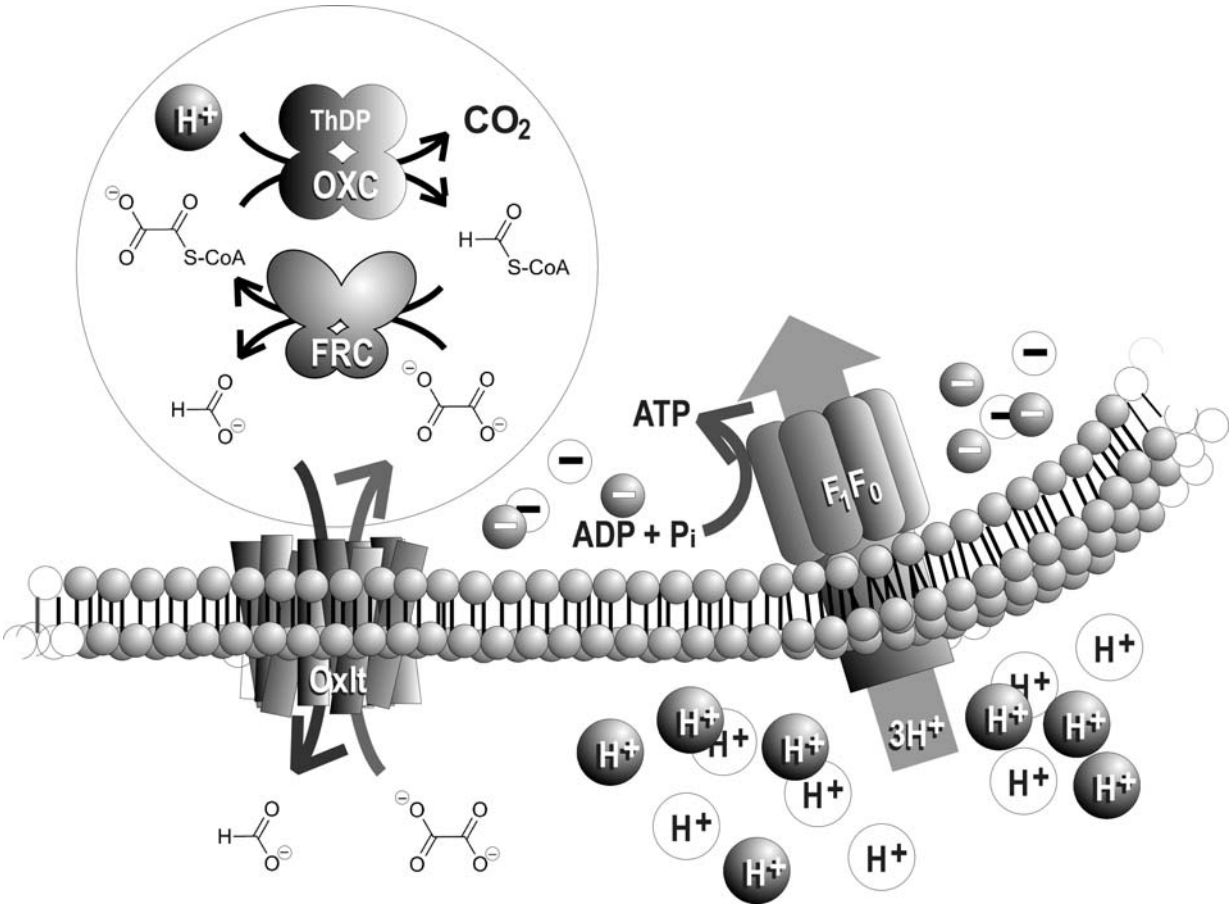

Figure. 1-1. Cartoon representation of the key metabolic enzymes of *O. formigenes*. OXC, oxalyl-CoA decarboxylase; FRC, formyl-CoA transferase; OxlT, formate:oxalate antiporter; and ATP synthase.

Formyl-CoA transferase (FRC)

Formyl-CoA transferase catalyzes the transfer of CoA from formyl-CoA to oxalate to yield oxalyl-CoA and formate (9, 124). FRC is the best-studied member of the Family III CoA transferases and will be discussed later in detail (see page 37).

Oxalyl-CoA decarboxylase (OXC)

OXC is a thiamine-dependent non-oxidative decarboxylase. The native enzyme was first purified from *O. formigenes* by Baetz et al; the 260 kDa homotetramer was reported to comprise four 65 kDa monomers (10). Steady-state kinetics studies demonstrated that specificity constant for OXC is about 3.8×10^6 $M^{-1}s^{-1}$, $K_{M(oxalyl\text{-}CoA)}$ is 23 μM, and k_{cat} is 88 s^{-1} (15). Adventitious ADP was found tightly bound in the 1.8 Å X-ray crystal structure in the same report. Analysis showed that micromolar concentrations of ADP were required for maximal enzymatic activity, whereas ATP had no effect. Considering the vital role that OXC plays in oxalate metabolism, this finding strongly suggests that ADP-dependent activation of OXC in *O. formigenes* is physiologically relevant.

Coenzyme A

History of Coenzyme A

Coenzyme A (CoA), is a cofactor essential to all living organisms, involved in over 100 different metabolic reactions, and purported to be utilized by about 4% of all known enzymes. The discovery of CoA is historically linked to the elucidation of the mechanism by which saturated fatty acids are utilized in living organisms and, as such, Franz Knoop's famous 1904 use of a labelled phenyl group to show that fatty acids are degraded by successive removal of two-carbon units (139) was to become the starting point for both understanding β-oxidation and identifying CoA. In 1942 Feodor Lynen demonstrated that after respiring yeast had exhausted their supply of substrates, a lag or induction period was required before the process of oxidizing

acetate could resume, and further, that the process could be facilitated by the addition of oxidizable substrates such as ethyl, propyl, or butyl alcohol (158). This lead to the theory that acetate must be "activated" in some fashion in order to be used as a substrate and, indeed, Lynen was later able to identify acetyl-CoA from starved yeast (159). At the same time, several independent research groups confirmed that some form of "active acetic acid" was required for the enzymatic acetylation of both sulfanilamide (152) and choline (80, 176, 177) and it was theorized that the same water soluble activator was involved in all cases. Fritz Lipmann (154) was able to purify this activator—coenzyme for acetylation—and demonstrated that it comprised pantothenic acid, or vitamin B_5, whose origin and nature had been reported in the 1930's (263), and, upon acid hydrolysis, β-alanine. The complete purification protocol, the presence of sulfur, as well as the identification of a pyrophosphate bridge to an adenylate group was reported in 1950 (153, 155). Snell and coworkers were able to show that the sulfur-containing component of CoA is cysteamine, or 2-amino-ethanethiol, linked to pantothenic acid by a peptide bond (228). Baddiley used a combination of analysis and synthesis to show that the pyrophosphate group binds to the 4-position of pantothenate (8). Kaplan demonstrated that the third phosphate is bound to the 3'-position of the adenylyl-bound ribose (223). With the composition of CoA understood and the availability of isolated acetyl-CoA, researchers would now have the tools necessary to unravel the mysteries of the processes involved in β-oxidation.

Coenzyme A Pool in Bacteria

In vivo CoA pools have been determined for *E. coli* by three methods. Radioisotopic methods were employed to assay the total CoA pool in β-alanine auxotrophs (*panD2*) grown on glucose-minimal medium. Concentrations were about 380 μM with about 80% found as acetyl-CoA(118). The three other major species were CoA, 52 μM; succinyl-CoA, 22 μM; and malonyl-CoA, 2 μM. Chohnan and coworkers employed their malonate decarboxylase-

dependent acyl-CoA cycling method (242) to amplify CoA levels in anaerobic and aerobic *E. coli*. They report that CoA thioester concentrations are 10 times higher under anaerobic conditions than aerobic and their value for the total CoA pool concentration agreed with the previous report (300 – 520 μM) (45, 46). Boynton *et al.* have used reverse-phase HPLC methods to analyse CoA thioesters in *Clostridium acetobutylicum* (ATCC 824) (26). The total CoA pool ranged from about 1.0 – 1.2 mM.

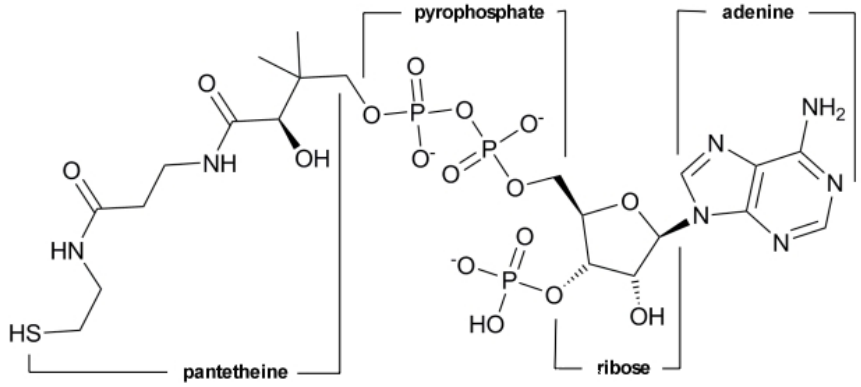

Figure. 1-2. Coenzyme A. CoA comprises an adenine ring and 3'-phosphorylated ribose linked to a pantetheine domain by a pyrophosphate linker.

Reactivity of Coenzyme A

Coenzyme A comprises an adenine ring, 3'-phosphorylated ribose linked to a pantetheine domain by a pyrophosphate linker (Figure 1-2). CoA both carries and activates acyl groups as thioesters formed by reaction with the nucleophilic CoA thiol in two ways—the carbonyl is more electrophilic and the α-carbon is more acid (pK_a~21) (171). Acyl groups can be transferred to another nucleophile, or the activated thioesters can undergo α-carbon condensation, 1,4-addition, or reduction reactions at the thioester carbonyl. Enzymatic reactions with acetyl-CoA involve either Claissen or aldol condensations as with citrate synthase, the gateway to the TCA cycle; acetyl-CoA carboxylase which catalyzes the synthesis of malonyl-CoA, the starting point for fatty acid synthesis; or, the acylation of compounds, e.g. the inactivation of antibiotics such as

chloramphenicol or kanamycin by acetylation in resistant bacteria (194, 195, 222). In β-oxidation of fatty acids, CoA is purported to stabilize the negative charge on the α-carbon for dehydrogenation and addition of water across the double bond (252).

In simple terms, the pantetheine and ADP moieties can be considered the structural components responsible for enzyme interaction and aligning the reactive sulfur atom. In a study by Jencks *et al*. it was demonstrated that the pantoic acid and ADP domains were critical for transition state stabilization and contributed significantly to k_{cat}/K_M (259). However, other studies have shown that in some cases the ADP moiety contributes little to binding and catalysis (55, 83),

Coenzyme A Transferases

Coenzyme A transferases, initially termed thiophorases or transphorases, catalyze the reversible transfer of coenzyme A from a thioester donor to a free acid. CoA transferases are found in all Eubacteria and Eukaryota (putative genes are found in Archaea) and play important roles in amino acid catabolism (12, 21, 32, 39, 218), ketone-body metabolism (22, 236), aromatic (132) and chloro-aromatic degradation (91), acetone-butanol fermentation (4, 122), and fatty acid fermentation (140). There are currently 16 enzymes listed as CoA transferases (EC 2.8.3; IUBMB, 2005); these can be further separated into three CoA Transferase Families based on function, structure, and sequence similarity (102).

In addition to other properties, the three Families are separated on the basis of kinetic mechanism. All three share a common group transfer mechanism summarized by the following equations:

$$A + B \rightleftharpoons P + Q \quad \text{or} \quad ACoA + B \rightleftharpoons A + BCoA$$

where CoA and is transferred from a donor acid (A) to an acceptor acid (B). Mechanisms of this type can be divided into those which proceed through a ternary complex, ordered or random, and those which pass through a substituted mechanism, i.e. ping-pong mechanism.

Family I CoA Transferases

Family I CoA transferases, specifically in EC 2.8.3.5-6 and 8-9, share two signature motifs: signature 1 (PS01273) is found in the N-terminal region of the α-subunit and may be involved in CoA binding. The second consensus sequence motif (PS01274) (S)ENG, where E is the active-site glutamate, is found in the N-terminal region of the β-subunit (162, 183). Family I CoA transferases, i.e. glutaconate-CoA transferase (35), involve an enzyme-CoA thioester intermediate and follow a substituted mechanism which can be identified by the set of initial velocity plots where 1/velocity vs. the reciprocal of one substrate yields a pattern of parallel lines (Figure 1-3). Evidence for the formation of the two anhydride intermediates, in addition to the enzyme-CoA intermediate, has been obtained from model reactions with citramalate lyase (30).

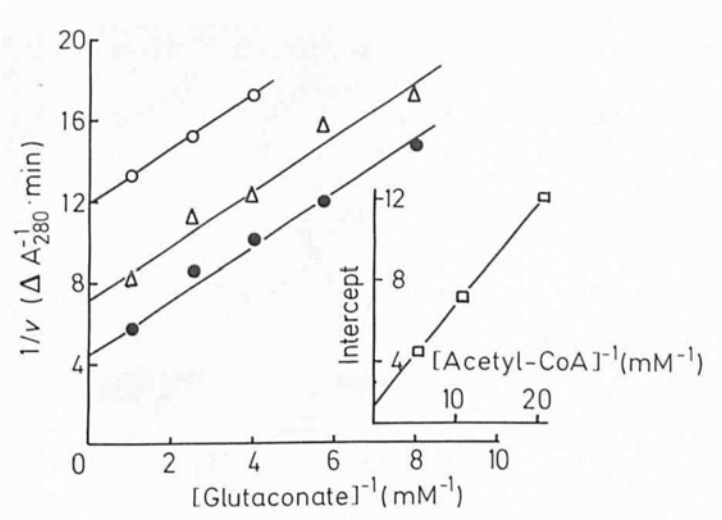

Figure. 1-3. Ping-pong kinetics of Family I glutaconate-CoA transferase (GCT) from *Acidaminococcus fermentan*. Taken from Buckel 1981 (35).

Propionate CoA transferase (EC 2.8.3.1)

The first reports of catalysis of the reversible transfer of CoA to various fatty acids was in cell-free extracts from *Clostridium kluyveri* (234), but propionate CoA transferase from *C. propionicum* was the first purified and reported to have a tetrameric quaternary structure comprising four identical 67 kDa subunits (214). Propionate CoA transferase is an important enzyme in the nonrandomizing alanine fermentation pathway of *C. propionicum*: alanine is converted to ammonia and pyruvate which is reduced to (R)-lactate, activated as (R)-lactoyl-CoA, and subsequently reduced to propionate. Propionate CoA transferase activates lactate as the CoA thioester using propionyl-CoA as the CoA donor (214). The enzyme is also implicated in the methylmalonyl-CoA pathway for the propionate-oxidizing metabolic pathway of *Pelotomaculum thermopropionicum* (140, 211). Glu-324 was identified as the active site carboxylate by MALDI-TOF MS of enzyme incubated with priopionyl-CoA, labelled with either borohydride (-14 Da) or hydroxylamine (+15 Da), and subsequently proteolytically digested individually by chymotrypsin, endoprotease-AspN, endoprotease-GluC, or trypsin (218). Further, propionate CoA transferase lacks the (S)ENG consensus motif shared by Family I CoA transferases.

Succinyl-CoA:oxalate CoA transferase (EC 2.8.3.2)

Quayle has done extensive study on the facultative autotroph *Pseudomonas oxalaticus*, now called *Cupriavidus oxalaticus* (249), and its metabolism of oxalate and formate (191-193). Limited characterization of cell lysates suggested the presence of a CoA transferase that reversibly transfers CoA between oxalate and succinate.

Acetyl-CoA:malonate CoA-transferase (EC 2.8.3.3)

Bacterial growth on malonate generates the end products acetate and CO_2 (for a review, see Dimroth (64)). The malonate decarboxylase complex in *Pseudomonas ovalis* comprises five

subunits (α-ε) (44). The 60 kDa α-subunit has malonate-CoA transferase activity (43); CoA is transferred from actetyl-CoA to form malonyl-CoA which is subsequently decarboxylated (100).

Succinyl-CoA:3-ketoacid CoA transferase (SCOT; EC 2.8.3.5)

SCOT activates acetoacetate by transferring CoA from succinyl-CoA (236) and is an essential enzyme in ketone-body metabolism. Acetoacetyl-CoA is catabolized to acetyl-CoA which can enter the TCA cycle or fatty-acid metabolic pathway. Bacterial SCOT comprises α- and β-subunits that form a heterodimer (54). Mammalian SCOT from sheep kidney and rat brain exist as homodimers (207, 221). Pig heart SCOT has been reported to exist as a homodimer (71, 106), as well as a homotetramer that dissociates slowly to homodimer in high potassium chloride (202). However, each monomer comprises two domains corresponding to the α- and β-subunits in other Family I CoA transferases (54, 183). Initial velocity studies and treatment with sodium boro[^{3}H]hydride show that SCOT catalyses a ping-pong reaction where an enzyme-CoA intermediate exists with CoA covalently bound to the enzyme through the γ-carboxylate of a glutamate residue at each active site in the protein (22, 106, 207, 229). Isotope labelling experiments where SCOT was incubated with [$^{18}O_4$]-succinate and acetoacetyl-CoA showed reversible incorporation of ^{18}O into some oxygen-containing group on the enzyme (14). This residue in pig heart SCOT has been identified as Glu-305 by mass spectrometry and the adventitious autolytic reaction that occurs with the thioesters of γ-carboxylates through a 5-oxyprolyl intermediate (115, 201, 264). Because of its relative stability (the rate constant for hydrolysis has been calculated as 0.10 min^{-1} at pH 8.1), the enzyme-CoA intermediate has been the target of several lines of research. Electrospray mass spectrometric analysis of SCOT identified peaks consistent with free SCOT, enzyme-CoA intermediate after incubation with either acetacetyl-CoA or succinyl-CoA, and the primary alcohol expected upon treatment with sodium borohydride (156). More interestingly, further experiments provided compelling

evidence for half-sites reactivity, where only one active site per dimer was required for full activity. Jencks and coworkers have used various hydroxylamine and hydroxamic acid derivatives to probe the nature of the reaction mechanism (187).

There are currently five solved X-ray crystal structures archived in the RCSB Protein Data Bank: three of SCOT at 2.5 (1m3e), 2.4 (1o9l), and 1.7 Å (1ooy) resolution, respectively (13, 53), and two ΔSCOT deletion variants where residues 249-254, a region easily cleaved by proteolytic enzymes, were removed (1ope and 1ooz) (53).

3-Oxoadipate CoA-transferase (EC 2.8.3.6)

Oxoadipate CoA transferase catalyses the transfer of CoA from succinyl-CoA to β-ketoadipate, and the product, β-ketoadipyl-CoA is subsequently converted to acetyl-CoA and succinyl-CoA by a thiolase in the degradation of aromatics (132). These activities were first isolated in the cell-free lysate of *Pseudomonas fluorescens* (132). Homogeneous proteins from both *Pseudomonas* and *Acetinobacter* have an $\alpha_2\beta_2$ oligomeric structure as determined by both gel filtration and gene analysis (183, 268). The genes for the two subunits (*pcaI* and *pacJ*) are separated by only 8 base pairs in *Pseudomonas putida* and it is proposed that a gene fusion event may explain the homodimeric structure of mammalian succinyl-CoA transferase (183). The transferase from *Pseudomonas* sp. strain B13 is involved in degradation of aromatics and chloroaromatics (131). K_M values for 3-oxoadipate and succinyl-CoA were 0.4 and 0.2 mM, respectively, at a pH optimum of 8.4. The B13 transferase is a heterotetramer of the type $\alpha_2\beta_2$ with an overall size of 120 kDa and subunits with molecular masses of 32.9 and 27 kDa.

Succinyl-CoA:citramalate CoA-transferase (SmtAB; EC 2.8.3.7)

SmtAB (87) is proposed to be involved in CO_2 fixation by *Chloroflexus aurantiacus*, a thermophilic green nonsulfur bacterial phototroph. The enzyme has been purified; it appears to

exist as a αβ heterohexamer (44 and 46 kDa subunits). Similar enzymes in *Pseudomonas* sp. and *Micrococcus* sp. activate itaconate to itaconyl-CoA which is converted to acetyl-CoA and pyruvate in a series of steps (49, 50).

Acetate CoA-transferase (AA-CoA transferase, atoDA; EC 2.8.3.8)

Acyl-CoA:acetate CoA-transferase activity was detected as early as 1968 in *E.* coli (250) and is associated with short fatty acid, e.g. butanoate and propanoate, metabolism. The transferase and a CoA lyase, both members of the *ato* operon, are upregulated when *E. coli* is grown on acetoacetate (184). Two subunits of molecular mass 26 kDa (atoD) and 24-26 kDa (atoA) compose the $\alpha_4\beta_4$ hetero-octameric protein (231). In an experiment similar to that of Solomon and Jencks (229), the catalytic glutamate residue on the β –subunit was detected by $NaBH_4$ treatment after incubation with acyl-CoA (231). The apparent K_M for acetyl-CoA with acetoacetate and K_M for acetoacetyl-CoA with acetate were 0.26 mM and 35 μM, respectively.

Butyrate-acetoacetate CoA-transferase (EC 2.8.3.9)

Butryate-acetoacetate CoA transferase was first purified from the acetoacetate degradation operon (*ato*) in constitutive *E. coli* (232), then later from lysine-fermenting *Clostridium SB4* (12) and solventogenic (acetone) *Clostridium acetobutylicum* ATCC 824 (261). The enzyme is important in detoxification of the medium from acetate and butyrate fermentation products. Enzymes from all three organisms were reported to comprise $\alpha_4\beta_4$ hetero-octameric quaternary structure with subunits of about 23 and 25 – 26 kDa each.

Acetyl-CoA: glutaconate CoA-transferase (GCT; EC 2.8.3.12)

Acidaminococcus fermentans, C. microsporum, Fusobacterium nucleatum, and *F. fusiformis* metabolize glutamate through the hydroxyglutarate pathway involving many transformations carried out at the CoA-ester level (31, 32). Like propionate CoA transferase, glutaconate CoA transferase does not have the (S)ENG motif. Recombinant proteins from

Acidaminococcus fermentans have been overexpressed in *E. coli* and the active protein exists as $\alpha_4\beta_4$ hetero-octamer where the two subunits have molecular masses of 35.5 kDa and 29 kDa respectively (35, 162). Initial velocity studies showed that the enzyme uses a ping-pong kinetic mechanism (35) and peaks of *m/z* consistent with the enzyme-CoA intermediate have been detected by MALDI-TOF mass spectrometry of enzyme incubated with only glutaryl-CoA (217). Glu-54 of the β-subunit was identified as the catalytic amino acid residue by reducing the enzyme-CoA thioester with sodium boro[^{3}H]hydride and detecting 2-amino-5-hydroxy[5-^{3}H]valeric acid in a peptide generated by trypsin proteolysis (35, 162). Site-directed mutagenesis experiments where Glu-β54 was replaced with alanine or asparagine completely abolished all activity while conversion to glutamine retained 1% of wild type activity (164). Intriguingly, when the βE54Q variant was incubated with substrates for 40 hours at 37º C nearly wild-type activity was restored. The enzyme has been converted from a CoA transferase to a thioester hydrolase by replacing Glu-54 with aspartate (163). Oxygen exchange between [$^{18}O_2$]-acetate, glutaconate CoA transferase, and glutaryl-CoA was further proof of the Family I mechanism (217) (see Figure 2-1). In addition, the βE54D hydrolase variant did not undergo ^{18}O uptake into the aspartate carboxylate. The first X-ray crystal structure (PDB 1POI) of a CoA transferase was solved for GCT (119).

Family II CoA Transferases

Family II transferases involve a ternary complex and yield a pattern of intersecting lines in the double-reciprocal plots when either substrate concentration is varied (see Figure 1-5). The transferase α-subunit of citrate or citramalate lyase complexes facilitate the direct transfer of CoA from acetate to citrate or citramalate without any covalent bond forming between enzyme and substrate (34, 63). The CoA cofactor is covalently bound to the both enzymes by a

phosphodiester linkage from Ser-14 to 2′-(5′′-phosphoribosyl)-3′-dephospho-CoA (19, 61, 200, 226) (see Figure 1-4).

Citrate CoA-transferase (EC 2.8.3.10)

Citrate lyase (EC 4.1.3.6) catalyses the reversible cleavage of citrate to yield oxaloacetate and acetyl-CoA used in fatty acid synthesis. Citrate CoA transferase is the largest subunit (α) of the three-subunit citrate lyase complex. Most biochemical characterization has been carried out by the enzyme purified from *Klebsiella pneumoniae* (formerly *Klebsiella aerogenes*). Neither initial velocity studies performed with varied citrate concentrations and varied fixed acetyl-CoA concentrations nor with varied citryl-CoA and varied fixed acetate showed the parallel line pattern expected in the double-reciprocal plots of ping-pong kinetics (65).

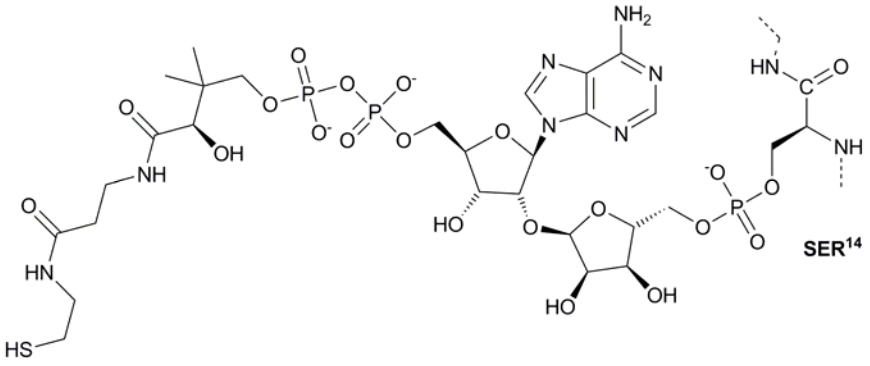

Figure. 1-4. Prosthetic cofactor of citrate lyase 2′-(5′′-phosphoribosyl)-3′-dephospho-CoA is bound to Ser-14 of the ACP subunit by the ribose 5'- phosphate linkage.

Further evidence for no enzyme-CoA intermediate includes: no isolable enzyme-CoA intermediate upon incubation of citrate CoA transferase with acetyl-CoA; no enzyme inhibition, nor acetyl-CoA hydrolysis, were detected when an enzyme/acetyl-CoA mixture was treated with excess borohydride; and, no increase in radiolabel was detected in acetate measured after the enzyme and [^{14}C]-acetyl-CoA were incubated together (65). Citrate blocks the reacetylation of the deacetylated lyase with acetic anhydride which has been shown to be an intermediate substrate analogue for citramalate lyase (30, 65).

Citramalate CoA-transferase (EC 2.8.3.11)

Citramalate lyase (EC 4.1.3.8) catalyses the cleavage of citramalate to pyruvate and acetate and comprises six copies each of three different proteins: γ-subunit, acyl-carrier protein (ACP); α-subunit, the citramalate CoA transferase; and β-subunit, citramalyl-CoA lyase (EC 3.1.2.16) (62). Citramalate CoA transferase purified from *Klebsiella aerogenes* catalyses the transfer of the thio-acyl carrier protein from (3S)-citramalyl-thio-acyl carrier protein to acetate to generate citramalate and acetyl-thio-acyl carrier protein (65). The β-subunit lyase catalyses the cleavage of citramalyl-CoA to pyruvate and acetyl-CoA in a Mg^{+2}-dependent reaction. As seen in Figure 1-5, there is no indication that the kinetics follow a ping-pong mechanism when either substrate is varied. Interestingly, the enzyme purified from the citrate lyase protein complex catalyses the acetyl-CoA:citramalate CoA transferase reaction more efficiently. Treatment with borohydride did not inactivate the transferase, and no enzyme-substrate intermediate could be isolated. The

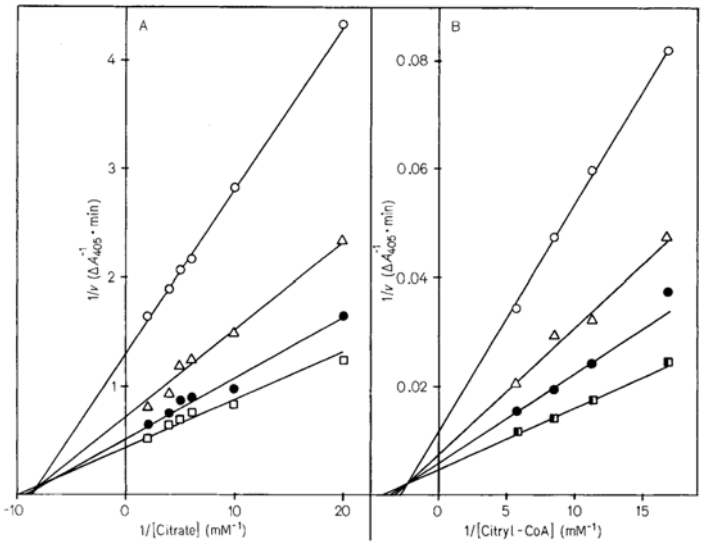

Figure. 1-5. Double-reciprocal plots of initial velocity data consistent with an ordered mechanism in Family II citramalate-CoA transferase from *Klebsiella aerogenes*. Taken from Dimroth 1977 (65).

subunits of citrate lyase and citramalate lyase are so similar that active hybrid enzyme complexes have been formed from the α- and β-subunits of citramalate lyase and the ACP (-subunit from citrate lyase (62).

Family III CoA Transferases

Previous work, including site-directed mutagenesis, steady-state kinetics, and product inhibition studies on recombinant FRC from *Oxalobacter formigenes*, the representative enzyme of Family III CoA transferases, have demonstrated that Asp-169 is a vital catalytic residue and that the reaction proceeds through a ternary complex where formyl-CoA binds first followed by oxalate followed by release of formate prior to oxalyl-CoA in an ordered sequential mechanism (124). Thus, unlike the Family I ping-pong kinetic mechanism, formate must remain in the active site until chemistry is complete. However, this does not exclude the possible formation of an enzyme-CoA thioester intermediate like that of glutaconate-CoA transferase during catalysis (35, 217). Indeed, an X-ray crystal structure in the study showed electron density consistent with an oxalyl-aspartyl mixed anhydride in the active site, evidence that just such a covalent enzyme-substrate intermediate may exist along the reaction pathway. Theoretical reaction mechanisms are shown in Figure 1-6.; Mechanism 1 in Figure 1-6 is a viable proposal conditional that formate remains in the active site. Two other likely mechanistic pathways exist: Mechanism 2, the direct attack of the formyl-CoA carbonyl by oxalate, in a mechanism analogous to that of Family II transferases, followed by the CoA thiolate attacking oxalate; and, Mechanism 3 proposed by Jónsson *et al.* (124) where nucleophilic attack of the formyl carbonyl by Asp-169 is followed by attack of oxalate on the resultant aspartyl-formyl mixed anhydride to form an aspartyl-oxalyl mixed anhydride intermediate which is finally attacked by CoA, which has remained in the active site , generating the final product.

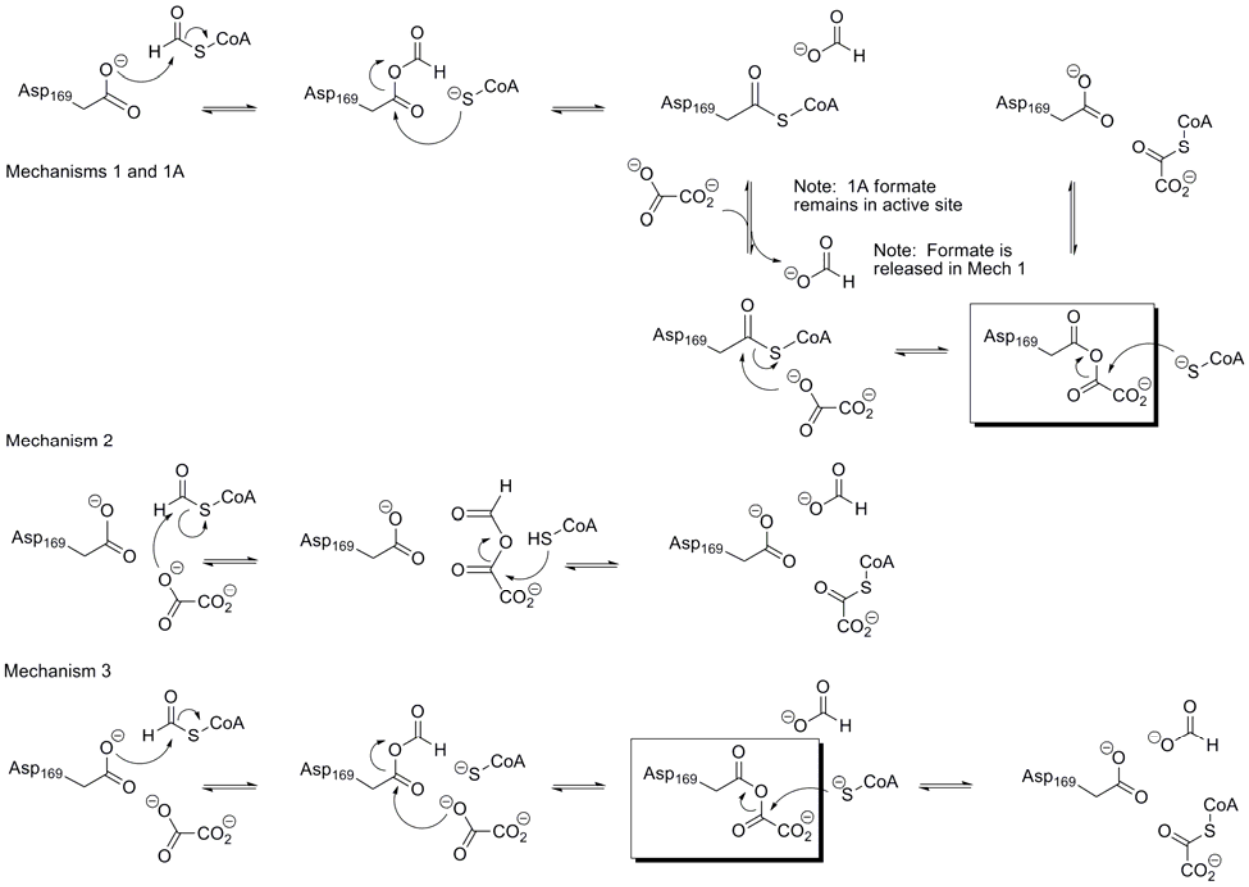

Figure. 1-6. Possible reaction mechanisms for FRC. Mechanism 1 corresponds to the Family III CoA transferase pathway that exhibits ping-pong kinetics. Mechanism 1A is the ordered sequential variation of Mechanism 1 where formate must remain in the active site until oxalyl-CoA is formed. Mechanism 2 is analogous to the enzyme stabilized direct-attack mechanism of Family II CoA transferases. Mechanism 3 is a third proposed mechanism that avoids the enzyme-CoA thioester intermediate of Mechanism 1 (124). Enzyme aspartyl-oxalyl mixed anhydride intermediates in the reaction pathways are highlighted. Putative tetrahedral intermediates have been omitted to save space.

Formyl-CoA transferase (FRC; EC 2.8.3.16)

Formyl-CoA transferase activity was first suggested by studies of *Pseudomonas oxalaticus* (192) and limited kinetic characterization was carried out on native formyl-CoA transferase (FRC) isolated from *Oxalobacter formigenes* (9). FRC has been detected in *Enteroccus faecalis* and identified by Western blotting using antibodies against *frc* from *O. formigenes* (111).

The *frc* gene has since been cloned from *O. formigenes*; recombinant wild-type FRC has 428 amino acids, pI of 5.2, a calculated monomeric mass of 47.3 kDa, and exists in solution as a homodimer (225). Steady state kinetics and product inhibition studies by Jónsson *et al.*, established that the enzyme exhibits an ordered sequential Bi-Bi kinetic mechanism where formyl-CoA binds first followed by oxalate (124). Subsequent to the chemistry step, formate is released first followed by oxalyl-CoA. FRC was initially reported to be a monomer (9), but later crystal structure data suggested that the catalytic subunit is dimeric (197). Size-exclusion chromatography experiments have since confirmed that active FRC exists as the dimer (124).

High resolution X-ray crystal structures of YfdW, a putative formyl-CoA transferase in *E. coli*, have been published independently by two groups (92, 97). YfdW, identified by structural genomics as part of the effort to annotate the many unknown genes in *E. coli* (251), shares 63% identity with FRC (see Figure 1-8) and is proposed to be a formyl-CoA transferase (97). YfdW is the gene product of the *yfdXWUVE* operon, where the *yfdX* gene is under the control of the EvGAS two-component regulatory system (see Figure 3-3), and has been implicated in acid resistance in *E. coli* (169).

In addition, *frc* and *oxc* genes also appear to be involved in acid protection mechanisms in *Lactobacillus acidophilus*. Variants with *frc* and *oxc* deletions challenged by exposure to pH 3.5 showed a reduced ability to survive compared to the wild type (7). Interest in possible probiotic treatments for oxalate stones has also prompted study of formyl-CoA transferase activity in *L. acidophilus*. Of the 60 *Lactobacillus* strains evaluated, several showed high oxalate degrading activity (247).

BaiF

Some prokaryotes are able to metabolize bile acids utilizing the bile acid inducible (*bai*) operon (see the review by Ridlon *et al*. (199)). BaiF, the protein product of the *baiF* gene, is

proposed to mediate CoA transfer between several cholic acid derivatives, i.e. CoA from 3-dehydro-4-cholenoic acid to cholic acid, 3-dehydro-4-chenodeoxycholenoic acid to chenodeoxycholic acid, or 3-dehydro-4-ursodeoxycholenoic acid to ursodeoxycholic acid. Baif has been isolated from the intestinal anaerobe *Eubacterium* sp. strain VPI 12708 (258). The recombinant protein has been overexpressed in *E. coli* (266). The K_M and V_{max} for the hydrolysis of cholyl-CoA were ca. 175 μM and 374 μmol/min mg, respectively. Although the 47.5 kDa protein has only been demonstrated to have bile acid-CoA hydrolase activity, its gene sequence does not contain a signature motif found in many thioesterases (266); it is proposed to be a CoA transferase and play an important role in ATP-independent recycling of CoA thioesters and, thus, conserving energy (102).

Succinyl-CoA:(*R*)-benzylsuccinate CoA-transferase (BbsEF; EC 2.8.3.15)

BbsEF is involved in the anaerobic degradation pathway of aromatic compounds in bacteria (for a review on anaerobic degradation of aromatics see Heider (103)). *Thauera aromatica* metabolizes toluene as well as phenol, *p*-cresol, anthranilate, and phenylalanine (104). In toluene metabolism, toluene is oxidized to benzoyl-CoA and succinyl-CoA in a proposed six step pathway. In one important step, CoA is transferred from succinyl-CoA to benzylsuccinate to form benzylsuccinyl-CoA. BbsEF has been purified from *T. aromatica* grown on toluene (149). BbsE (44 kDa) and BbsF (46 kDa), the two subunits that compose the active $\alpha_2\beta_2$ protein, are products of the the *bbs* operon (β-oxidation of benzyl-succinate) (148). Double-reciprocal plots of the intial velocity kinetics are consistent with an ordered sequential mechanism. The K_M values for the reverse reaction were 40 μM for 2- and 3-(*R*)-benzylsuccinyl-CoA and 160 μM for succinate. BbseF could be inactivated in a benzylsuccinyl-CoA concentration dependent manner with high concentrations (1 and 10 mM) $NaBH_4$, but lower concentrations (0.1 mM) and hydroxylamine had no effect.

Crotonobetainyl/γ-butyrobetainyl-CoA:carnitine CoA-transferase (CaiB)

Carnitine is an organic molecule important in long-chain fatty acid transfer across the mitochondrial inner membrane in humans. *E. coli* is able to utilize carnitine as an osmoprotectant (128) and as a terminal electron acceptor under anaerobic conditions (138). Carnitine is metabolized to (-butyrobetaine by a three-enzyme system comprising CaiA, CaiB, and CaidD (74, 75, 190). Carnitine is activated by the CoA transferase CaiB; carnitine is added to CoA from γ-butyrobetainyl-CoA to form carnitinyl-CoA and γ-butyrobetaine. Carnityl-CoA is reduced to γ-butyrobetainyl-CoA by CaiD, a dehydratase, and CaiA, reductase. The end result is a 2 electron reduction coupled to the regeneration of γ-butyrobetainyl-CoA which is used for the next cycle. CaiB also catalyzes transfer from crotonyl-CoA (74). A fourth enzyme, CaiC, is thought to prime the cycle by ATP-dependent formation of carnityl-CoA (102). Dimeric X-ray crystal structures of CaiB from *E. coli*, CaiB/CoA, and CaiB/CoA/Crotonyl-CoA complexes have been solved (196, 235) and these structures share high structural similarity with FRC structures. CaiB is missing the tetraglycine loop of FRC and has a larger active site consistent with its larger substrates. The small and large domains appear to close together upon substrate binding (196, 235).

Cinnamoyl-CoA: phenyllactate CoA-transferase (FldA; EC 2.8.3.17)

Phenyllactate CoA transferase is one of three enyzmes in the heterotrimeric phenyllactate dehydratase complex important in L-phenylalanine fermentation in strictly anaerobic *Clostridium sporogenes* (210). FldA forms activated phenyllactyl-CoA by transferring CoA from cinnamoyl-CoA. The remaining enzymes in the $[4Fe\text{-}4S]^{2+}$-containing complex, FldB and FldC, remove water to regenerate cinnamoyl-CoA and (E)-cinnamate. FldA has a molecular weight of 46 kDa and when purified alone appears as a dimer (97 kDa) in gel filtration analysis (60). The lines on the double-reciprocal plot of 1/v vs 1/[phenylpropionate] and 1/[cinnamoyl-CoA] intersected in

the 2nd quadrant consistent with an ordered sequential kinetic mechanism. Micromolar K_M values for both substrates were reported. FldA activity was reduced 50% when incubated with cinnamoyl-CoA and treated with $NaBH_4$, but hydroxylamine had no effect.

2-Hydroxyisocaproate CoA transferase (HadA)

HadA is one five enzymes important in the leucine fermentation pathway of *Clostridium difficile*, a gram positive, non-spore forming strict anaerobe implicated in antibiotic-related diarrhea and psueodmembranous colitis in man (25, 188, 230). In the fermentation pathway where leucine is both oxidized to 3-methylbutyrate and reduced to isocaproate (28, 73). Recombinant HadA has been cloned from *C. difficile*, expressed, and purified by streptavidin-affinity chromatography (137). Variants where the cognate Asp-171 is changed by site-directed mutagenesis to either an N or A showed activity 2000 times less than the wild-type enzyme. This compares to the D169A FRC variant where activity was reduced ~1300-fold, but conflicts with the D169E variant that was completely inactive (124). HadA showed up to 88% inactivation with $NaBH_4$ and 94% with NH_2OH when the enzyme was incubated with 200 μM (R)-2-hydroxyisocaproyl-CoA, but no inactivation in the absence of substrate (137). Wild-type activity could be restored by incubating inactivated HadA with 2-hydroxyisocaproate and isocaprenoate for 20 hours at pH 8.0 and 25°C. Further, HadA could be activated by incubation with the two acids, to a maximal activation of 120% of wild-type activity before returning to 100%. However, in contrast to GCT, the D171N and D171N variants could not be induced to recover from inactivation. MALDI-TOF mass spectrometric analysis of the tryptic peptide showed only *m/z* of the untreated enzyme suggesting that Asp-171 may act in an alternate manner than Asp-169 in FRC.

α-Methyl-CoA racemase (MCR and Amacr)

Amacr, or α-methyl-CoA racemase, catalyzes the racemization of the (S)- and (R)-enantiomers of a variety of α-methyl-branched chain-CoA substrates in the β-oxidation of fatty acids (107) , bile acid synthesis (206), and ibuprofen bioactivation (37). The protein has been purified from rat and human liver (212, 213). Although, the catalytic oligomeric form is unknown, the monomer has a molecular mass of 45 kDa. It is proposed to be a member of Family III CoA transferases due to sequence similarity with other members (102). X-ray crystal structures have been reported for the homologous recombinant apoenzyme from *Mycobacterium tuberculosis* (MCR) (210) and for substrate-enzyme complexes with several substrates, including ibuprofenyl-, methylmyristoyl-, and acetyl-CoA, bound to the protein (20). On the basis of the active site geometry and kinetic results from several MCR variants prepared by site-directed mutagenesis (210), the two catalytic acid-base residues have been identified as His-126 and Asp-156 (analogous to Asp-169 in FRC). K_M and V_{max} for the release of ^3H from [2-^{3}H]pristanoyl-CoA were 41 μM and 214 μmol/min mg, respectively. Thus, it appears that MCR (and the mammalian Amacr enzymes) with its high sequence and structural similarity has taken the FRC scaffold and evolved a new enzymatic activity.

Conserved Structure of Family III CoA Transferases

Since Heider categorized the CoA transferases based on sequence similarity (102), X-ray crystallography studies have revealed that Family III CoA transferases also share a remarkable 3-dimensional tertiary structure that is more conserved than expected from the only ca. 25% sequence similarity. Family III transferases are dimers (BbsEF is reported as a tetramer); FRC, homologue YfdW, CaiB, and MCR comprise two subunits that thread through one another like links in a chain (97, 197, 210, 235). The N-terminus begins in the large domain, travels down

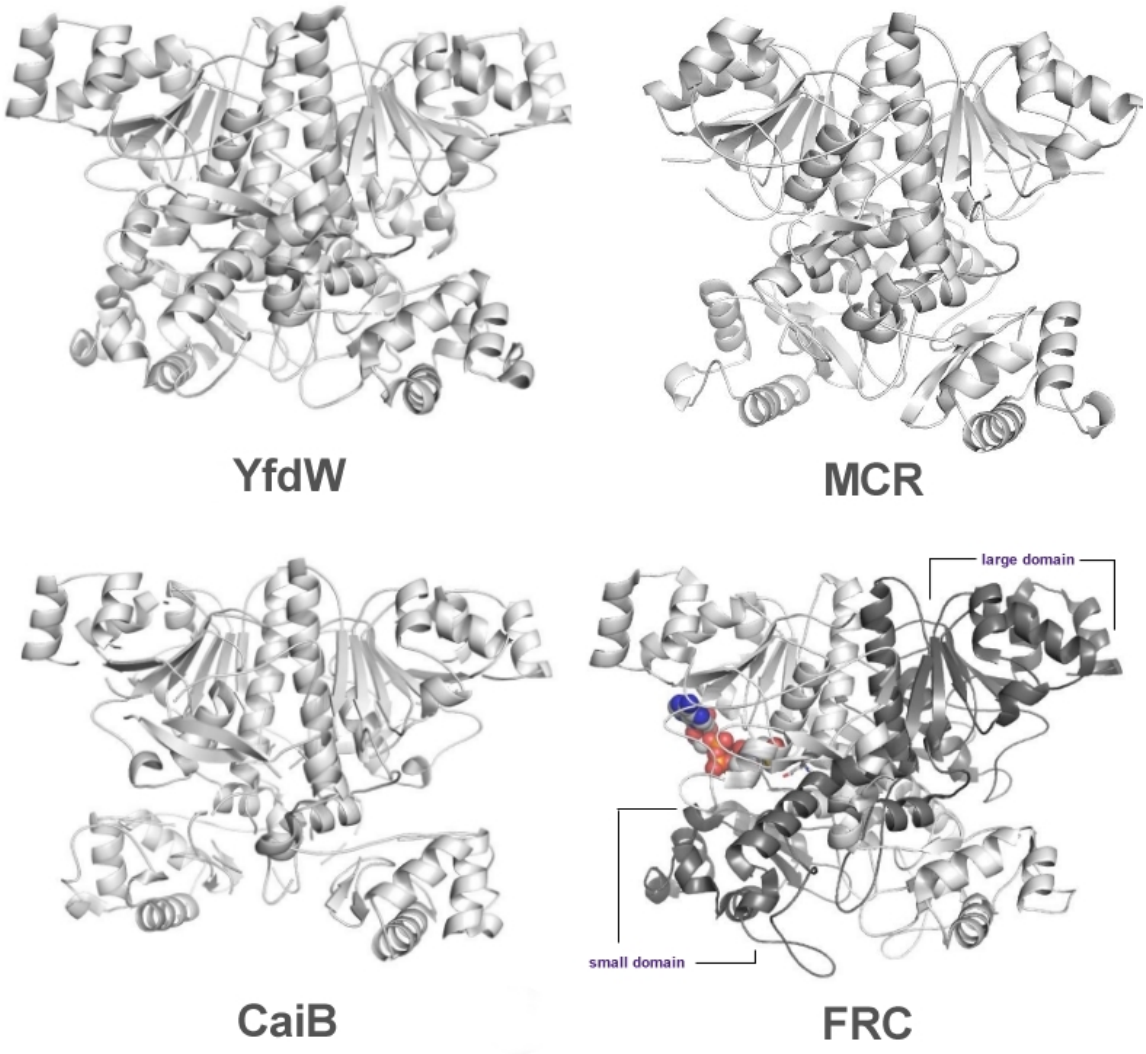

Figure. 1-7. Cartoon representations of Family III CoA transferases. *E. coli* YfdW (pdb 1pt5), *Mycobacterium tuberculosis* α-methylacyl-CoA racemase (MCR; pdb 1x74) (210), *E. coli* crotonobetainyl-CoA–carnitine CoA transferase (CaiB; pdb 1xa3) (235), and *O. formigenes* FRC (Protein Data Bank accession number 1p5h). Monomers in FRC are shown in black and white. CoA is shown *in spheres* bound in the active site, at the interface of the large and small domains, just above the catalytic Asp-169 residue, *sticks*.

through a linker domain to the small domain and then back up to terminate in the large domain. The four structures were aligned and a structural sequence comparison was constructed (Figure 1-7). The large domains have relatively high similarity, while more diversity is apparent in the small domains. Substrate specificity, ranging from formyl-CoA to bulky steroids in MCR,

Table 1-1. Summary of Family III CoA Transferases. Structural data are summarized for the known Family III CoA transferases. AA refers to the number of amino acids in the monomer and %FRC is sequence identity with FRC.

Name	Description	X-ray Structure	Quaternary Structure	Subunit MW (kDa)	AA	% FRC	Organism/Pathway
BaiF (266)	cholyl-CoA hydrolase; proposed CoA transferase	--	--	47.5	426	27	anaerobic bile acid transformation
BbsEF (149)	succinyl-CoA: (R)-benzylsuccinate CoA transferase	--	$\alpha_2\beta_2$	44 and 45	410, 409	23, 28	first step of anaerobic toluene catabolism in *Thauera aromatica*
CaiB (79)	γ-butyrobetainyl-CoA: (R)-carnitine CoA transferase	apo, CoA	homodimer		405	24	anaerobic carnitine metabolism in *E. coli* and *Proteus* sp.
FldA (137) (PLCT)	(E)-cinnamoyl-CoA: (R)-phenyllactate CoA transferase	--	homodimer, heterotrimeric complex with FldABC	46	405	25	Stickland-fermentation in *Clostridia* (*sporigenes* and *difficile*)
FRC (124)	formyl-CoA: oxalate CoA transferase	multiple ligands (see text)	homodimer	47.2	428	100	oxalate metabolism in *Oxalobacter formigenes*
HadA (137)	(*R*)-2-hydroxyisocaproyl-CoA: (*E*)-2-isocaprenoate CoA transferase		homodimer	43		25	leucine fermentation in *Clostridum difficile*
MCR (210) (Amacr)	α-methylacyl-CoA racemase	multiple ligands (see text)	homodimer	39 (89)	360	23	bile acid synthesis in *Mycobacterium tuberculosis*
YfdW (97, 245)	formyl-CoA transferase	apo, Ac-CoA	homodimer	48.3	415	60	*E. coli*

appears to result from variation in the residues at the interface of the large and small domains, as well as from large differences in both the linker and small domains. Another key difference is that the formyl-CoA transferases all share a tetraglycine loop that is proposed to protect the active site and prevent hydrolysis of labile formyl-CoA (197).

Research Objectives

Three Families of CoA transferases, based on sequence similarity and kinetic mechanism, have been reported. Family I transferases use a ping-pong mechanism with an enzyme-CoA intermediate. Family II transferases form a ternary complex that involves direct attack of the incoming receptor acid on to the donor acyl-CoA substrate. So far, the kinetic mechanism of Family III CoA transferases, of which FRC is the representative and best characterized enzyme, is not completely understood. It is known that FRC forms a ternary complex with formyl-CoA binding first followed by oxalate in a sequential mechanism. X-ray crystal structures of FRC and OXC show variations in the conformation of peptide loops near the active site. It is proposed that these motions play an important role in catalysis. Finally, the gene product of *yfdW* in *E. coli* has been expressed, purified, and crystallized. This enzyme is a putative formyl-CoA transferase based on sequence homology and structural similarity; however, *E. coli* has no reported ability to metabolize oxalate. Confirming that YfdW is in fact a formyl-CoA transferase would be validation of structural genomics. The goals of this project were to

1. Determine if the mechanism of FRC includes an enzyme-substrate intermediate like that of Family I transferases, and if so, to determine the nature of the intermediate species;
2. Examine the nature of the tetraglycine loop in FRC and the C-terminal loop in OXC by site-directed mutagenesis and steady steady state kinetics; and,
3. Test YfdW for formyl-CoA transferase activity.

Figure. 1-8. Structure-based sequence alignment of Family III CoA transferase family members. This alignment, *following page*, was generated by the superimposition of the crystal structures of FRC (pdb 1p5h), YfdW (pdb 1pt5), MCR (pdb 1x74) (210), and CaiB (pdb 1xa3) (235). α-Helical and β-strand secondary structural elements are colored *orange* and *blue*, respectively. Specific residues discussed in the text are highlighted. Asterisks indicate residues identical in all four transferases. Taken from Toyota 2008 (245).

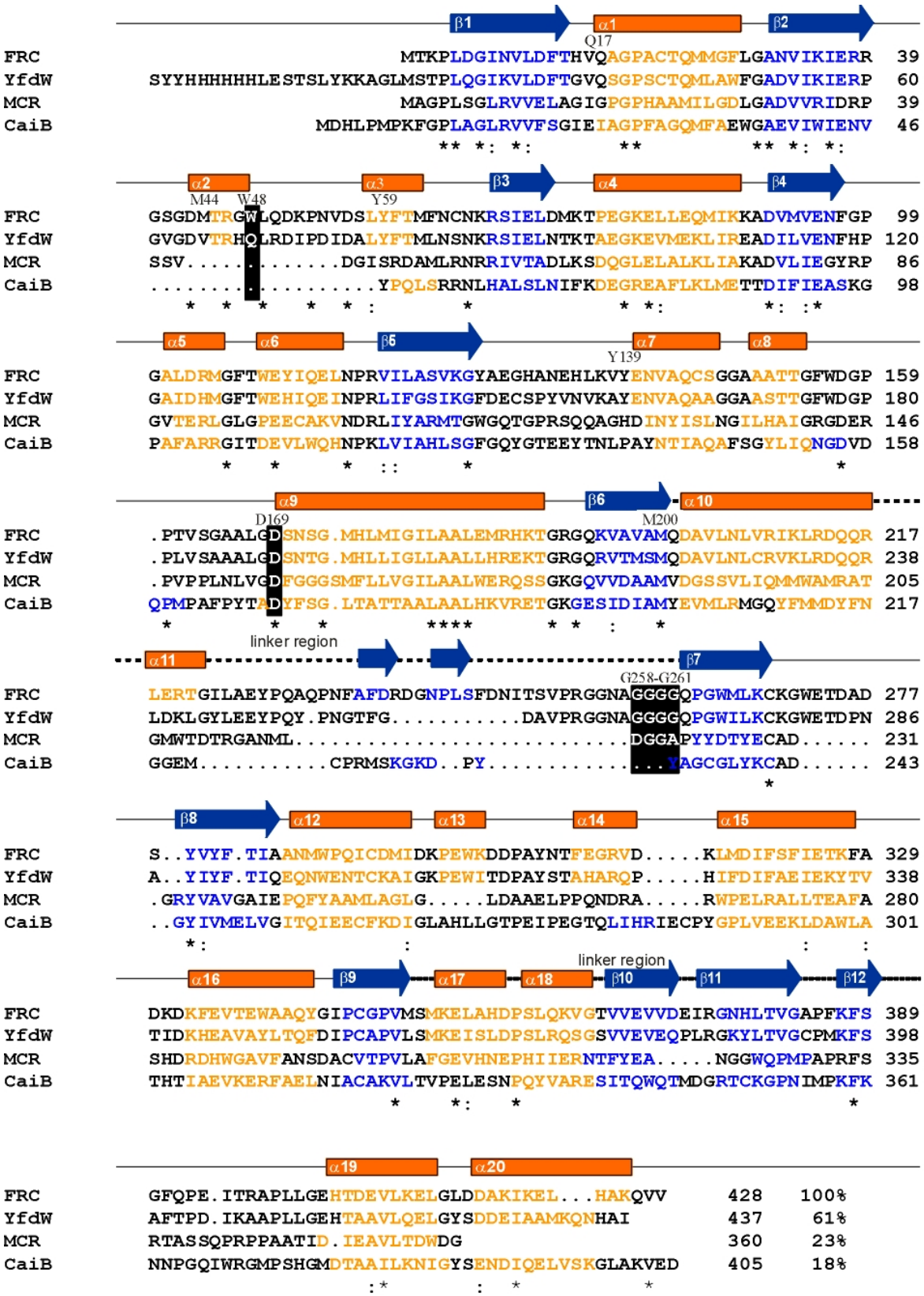
β1
α1
β2
Q17
FRC MTKPLDGINVLDFTHVQAGPACTQMMGFLGANVIKIERR 39
YfdW SYYHHHHHHLESTSLYKKAGLMSTPLQGIKVLDFTGVQSGPSCTQMLAWFGADVIKIERP 60
MCR MAGPLSGLRVVELAGIGPGPHAAMILGDLGADVVRIDRP 39
CaiB MDHLPMPKFGPLAGLRVVFSGIEIAGPFAGQMFAEWGAEVIWIENV 46
α2
α3
β3
α4
β4
M44
W48
Y59
FRC GSGDMTRGWLQDKPNVDSLYFTMFNCNKRSIELDMKTPEGKELLEQMIKKADVMVENFGP 99
YfdW GVGDVTRHQLRDIPDIDALYFTMLNSNKRSIELNTKTAEGKEVMEKLIREADILVENFHP 120
MCR SSV.....DGISRDAMLRNRRIVTADLKSDQGLELALKLIAKADVLIEGYRP 86
CaiB .....YPQLSRRNLHALSLNIFKDEGREAFLKLMETTDIFIEASKG 98
α5
α6
β5
α7
α8
Y139
FRC GALDRMGFTWEYIQELNPRVILASVKGYAEGHANEHLKVYENVAQCSGGAAATTGFWDGP 159
YfdW GAIDHMGFTWEHIQEINPRLIFGSIKGFDECSPYVNVKAYENVAQAAGGAASTTGFWDGP 180
MCR GVTERLGLGPEECAKVNDRLIYARMTGWGQTGPRSQQAGHDINYISLNGILHAIGRGDER 146
CaiB PAFARRGITDEVLWQHNPKLVIAHLSGFGQYGTEEYTNLPAYNTIAQAFSGYLIQNGDVD 158
α9
β6
α10
D169
M200
FRC .PTVSGAALGDSNSG.MHLMIGILAALEMRHKTGRGQKVAVAMQDAVLNLVRIKLRDQQR 217
YfdW .PLVSAAALGDSNTG.MHLLIGLLAALLHREKTGRGQRVTMSMQDAVLNLCRVKLRDQQR 238
MCR .PVPPLNLVGDFGGGSMFLLVGILAALWERQSSGKGQVVDAAMVDGSSVLIQMMWAMRAT 205
CaiB QPMPAFPYTADYFSG.LTATTAALAALHKVRETGKGESIDIAMYEVMLRMGQYFMMDYFN 217
linker region
α11
β7
G258-G261
FRC LERTGILAEYPQAQPNFAFDRDGNPLSFDNITSVPRGGNAGGGGQPGWMLKCKGWETDAD 277
YfdW LDKLGYLEEYPQY.PNGTFG.....DAVPRGGNAGGGGQPGWILKCKGWETDPN 286
MCR GMWTDTRGANML.....DGGAPYYDTYECAD..... 231
CaiB GGEM.....CPRMSKGKD..PY.....YAGCGLYKCAD..... 243
β8
α12
α13
α14
α15
FRC S..YVYF.TIAANMWPQICDMIDKPEWKDDPAYNTFEGRVD.....KLMDIFSFIETKFA 329
YfdW A..YIYF.TIQEQNWENTCKAIGKPEWITDPAYSTAHARQP.....HIFDIFAEIEKYTV 338
MCR .GRYVAVGAIEPQFYAAMLAGLG.....LDAAELPPQNDRA.....RWPELRALLTEAFA 280
CaiB ..GYIVMELVGITQIEECFKDIGLAHLLGTPEIPEGTQLIHRIECPYGPLVEEKLDAWLA 301
linker region
α16
β9
α17
α18
β10
β11
β12
FRC DKDKFEVTEWAAQYGIPCGPVMSMKELAHDPSLQKVGTVVEVVDEIRGNHLTVGAPFKFS 389
YfdW TIDKHEAVAYLTQFDIPCAPVLSMKEISLDPSLRQSGSVVEVEQPLRGKYLTVGCPMKFS 398
MCR SHDRDHWGAVFANSDACVTPVLAFGEVHNEPHIIERNTFYEA.....NGGWQPMPAPRFS 335
CaiB THTIAEVKERFAELNIACAKVLTVPELESNPQYVARESITQWQTMDGRTCKGPNIMPKFK 361
α19
α20
FRC GFQPE.ITRAPLLGEHTDEVLKELGLDDAKIKEL...HAKQVV 428 100%
YfdW AFTPD.IKAAPLLGEHTAAVLQELGYSDDEIAAMKQNHAI 437 61%
MCR RTASSQPRPPAATID.IEAVLTDWDG 360 23%
CaiB NNPGQIWRGMPSHGMDTAAILKNIGYSENDIQELVSKGLAKVED 405 18%

CHAPTER 2
CATALYTIC MECHANISM OF FORMYL-COA TRANSFERASE[1]

Introduction

CoA-transferases catalyze reversible transfer reactions of coenzyme A carriers from CoA-thioesters to free acids. Most members of the enzyme class are grouped into the well characterized Family I and II CoA-transferases, but recently a third class of enzymes was identified, differing in sequence and three-dimensional structure to the other CoA-transferases (102). Members of this third class are mostly from bacteria, but putative genes have been identified in Archaea and Eukarya as well. Family III enzymes are known to be involved in Stickland fermentation and the metabolism of oxalate, carnitine, toluene, and bile acid. The first Family III CoA-transferase identified was formyl-CoA transferase (FRC) from *Oxalobacter formigenes* (102).

The first Family III CoA-transferase identified was formyl-CoA transferase from *Oxalobacter formigenes* (102). Formyl-Coenzyme A transferase is the first of two enzymes involved in oxalate degradation in the gut-dwelling bacterium *O. formigenes* (1). Formyl-CoA transferase catalyzes the transfer of a CoA moiety between formyl-CoA and oxalate and thereby activates oxalate in the form of oxalyl-CoA (9, 191). Oxalyl-CoA is then decarboxylated by the second enzyme on the pathway, oxalyl-CoA decarboxylase, which regenerates formyl-CoA (10, 15). Oxalate catabolism has a central role in *O. formigenes*, where oxalate serves as vital source of energy as well as carbon (1, 51). The crystal structure of formyl-CoA transferase revealed an interesting new fold composed of two subunits linked together in an interlocked dimer like two rings of a chain (197) (Figure 2-3). This fold proved to be characteristic for the Family III

[1] Reproduced in part with permission from Journal of Biological Chemistry, Vol. 283 (10), Berthold, C. L., Toyota, C. G., Richards, N. G., and Lindqvist, Y. Pages 6519-6529. Copyright 2008 Journal of Biological Chemistry

family as the crystal structures of the formyl-CoA transferase ortholog in *Escherichia coli* coded by the *yfdW* gene (97) and the close homolog (-butyrobetaine-CoA:carnitine CoA transferase (196, 235) were determined. The Family I CoA-transferases, including mostly enzymes involved in fatty acid metabolism, have a well established mechanism described in Figure 2-1 (*Mechanism 1*). The formation of covalent intermediates involving a glutamate residue of the enzyme results in a classical ping-pong mechanism with exchanging substrate product glutamyl-acyl anhydrides and γ-glutamyl-CoA thioesters (217, 229). The γ-glutamyl- CoA thioester was

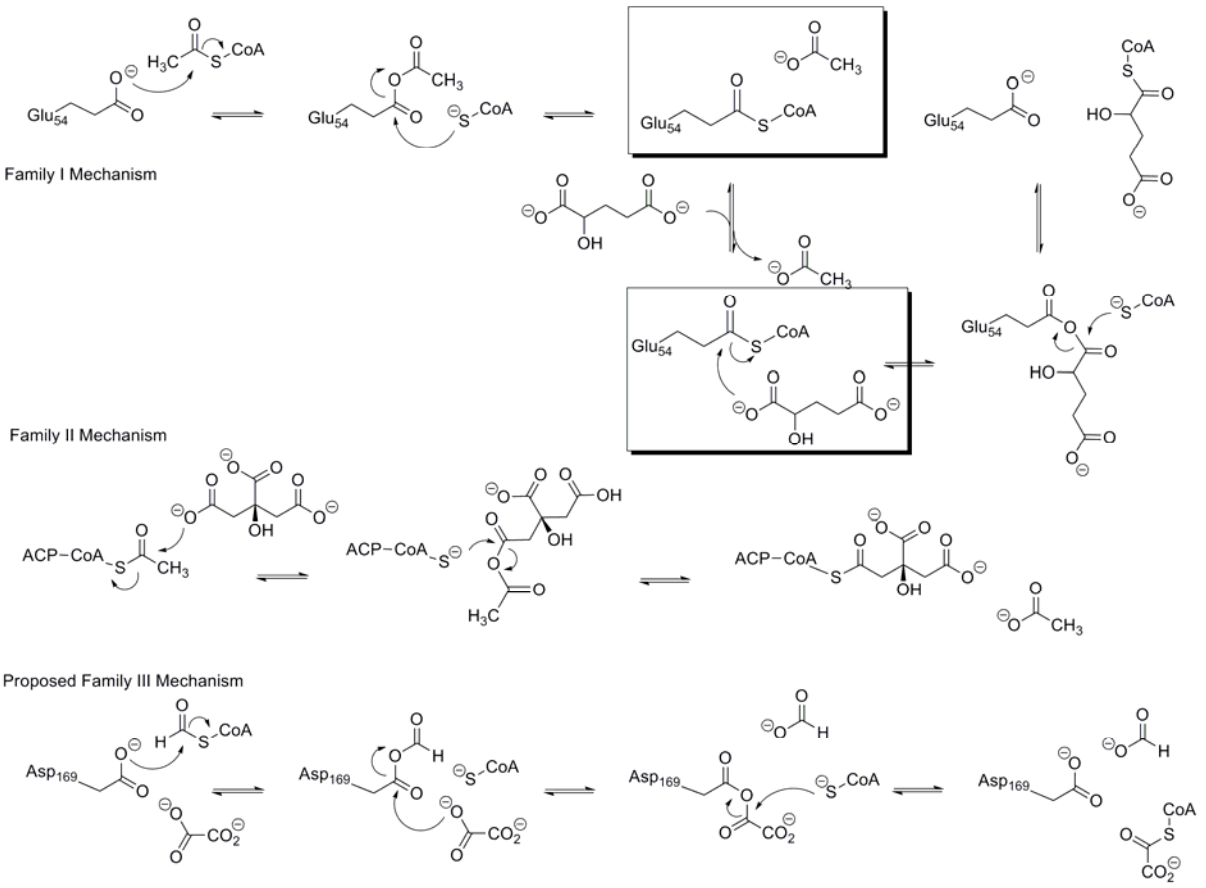

Figure. 2-1. Summary of kinetic mechanisms for the three known CoA transferase Families. Mechanism 1 is the ping-pong scheme shown for GCT. The enzyme-CoA covalent intermediate is highlighted. Mechanism 2 is the transferase reaction with acetyl-CoA and citrate in citrate lyase. Mechanism 3 is the 2004 proposed kinetic mechanism for Family III CoA transferases from (124). Putative tetrahedral intermediates have been omitted to save space.

first identified in a Family I transferase in 1968 by electrophoresis and chromatography studies with isotope-labeled borohydride (229) and was recently trapped in a crystallographic study, giving the first structural proof of its existence (196). The smaller group of Family II CoA-transferases catalyzes a partial reaction in the citrate and citramalate lyase complexes. These reactions do not include covalent enzyme intermediates, and the transfer of a dephospho-CoA, which is covalently bound to an acyl carrier protein (ACP) in the enzyme complex, is carried out through a ternary complex where a mixed anhydride is formed between the two acids during the transition state (Figure 2-1, *Mechanism 3*) (33, 63).

During initial studies of the Family III CoA-transferases, steady state kinetics showed that the reaction is not consistent with a ping-pong mechanism as in the Family I CoA-transferases. The mechanism was instead interpreted to proceed through a ternary complex, where both formyl-CoA and oxalate need to be bound to the enzyme before catalysis (60, 124, 149). The crystal structure of an aspartyl-oxalyl mixed anhydride led to the suggestion that the reaction was initiated in the ternary complex with both substrates by the formation of an aspartyl-formyl anhydride and CoA-S^-. The CoA-S^- was then kept bound in the active site as a spectator while oxalate replaced formate, before attacking the aspartyl-oxalyl anhydride yielding oxalyl-CoA (124). A freeze-trapped crystal structure reveals that the enzyme-β-aspartyl-CoA thioester intermediate is also formed during catalysis by formyl-CoA transferase, a finding leading to reassessment of the catalytic mechanism of Family III CoA-transferases. The mechanistic investigation is complemented with the crystal structure of a trapped aspartylformyl anhydride similar to the previously characterized aspartyloxalyl anhydride complex (124) and two mutant protein structures, where one contains the complex with β-aspartyl-CoA and oxalate. Central to the catalyzed reaction is a glycine-rich loop that adopts two different conformations controlling

the accessibility of the active site. Mutations in the loop seriously affect the activity, proving its importance during catalysis. A modified mechanism in concordance with all information obtained is proposed, where catalysis includes formation of both the aspartyl-formyl and -oxalyl anhydrides and the β-aspartyl-CoA thioester and where the carboxylate product remains bound to the enzyme until release of the acceptor thioester.

Results

Wild-Type FRC Activity

By first determining the inhibitory effects of free CoA (Table 2-5), a ubiquitous contaminant resulting from the hydrolysis of formyl-CoA, the kinetic parameters for FRC and mutant variants were improved (see Figure 2-2). The values obtained for FRC by this method were similar to previously reported values (124). Fortuitiously, the inhibition constant for CoA (K_{iCoA}) was 16.7 ± 0.7 μM and high enough that there was little effect on the original kinetic analysis.

Enzyme-β-Aspartyl-CoA Thioester Complexes

Crystals, produced with a precipitant mixture of polyethylene glycol and magnesium chloride, were soaked with formyl-CoA for 1, 5, and 10 min respectively and with oxalyl-CoA for 2, 4, and 10 min, respectively. Inspection of the crystal structures from different soaking times revealed that all formyl-CoA soaked crystals contained the same intermediate and all oxalyl-CoA soaked crystals contained the same intermediate, with no difference over time. The best data set of each, formyl-CoA soaked for 2 min and oxalyl-CoA soaked for 5 min, were used for further analysis.

Close inspection of the freeze-trapped formyl-CoA and oxalyl-CoA intermediates, show that the formyl- as well as the oxalyl moieties are cleaved off by the enzyme, and a covalent bond is formed between the carboxyl group of Asp-169 and the thiol-group of the CoA carrier.

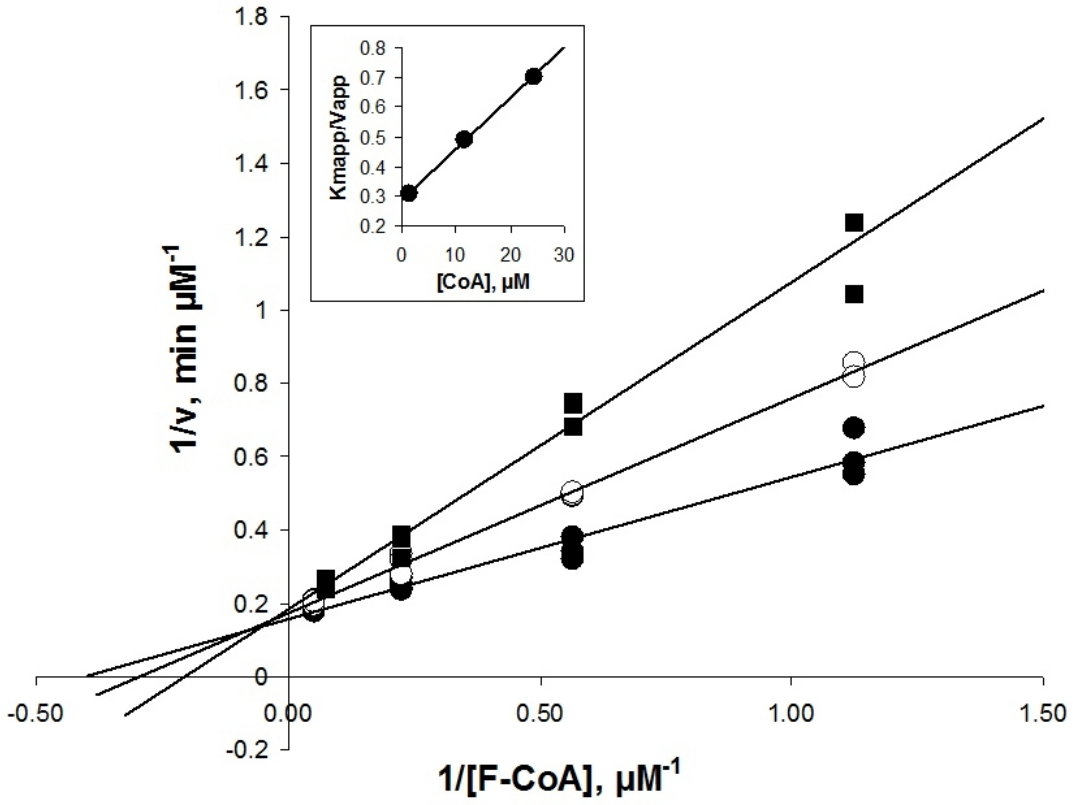

Figure. 2-2. Double-reciprocal plot for the inhibition of FRC by free CoA against varied [formyl-CoA] at constant saturating [oxalate] = 77 mM showing lines fitted to the data by linear-regression methods. CoA concentrations were 1.5 µM (●), 11.5 µM (○), and 24.3 µM (■). $K_{i(CoA)}$ of 16 .7 ± 0.7 µM was determined from the replot of K_{Mapp}/V_{app} vs. [CoA] (*insert*).

The resulting intermediates from the formyl-CoA and oxalyl-CoA soaks are thus highly similar and the dimeric structures superimpose with an r.m.s. deviation of 0.3 Å over 851 Cα atoms. An intriguing feature is that in both complexes, the two subunits of the dimer adopt different active site conformations with the pantetheine arm of the CoA molecule bound in different orientations (Figures 2-4 and 2-6). Several residues show different conformations in the two subunits of the dimer. Tyr-139 is centrally positioned in the active site and moves with the side chain hydroxyl group shifted approximately 3 Å, allowing the two different orientations of the pantetheine moiety. Lys-137 is positioned on the same side of the CoA molecule and shows a shift of 4.5 Å

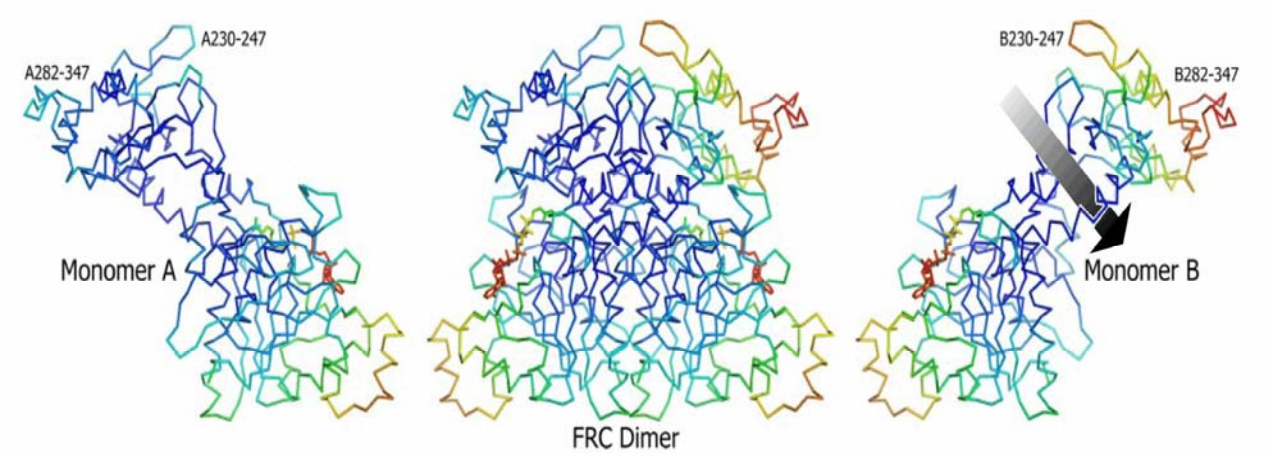

Figure. 2-3. Two formyl-CoA transferase monomers displayed separately and in the dimer. The figure displays the structure of the β-aspartyl-CoA thioester derived from oxalyl-CoA. The Cα trace and CoA molecules (shown as *stick models*) are coloured by B-factor, with *blue* representing the lowest B-factor and *red* the highest. The arrow indicates the central hole in Monomer B. Modified from Berthold 2008 (18).

at the side chain amino group. Residues Arg-38 and His-15 also adopt different side chain conformations in order to adapt to the two CoA conformations. Finally, Gln-17 takes on two different rotamer conformations, with a position behind Asp-169 in subunit A and above the thioester bond in subunit B. As was observed already for the apo-enzyme the side chain conformation of Trp-48 is flipped 90° between the two monomers and the glycine loop (^{258}GGGGQ^{261}) then assumes the open and closed conformations in subunits A and B, respectively (Figure 2-4).

Neither formate nor oxalate was detected in the active site. Interestingly, subunit A contains density interpreted as one chloride ion bound behind the active site residue Asp-169, at a position occupied by residue Gln-17 in the other subunit, and subunit B has density interpreted as two chloride ions bound, one on each side of the pantetheine arm of CoA, where one chloride ion is interacting with the closed glycine loop and the other with the main chain amides of Gln-17 and Ala-18 (Figure 2-4).

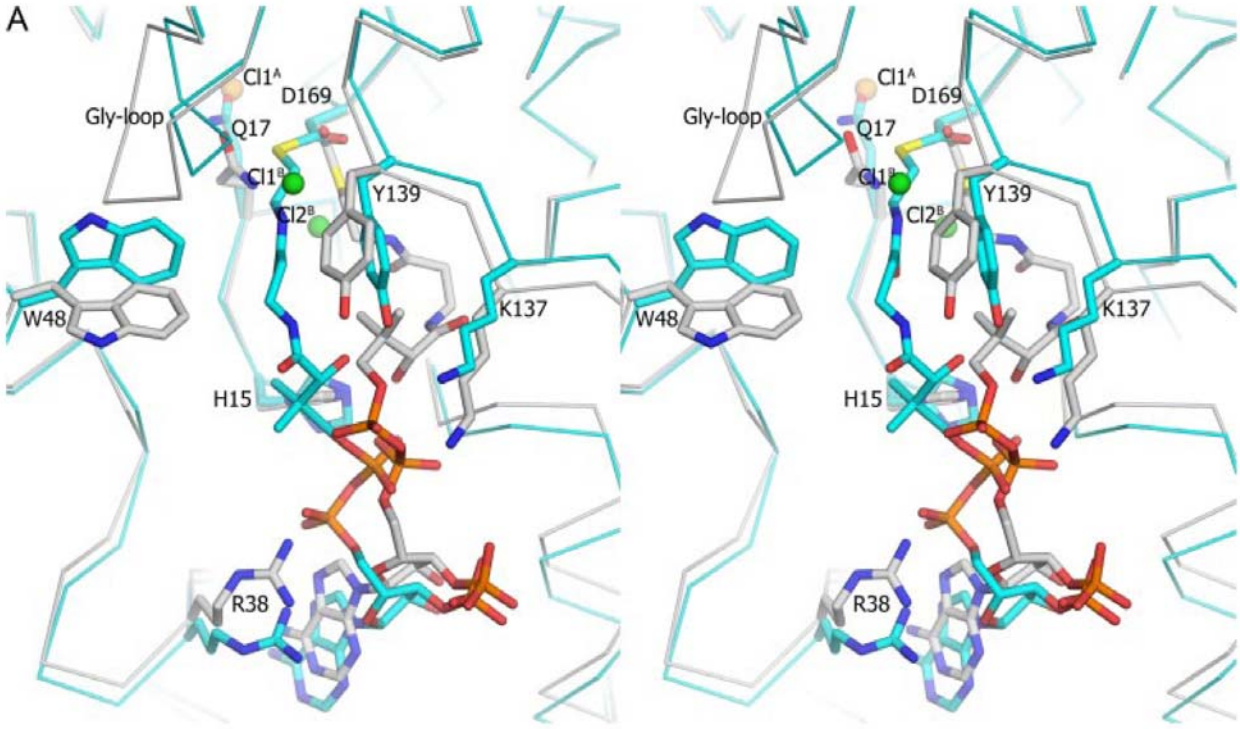

Figure. 2-4. Stereoview of the overlay of the two active site conformations of the β-aspartyl-CoA thioester complex. The "resting" conformation A, shown in *grey* with one bound chloride ion in *orange*, was observed in subunit A with an open glycine loop. The other "activated "conformation in *cyan* shows two bound chloride ions (*green*) and subunit B with a closed glycine loop. Note the two rotamer conformations of Q17. Taken from Berthold 2008 (18).

In both complexes Val-16 is positioned in the disallowed or generously allowed part of the Ramachandran plot in both monomers which was also observed in the complex of FRC with bound CoA reported earlier (197). Inspection of the structures reveals that Val-16 has a strained conformation in order to fit the CoA moiety. In the β-aspartyl-CoA thioester complex, Glu-140 is in the disfavored part of the Ramachandran plot in subunit B, which can be explained by the structure adopted by the adjacent residue Tyr-139, enforced by the different conformation of the CoA-moiety in that subunit. The B-factors show a clear difference in the region of the small domain comprising the two loops 230-247 and 282-347 between the two subunits (Figure 2-3).

Table 2-1. Data collection and refinement statistics. Values in parentheses represent the highest resolution shell.

Data Collection	β-aspartyl-CoA thioester from formyl-CoA	β-aspartyl-CoA thioester from oxalyl-CoA	Aspartyl-formyl anhydride	Q17A-β-aspartyl-CoA thioester and oxalate	G260A FRC
Beamline	ID14 eh1	ID14 eh1	I911-2	I911-2	ID23 eh2
Space group	I4	I4	I4	I4	$P4_32_12$
Unit cell a,b,c (Å)	151.8, 151.8, 100.1	151.9, 151.9, 99.5	151.7, 151.7, 98.9	153.6, 153.6, 98.1	97.3, 97.3, 193.4
Resolution (Å)	2.0 (2.11-2.0)	2.0 (2.11-2.0)	1.87 (1.97-1.87)	2.2 (2.32-2.2)	2.0 (2.11-2.0)
R_{sym}	0.11 (0.39)	0.11 (0.30)	0.067 (0.36)	0.12 (0.57)	0.15 (0.50)
Mn(I/σ(I))	8.7 (1.8)	10.1 (2.4)	15.9 (4.2)	9.3 (1.9)	7.2 (2.5)
Completeness (%)	98.3 (94.3)	99.2 (97.2)	97.1 (81.1)	99.5 (100)	99.6 (99.9)
Wilson B-factor	28	25	23	34	14
Refinement					
Resolution (Å)	30-2.0	30.0-2.0	30-1.87	30-2.2	30-2.0
Reflections in working set	71459	74942	85088	54545	59799
Reflections in test set	3765	3910	4473	2894	3206
R-factor / R-free (%)	19.7 / 24.1	17.3 / 21.4	17.2 / 20.3	20.7 /24.8	16.9 / 21.5
Atoms modeled	7565	7565	7509	7197	7566
No. of amino acids / B-factor ($Å^2$)	854 / 35.4*	854 / 29.7*	854 / 25.1*	854 / 33.0	854 / 12.5
Number of ligands / B-factor ($Å^2$)	2 / 47.3**	2 / 42.4**	4 / 30.5**	3 / 41.3	0 / -
Number of waters / B-factor ($Å^2$)	693 / 38.2	788 / 35.5	737 / 31.6	430 / 29.2	873 / 21.8
RMS Deviations from ideals					
Bonds (Å)	0.007	0.008	0.008	0.008	0.009
Angles (°)	1.08	1.12	1.06	1.15	1.16
Ramachandran zone distribution (%)	92.1, 7.5, 0.1, 0.3	92.5, 7.2, 0.1, 0.1	91.8, 7.9, 0.3, 0	92.1, 7.6, 0.3, 0	92.0, 7.6, 0.3, 0.1
PDB Accession code	2vjl	2vjk	2vjm	2vjo	2vjn

(includes amino acid part of residue 169) ** (includes CoA/formyl part of covalent complex at residue 169)

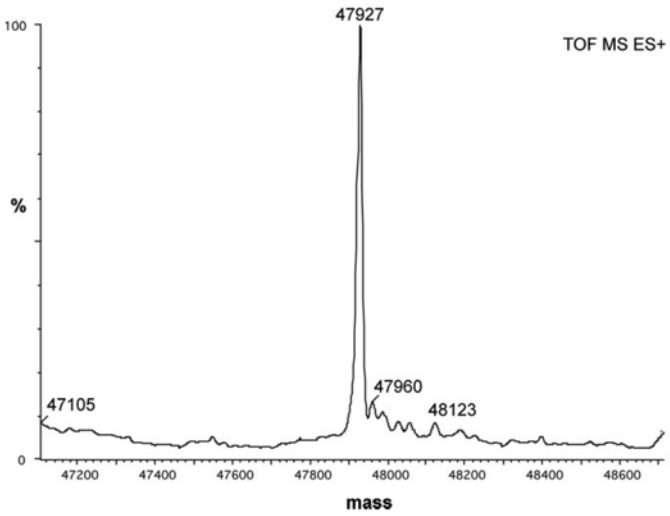

Figure. 2-5. Mass spectrum of formyl-CoA transferase incubated with formyl-CoA. The main peak of 47,927 Da corresponds with the covalent aspartyl-CoA thioester intermediate. No peak is observed at the molecular mass of the monomer (47,196 Da). Taken from Berthold 2008 (18).

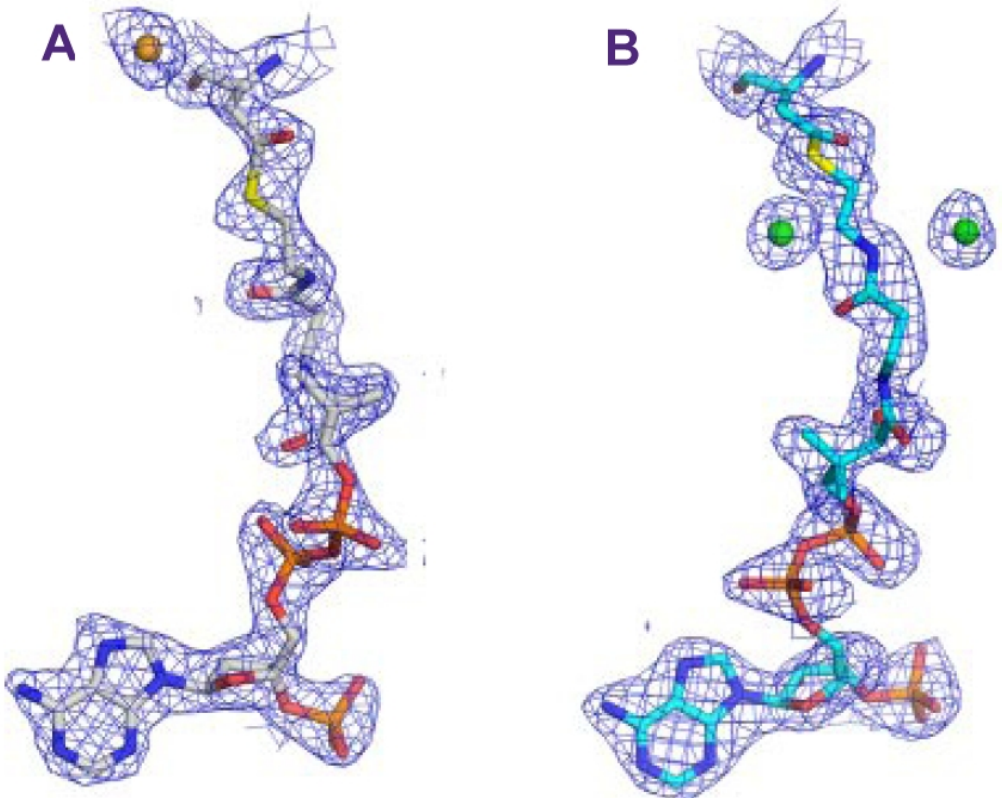

Figure. 2-6. Electron density maps of β-aspartyl-CoA thioester and chloride ions. Annealed composite omit $2F_o$-F_c electron density maps are contoured at 1σ around the β-aspartyl-CoA thioester and chloride ions. Subunits are labeled A and B. Figure courtesy of Catrine Berthold. Taken from Berthold 2008 (18).

In subunit B this region is much more flexible, and in the β-aspartyl-CoA thioester complex obtained from formyl-CoA, residues 286-316 have no interpretable electron density and are modeled with zero occupancy. Inspection of the crystal packing reveals that the corresponding region of subunit A forms crystal contacts with the adjacent molecule while this region in subunit B is freely exposed to solvent.

Inhibition of FRC by Chloride Ions and Glyoxalate

The identification of chloride ions bound in the active sites was followed up by kinetic measurements showing that chloride has an inhibitory effect on the transferase activity in FRC. Chloride is a weak competitive inhibitor against oxalate with K_{ic} of 3 ± 2 mM (Figure 2-7). Glycolate may act as an oxalate analogue and be a good tool for ascertaining the oxalate binding

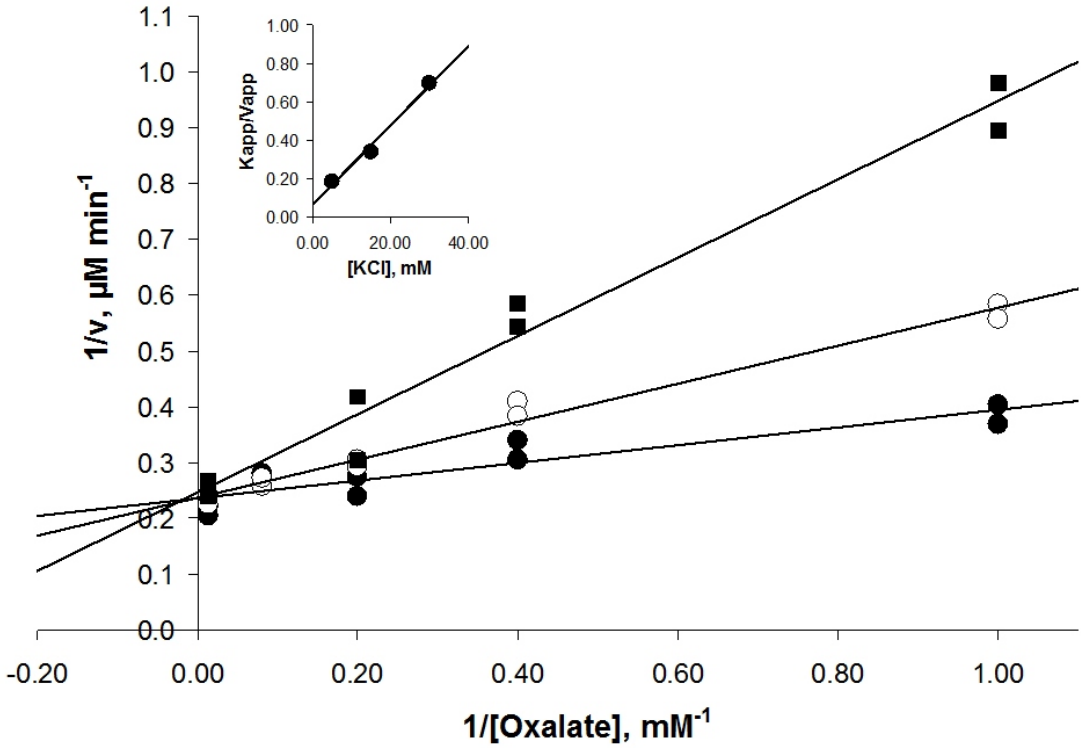

Figure. 2-7. Double-reciprocal plot of competitive Cl^- inhibition of FRC against varied [oxalate] (1.0 – 77.0 mM) at 21.4 µM [formyl-CoA] and 10 µM [CoA] with 8.8 nM enzyme. KCl concentrations were 5 mM (●), 15 mM (○), and 30 mM (■). K_{ic} = 3 ± 2 mM was determined from the replot of K_{Mapp}/V_{app} vs. [KCl] (*insert*). Taken from Berthold 2008 (18).

site in FRC. Thus, the effect of glycolate on FRC activity was determined. Glycolate is also a competitive inhibitor against oxalate with K_{ic} = 6 ± 6 mM.

Hydroxylamine and Sodium Borohydride Trapping

Family I CoA-transferases are inactivated by hydroxylamine and sodium borohydride in the presence of donor CoA-thioesters (217, 229). In the Family I enzymes treatment with hydroxylamine gives formation of a hydroxamate at the glutamate bound in the γ-glutamyl-CoA thioester while sodium borohydride reduces glutamyl-CoA to the corresponding alcohol. The effect of both these inhibitors on FRC preincubated with formyl-CoA at different concentrations were tested. Previous experiments on Family III transferases have yielded ambiguous results.

Table 2-2. Formyl-CoA dependence of inactivation of FRC (0.52 μM) by hydroxylamine trapping under turnover conditions with saturating oxalate (77 mM) and varied concentration of formyl-CoA.

[Formyl-CoA] (μM)	Residual Activity (%)	Residual Activity (U/mg)
0.0	100 ± 7	7.4 ± 0.5
5.5	81 ± 2	6.0 ± 0.1
10.0	75 ± 6	5.6 ± 0.3
38.0	33 ± 3	2.4 ± 0.1
77.0	12 ± 18	0.9 ± 0.2

Table 2-3. Formyl-CoA dependence of inactivation of FRC (0.26 μM) by hydroxylamine and borohydride trapping in the absence of oxalate.

[Formyl-CoA] (μM)	Hydroxylamine Residual Activity (%)	Sodium Borohydride Residual Activity (%)
0.0	100 ± 3	100 ± 5
0.1	71 ± 7	
0.2		93 ± 2
0.3	32 ± 2	
1.1	19 ± 1	
2.4	12 ± 0.2	
5.0	13 ± 1.4	
24.0	14.8 ± 0.3	
188.0	15 ± 7	
262.0		1 ± 0.1

The (*E*)-cinnamoyl-CoA:(*R*)-phenyllactate CoA transferase from *Clostridium sporogenes* was not inactivated by hydroxylamine and retained 50% activity when treated with $NaBH_4$ (60). Activity of succinyl-CoA:(*R*)-benzylsuccinate CoA transferase from *Thauera aromatica* was also unaffected by hydroxylamine but could be reduced to 3.5% in the presence of benzylsuccinyl-CoA and 10 mM $NaBH_4$ (149). The effect of both of these inhibitors on formyl-CoA transferase preincubated with formyl-CoA at different concentrations was examined.

FRC incubated with oxalate and formyl-CoA was subsequently treated with hydroxylamine. As any activated acyl groups are expected to be trapped as hydroxylamine adducts, oxalyl- and formyl-acyl as well as acyl-thioester intermediates in the transferase reaction should be trapped. The enzyme showed a reduced activity after removing all small molecules (i.e. excess CoA and hydroxylamine) by gel filtration. Table 2-2 shows that the addition of 77 μM formyl-CoA followed by hydroxylamine reduces the activity about 88%. The same experiment performed without addition of oxalate also displayed a trapping effect by hydroxylamine (Table 2-3). A clear dependence on formyl-CoA concentration was discovered for the inactivation of FRC by hydroxylamine.

Trapping experiments with sodium borohydride to reduce possible thioester intermediates in FRC also led to reduced activity (Table 2-3). The resulting alcohol from the borohydride reduction has not been identified.

Comparison with Previous FRC Complexes

Previously determined structures of wild type FRC include the apoenzyme structure (pdb code: 1p5h) , an inhibitory complex with CoA bound in the active site (pdb code: 1p5r) and a structure where co-crystallization with oxalyl-CoA resulted in a crystal structure where CoA is bound in both subunits, but where one subunit also contains the aspartyl-oxalyl mixed anhydride (pdb code: 1t4c) . Superimposition of these three existing structures with the β-aspartyl-CoA

thioester intermediate structures results in r.m.s. deviations of 0.4-0.5 Å over 854 Cα atoms for the dimer. The differences between the structures are mainly found in the flexible segments of the small domain in subunit B (residue 230-247 and 282-347) and among the active site residues that shift orientations in the two active sites. The orientation of the CoA moiety observed in subunit B of the β-aspartyl-CoA thioester complex (Figure 2-4 and 2-6B) has not been observed before and most probably represents a new state in the catalytic cycle. This conformation will be referred to as the "activated" conformation of CoA while the conformation in subunit A is described as the "resting" conformation.

Aspartyl-Formyl Anhydride Complex

A structure of FRC containing the aspartyl-formyl anhydride complex was obtained in the absence of chloride ions and oxalate upon flash-freezing a crystal 10 min after addition of formyl-CoA. At a resolution of 1.87 Å, subunit A of the dimer was interpreted to contain the covalent β-aspartyl-CoA thioester and subunit B the β-aspartyl-formyl anhydride and free CoA (Figure 8B). The formyl group of the aspartyl-formyl anhydride was modeled at occupancy 0.6 to best fit the observed electron density. In the subunit containing the trapped mixed anhydride, the active site is nicely shielded by the glycine loop which adopts the closed conformation. The other subunit has an open glycine loop and noise in the electron density map indicates flexibility/disorder in the active site, especially in the region of the glycine loop and Tyr-139. The CoA moieties are found in the resting conformation in both subunits. Superposition of the aspartyl-formyl anhydride and aspartyl-oxalyl anhydride (pdb code: 1t4c) complex structures results in an r.m.s. deviation of 0.4 Å over 427 Cα atoms of the monomer (Figure 8A). The structures show very small changes in the enzyme core and the active sites are highly similar, while the flexible solvent exposed areas display some differences.

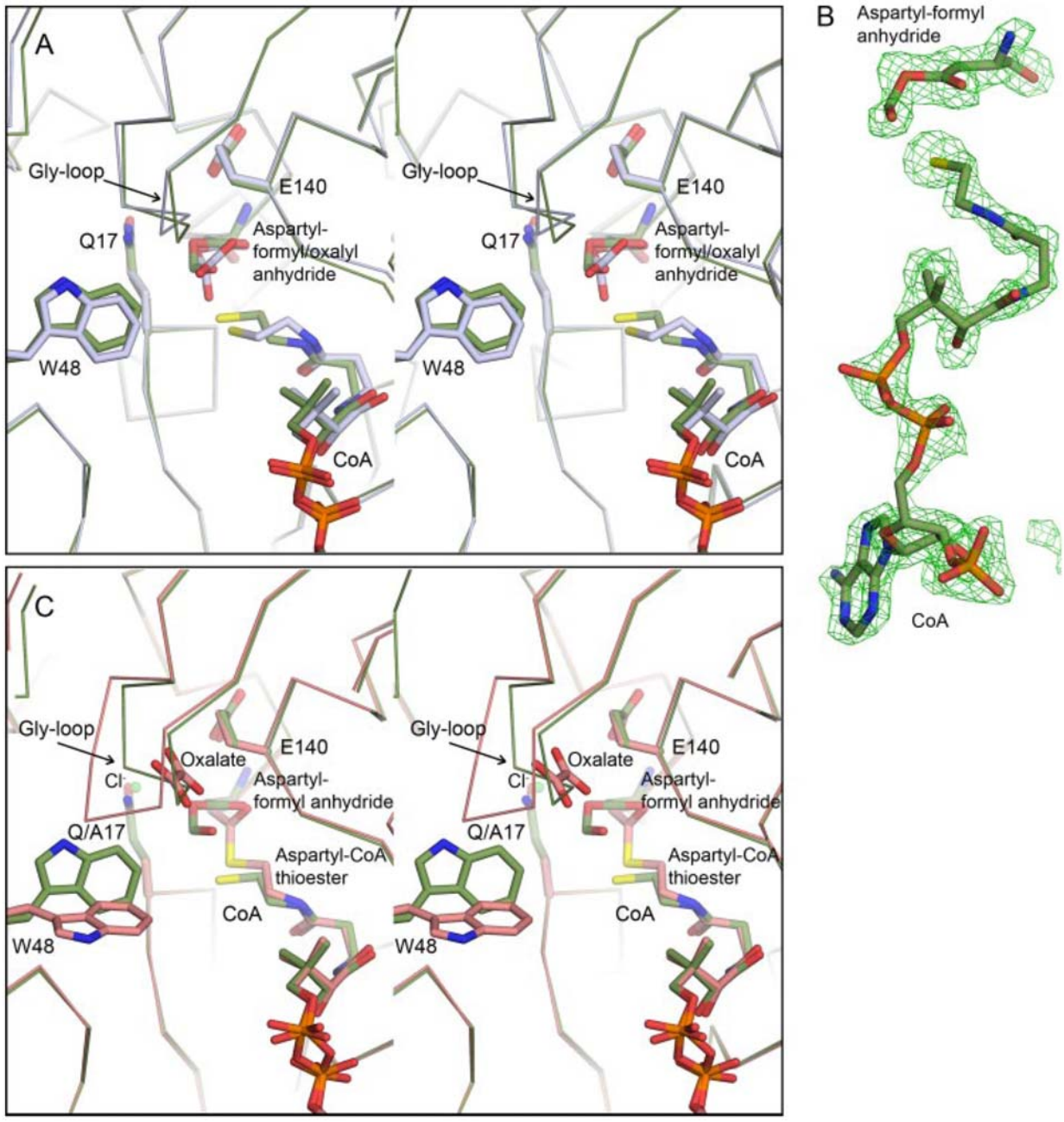

Figure. 2-8. Steroview overlay of FRC aspartyl-formyl and aspartyl-oxalyl anhydride active sites. *A*, the aspartyl-formyl active site is shown in *green* and the aspartyl-oxalyl is shown in *light blue*. The glycine loop is in the closed conformation in both structures. The Cα trace of the enzyme is displayed. *B*, F_o-F_c electron density map contoured at 3σ, calculated with the aspartyl-formyl anhydride and CoA molecule omitted from the structure. *C,* stereoview overlay of the aspartyl-formyl anhydride active site (*green*) and the Q17A formyl-CoA transferase mutant enzyme active site with the aspartyl-CoA thioester and oxalate bound to the open glycine loop (*pink*). Taken from Berthold 2008 (18).

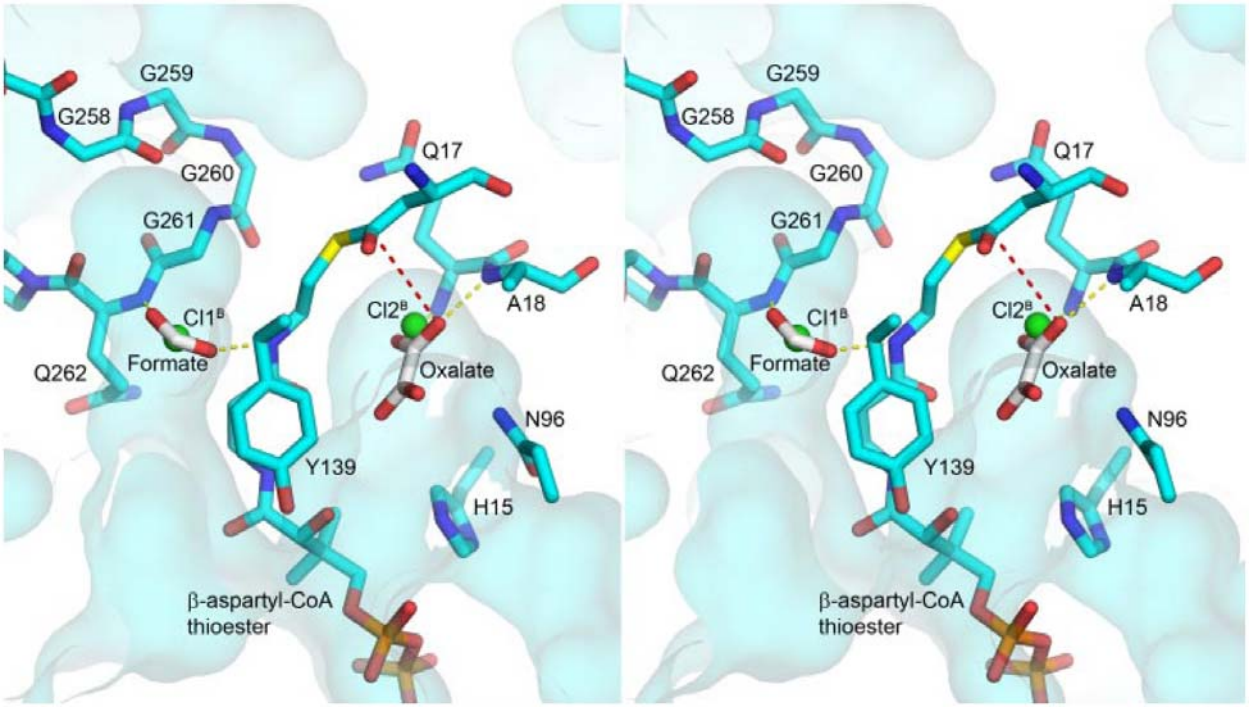

Figure. 2-9. Stereoview of oxalate and formate modeled into the FRC active site. Oxalate and formate are modeled into the anion binding sites occupied by chloride ions in subunit B of the β-aspartyl-CoA thioester complex. Pockets are calculated with a probe radius of 1.4 Å and are displayed in a surface representation. Both of the pockets have a connecting channel to the surface. The glycine loop in the closed conformation protects the thioester from an attack from above. Hydrogen bonds are indicated by *dashed yellow lines* and the *red dashed line* shows where nucleophilic attack will take place. Taken from Berthold 2008 (18).

Q17A FRC Mutant and Oxalate Binding

The active site residue Gln-17, positioned in the close proximity of Asp-169, has two distinct rotamer conformations corresponding to the two different active site conformations in the β-aspartyl-CoA thioester complexes (Figure 2-4). Replacement of this residue by an alanine results in severely impaired activity, with a 45-fold reduced k_{cat} (Table 2-4). A crystal structure of the Q17A mutant was solved to 2.2 Å resolution from a crystal incubated with formyl-CoA and oxalate. The enzyme variant still could bind formyl-CoA and the reaction proceeded until formation of the β-aspartyl-CoA thioester, which was observed in the resting conformation in both active sites of the dimer. Interestingly, the glycine loop displayed the open

conformation in both subunits and an oxalate molecule was bound to the loop in subunit B (Figure 2-8C). Oxalate is hydrogen bonded with one of its carboxyl groups to the main chain nitrogens of Gly-260 and Gln-262 in the loop while the other carboxyl group points towards the active site and mainly interacts with water molecules. The distance between the closest oxygen of oxalate and Cγ of Asp-169 is 5.3Å in this conformation and the orientation is not favorable for a nucleophilic attack by oxalate. Behind Asp-169, where the Gln-17 side chain normally is positioned when the glycine loop takes the closed conformation, a strong spherical electron density is present. A chloride ion, like in the β-aspartyl-CoA thioester complex structures, could be refined into this position forming a strong interaction with Ser-170. The crystallization

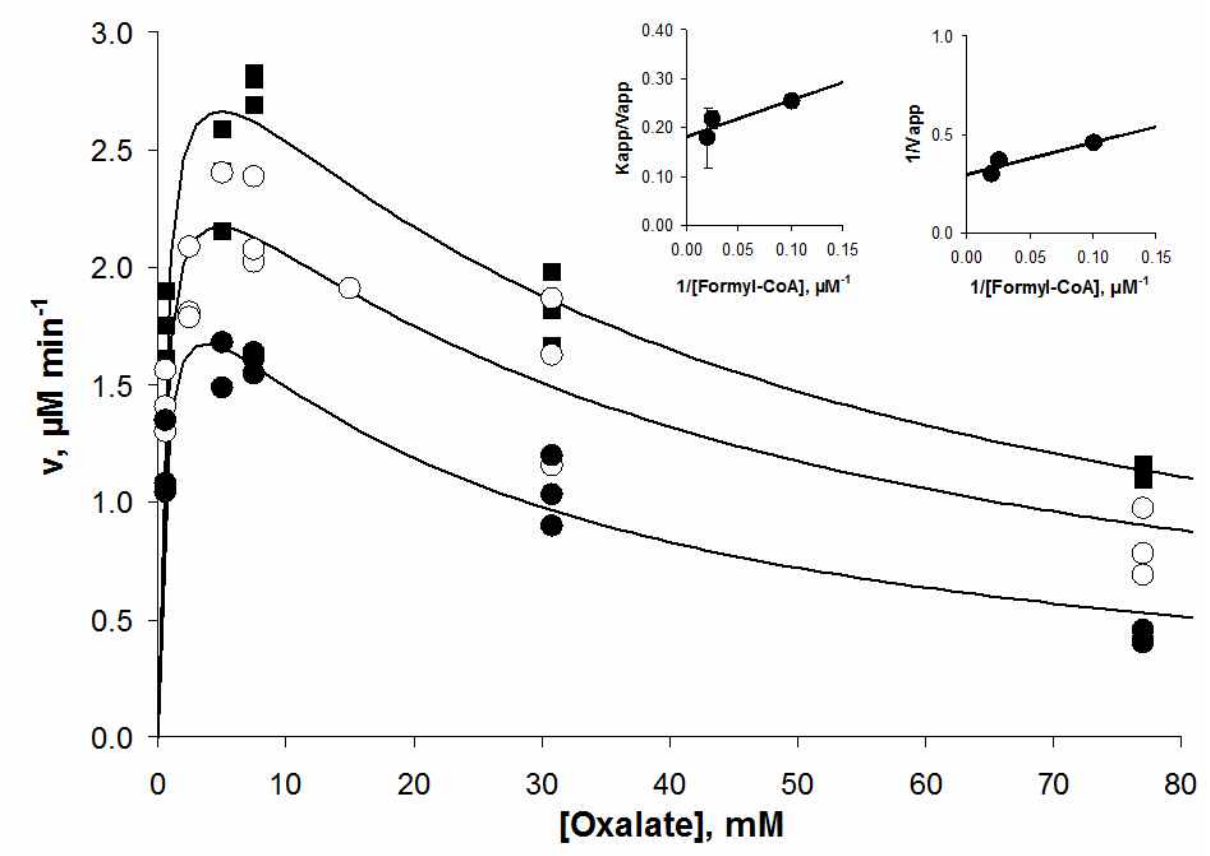

Figure. 2-10. Initial velocity plot of initial velocities of G261A variant against varied [oxalate] (0.063 – 77.0 mM) at 9.9 (●), 39.2 (○), and 78.4 μM [formyl-CoA] with 45.3 nM enzyme. Data were fitted with the Michaelis-Menten equation modified for substrate inhibition (Equation 2).

conditions or protein buffer for this complex contained no chloride ions and it is likely that the ion was bound during expression or purification of the mutant and remained due to the lack of a glutamine side chain occupying the site.

G259A, G260A, and G261A FRC Loop Mutants

Three FRC variants, where Gly-259, Gly-260, and Gly-261 were mutated into alanine residues, were prepared to investigate the importance of the glycine loop. The mutations were expected to impact the loop movement, because the peptide geometries of the Gly-259 and Gly-260 residues are positioned in the disallowed region of the Ramachandran plot for alanine. As

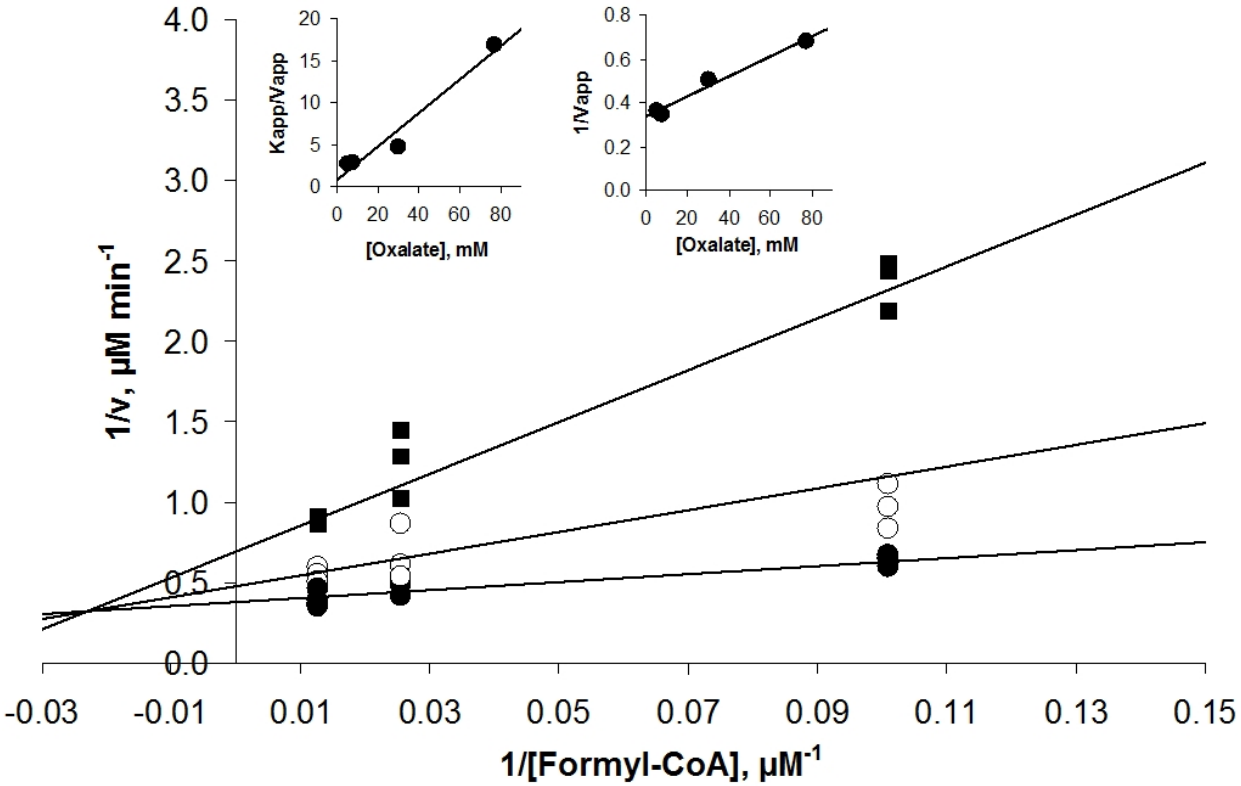

Figure. 2-11. Substrate inhibition of the G261A variant by oxalate against varied formyl-CoA. Initial velocity plot of initial velocities against varied [formyl-CoA] (9.9 mM – 78.4 µM) at 7.5 (●), 30.5 (○), and 77.0 mM [oxalate] with 45.3 nM enzyme. Data were fitted to the Lineweaver-Burk equation. Apparent inhibition constants for substrate inhibition by oxalate, K_{ic} = 4 mM and K_{iu} = 73 mM, were determined from the replots of slopes and intercepts.

expected the mutated enzyme is impaired. For the G260A mutant, the K_M value for oxalate increases almost 5 times and k_{cat}/K_M is 75 times reduced (Table 2-4). The 2.0 Å resolution crystal structure of the G260A mutant, showed clear strain in the loop, which could not adopt the same conformation as in the wild type enzyme in the closed form (Figure 2-12). The mutation containing loops were modeled in the most probable conformation based on the electron density in an omit map, although difference density around the loops shows them to be partly disordered.

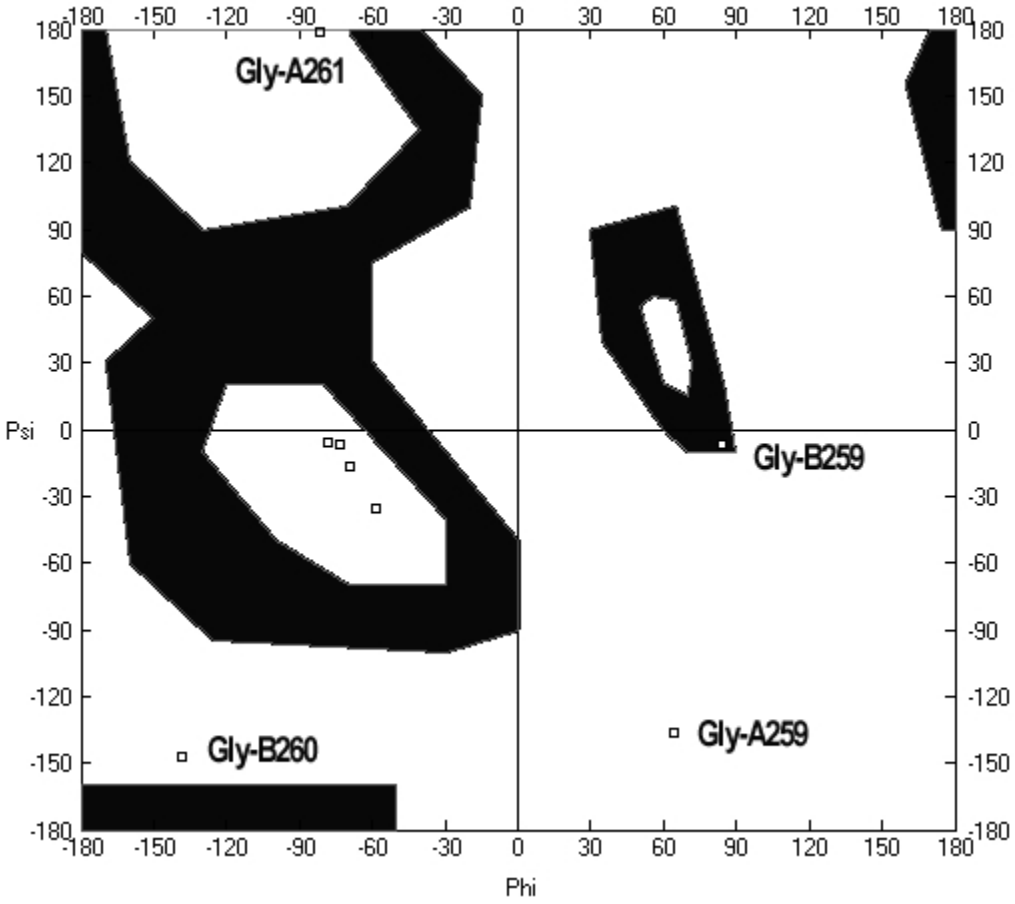

Figure. 2-12. Ramachandran plot showing loop glycine residues (^{258}GGGG^{261}). Plot generated in Swiss-PDB Viewer V3.7 from the apo-enzyme structure (1p5r). Chain A is in the closed conformation and chain B is in the open conformation. The *black* regions represent the generously allowed regions.

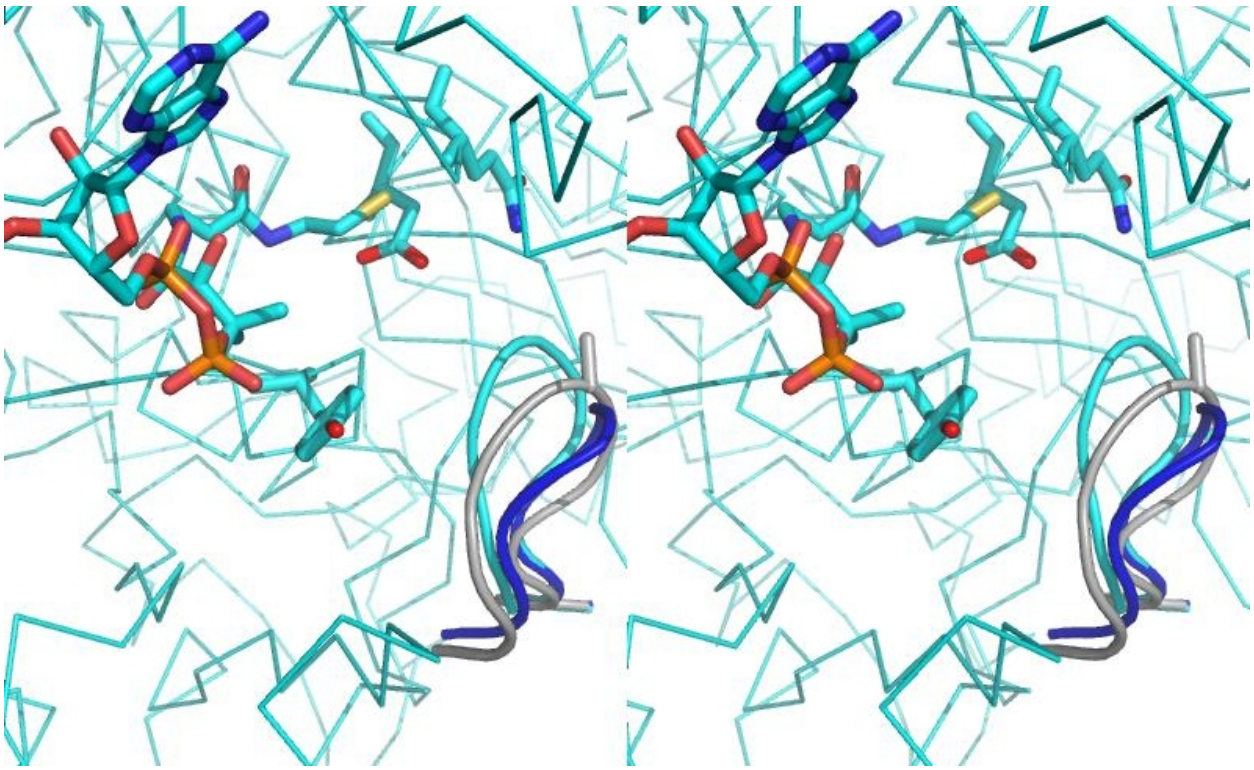

Figure. 2-13. Stereoview of G260A tetraglycine loop. The open, *blue*, and closed, *cyan*, loops of FRC are shown as ribbons. The *grey* loop in the G260A variant is unable to fully close.

The specificity constant for G261A variant was reduced nearly 50 times relative to wild-type FRC, primarily due to an order of magnitude increase in K_M for formyl-CoA (26.6 μM). In contrast to the other loop mutants, k_{cat}/K_M for oxalate increases slightly for the G261A variant and oxalate was a mixed-type substrate inhibitor of G261A with an apparent K_{ic} of 4 mM and K_{iu} of 73 mM (see Figures 2-10 and 2-11). Assuming that there is only one oxalate binding site (per monomer) in G261A, there are two plausible explanations for this behaviour: the role of the glycine loop is primarily that of protecting the active site or it is implicated in half-sites regulation of the second site. If the ability of the tetraglycine loop is disrupted, oxalate may be allowed to bind first and exclude formyl-CoA from the active site. If the G261A variant exhibits half-sites reactivity and the loop is critical to that reactivity, i.e. loop A closes down on the active

site allowing loop B to open, then disruption may allow oxalate to again bind out of turn in the second site. The competitive and uncompetitive components of CoA inhibition, 2 μM and 41 μM, respectively, are the lowest seen for any FRC variant and these results also support the critical nature of the loop.

Table 2-4. Summary of kinetic constants for wild-type FRC and mutants

	k_{cat} (s^{-1})	$K_{M(F\text{-}CoA)}$ (μM)	$k_{cat}/K_{M(F\text{-}CoA)}$ ($s^{-1}M^{-1}$)	$K_{M(oxalate)}$ (mM)	$k_{cat}/K_{M(oxalate)}$ ($s^{-1}M^{-1}$)
FRC	5.3 ± 0.1	2.0 ± 0.3	$2.7 \pm 0.4 \times 10^6$	3.9 ± 0.3	$1.4 \pm 0.1 \times 10^3$
G259A	1.9 ± 0.1	4.7 ± 0.8	$4.1 \pm 0.6 \times 10^5$	12.1 ± 0.5	160 ± 7
G260A	0.23 ± 0.02	18 ± 3	$1.3 \pm 0.2 \times 10^4$	18.0 ± 1.6	12 ± 1
G261A	1.65 ± 0.01	26.6 ± 0.9	$6.2 \pm 0.2 \times 10^4$	0.47 ± 0.08	$3.5 \pm 0.2 \times 10^3$
Q17A	0.12 ± 0.1	3.3 ± 0.5	$3.6 \pm 0.6 \times 10^4$	13.2 ± 0.6	8.7 ± 0.9

Table 2-5. Summary of the inhibition constants and patterns for wild-type FRC and mutants.

(μM)	FRC	Q17A	G258A	G259A	G260A	G261A
CoASH	competitive	mixed-type		mixed-type	mixed-type	mixed-type
K_{ic}	16.7 ± 0.7	16.0 ± 0.6		6.0 ± 1.0	55 ± 19	2 ± 1
K_{iu}	--	100 ± 14		460 ± 129	290 ± 5	41 ± 1

Hydroxylamine Trapping of G261A Variant

The proposed mechanism for formyl-CoA dependent hydroxylamine inactivation requires that the nucleophilic hydroxylamine attacks the carbonyl of Asp-169 in the putative formyl-aspartyl anhydride. Chemically, it makes better sense for the attack to occur at the formyl group. An explanation is that the enzyme active site protects the formyl carbonyl from attack; interference with tetraglycine loop may allow addition to the less hindered formyl group. If this is the case, a reduction in effective inactivation is expected. Thus, the G261A variant was tested

Table 2-6. Formyl-CoA dependent inactivation of G261A (0.27 μM) by hydroxylamine

[Formyl-CoA] (μM)	G261A Residual Activity (%)
0	100 ± 8
77	30 ± 10
260	30 ± 14

for inactivation by hydroxylamine in the presence of formyl-CoA. At up to 260 μM formyl-CoA, the G261A variant was only inactivated about 70%.

Mass Spectrometry Analysis of Proteolysed FRC

In order to confirm the formation of enzyme-substrate anhydride intermediates during FRC turnover, an ^{18}O-oxalate labeling experiment was designed where the Asp-169-containing peptide could be monitored for isotopic label by MS. However, the Asp-containing proteolytic peptide was not reliably detected. Cleavage by glutamyl endopeptidase (V8) was expected to generate a M+H 1041.48 *m/z* peptide (GPPTVSGAALGD^{169}) and this peptide was detected once (see Figure 2-13), but these conditions could not be reproduced. A proteolysis map for FRC was generated by digestion with trypsin or glutamyl endopeptidase with both denatured and folded FRC (Figure 2-14). MS data were analysed by ESI-MS and peptides were

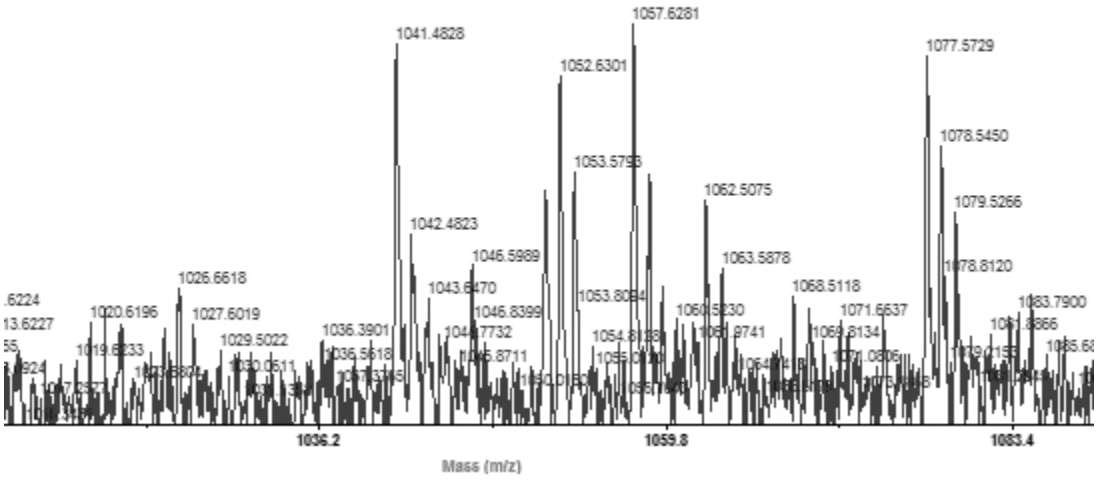

Figure. 2-14. Spectrum of FRC digested with glutamyl endopeptidase and analysed by MALDI-TOF mass spectrometry. The Asp-169-containing peptide (1041.48 *m/z*) was detected, but not reproducibly.

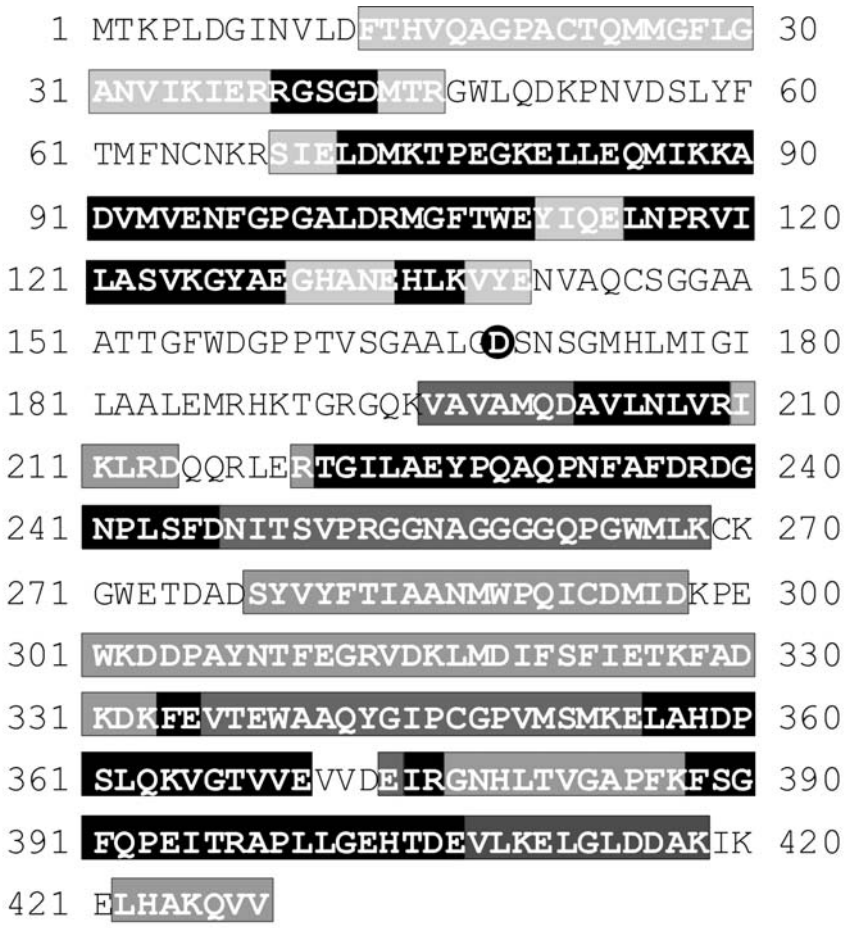

Figure. 2-15. Combined sequence coverage by mass spectrometric peptide analysis was 74%. Peptides identified from trypsin digest are shown in *dark grey*; peptides from glutamyl endopeptidase are shown in *light grey*; and, regions of overlap are shown in *black*. Identification was accomplished by tandem MS with the Mascot MS/MS ions search (185). The catalytic Asp-169 is highlighted with a *black circle*.

identified by MASCOT search engine (185). The central helix proved to be remarkably resistant to proteolysis (or detection by MS). Of the undetected residues (26%), the majority were from this region in the protein.

Engineering Trypsin-Friendly FRC

In an effort to facilitate detection of this residue, an arginine residue was engineered into FRC to afford a 28-residue peptide with mass 2908.46. The P159R mutant was designed after close analysis of a structural sequence alignment of FRC, YfdW, CaiB, and MCR (Figure 1-8).

Pro-159 corresponds to Arg-146 in MCR and both residues are found in a small, solvent-accessible loop connected to α-helix-9. Clostripain, a cysteine protease from *Clostridium hystolytica*, was chosen as an alternative to trypsin as it cleaves Arg-Pro peptide bonds (172). The peptide was expected to retain a positive charge upon ionization and should be a good candidate for MALDI-TOF MS. However, the protein was not overexpressed under the normal expression and purification conditions.

Half-Sites versus Independent Active Sites Reactivity

Half-sites reactivity is an extreme limit of negative cooperativity (see Seydoux for a review (220))—ligand-binding induces structural changes and alterations in subunit interactions lower enzyme affinity for the substrate in a second, otherwise equivalent, active site. Half-sites reactivity is common in nature, examples include glyceraldehye-3-phosphate dehydrogenase (48), thymidylate synthase (121), and the pyruvate dehydrogenase complex, where a "proton wire" is proposed to mediate half-sites reactivity (86). Family I CoA transferases exhibit this form of cooperativity, e.g. SCOT (156) and acetyl-CoA transferase from *E. coli* (233), mass spectrometric analysis of $NaBH_4$-treated protein, and use of the $1,N^6$-etheno-CoA, a fluorescent CoA analogue, demonstrated that in both cases, only one monomer was active at a time. Based on the asymmetry of the FRC structure with CoA bound, it has been suggested that the dimer might exhibit half-sites reactivity as well (124). A construct in the Novagen pET-Duet vector containing two cloning sites was therefore prepared allowing co-expression of FRC with the D169S inactive mutant . Constructs with a poly-histidine tag on FRC or the D169S mutant allowed the purification of heterodimers and histidine-tagged homodimers. If dimer formation is statistical, a 1:2:1 ratio of histidine-homodimer: histidine-heterodimer: heterodimer can be expected. Table 2-7 shows the predicted specific activities for both independent and half-sites

models and the experimental specific activities assayed with saturating formyl-CoA and oxalate. It appears that the active sites of FRC work independently of each other.

Table 2-7. Predicted and experimental activities of half-sites constructs.

S.A. (U/mg)	% wild type		Half-sites (%)	Independent (%)
WT-FRC	6.5 ± 0.4	100 ± 6		
DuetHisWT/D169S	4.0 ± 0.4	62 ± 6	100	66
DuetHisD169S/WT	1.8 ± 0.2	28 ± 2	66	33

Discussion

The reaction catalyzed by both Family I and III of CoA-transferases includes the formation of aspartyl- (Family III) or glutamyl- (Family I) mixed anhydride intermediates with the oxyacids, as well as covalent thioester intermediates to the CoA moiety (Figures 2-1 and 2-15). A distinction between the two families is that the Family I enzymes catalyze a classical ping-pong reaction while the kinetics of Family III enzymes differ; release of donor oxyacid is not observed prior to binding of the acceptor oxyacid. This leaves two possibilities, either the requirement of a ternary complex for catalysis, or the completion of the reaction before any product can be released. It can be settled from the kinetic trapping experiments and crystal structures presented above that hydrolysis of both formyl-CoA and oxalyl-CoA as well as formation of the mixed anhydride can be accomplished in FRC in the absence of acceptor carboxylic acid. Thus, the reaction does not need the formation of a ternary complex to proceed and the most probable interpretation of the kinetic data is that the leaving oxyacid remains bound in the enzyme and is released together with the acceptor thioester. Based on all available data a new proposal for the FRC reaction mechanism is presented in Figure 2-15. The glycine loop (^{258}GGGGQ^{261}) plays a central role during catalysis in FRC, and together with Gln-17, it protects the different intermediates from hydrolysis. The X-ray data suggest that upon binding of formyl-CoA, the CoA carrier adopts the resting conformation observed in most structures

including the mixed anhydride complexes. The glycine loop is presumed to close down upon formation of the aspartyl-formyl anhydride complex [B] in Figure 2-15. The Gln-17 side chain is positioned behind Asp-169. During the next catalytic step, $CoAS^-$ performs a nucleophilic attack on the mixed anhydride resulting in the β-aspartyl-CoA thioester [C]. Now the glycine loop opens up and Gln-17 flips its side chain out above the thioester, protecting it from hydrolysis. The released formate molecule binds to the open glycine loop at the site where oxalate was observed in the Q17A mutant structure (Figure 2-8C). As the loop closes, formate is pushed

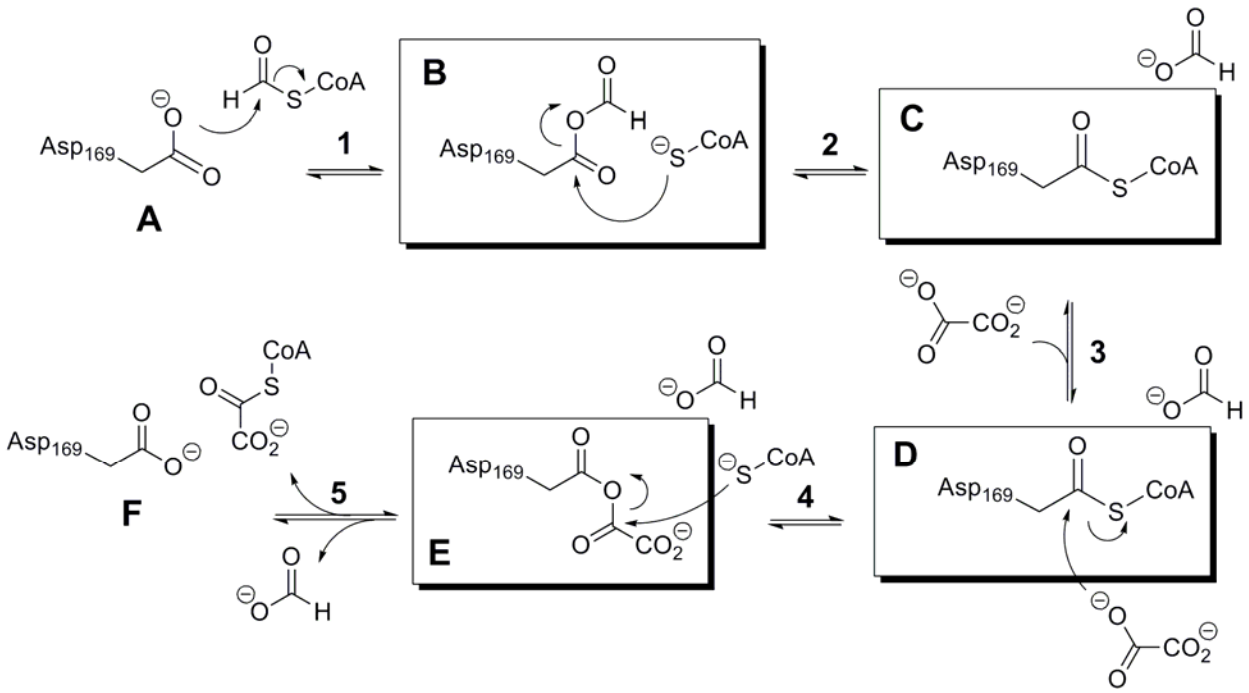

Figure. 2-16. The proposed reaction mechanism for formyl-CoA transferase. All complexes observed in crystal structures are highlighted. Letters and numbers correspond to structures and steps seen in Figure 2-17. The mechanism corresponds to Mechanism 1a in Figure 1-6. Putative tetrahedral intermediates are not shown to save space.

down in the active site simultaneously as the CoA moiety reorganizes [C] into the newly observed activated conformation and Gln-17 moves back above Asp-169. The thioester is at this stage protected from hydrolysis by the closed glycine loop and formate is bound in one of the anion sites identified in subunit B of the β-aspartyl-CoA thioester complex (Cl_1^B in Figures 2-4

and 2-6B). Binding of formate at this site can result in hydrogen bonds to both the pantetheine arm and the main chain amide of Gln-262 (Figure 2-9). The activated CoA conformation creates a cavity below the β-aspartyl-CoA thioester with connection to the surface, where oxalate can enter and bind in the second anion site identified in subunit B of the β-aspartyl-CoA thioester complex (Cl_2^B in Figures 2-4 and 2-6B). Manual modeling of oxalate at this site results in strong hydrogen bonds to the amides of Gln-17 and Ala-18 and minor shifts would place also His-15 and Asn-96 within hydrogen bonding distances, ensuing bonds to all four oxygens of oxalate (Figure 2-9). With a favorable orientation, and a distance of approximately 3.7 Å to Cγ of Asp-169, oxalate is perfectly aligned for a nucleophilic attack at the β-aspartyl-CoA thioester [D].

The second mixed anhydride, the aspartyl-oxalyl anhydride results, and $CoAS^-$ shifts back to its resting conformation. The final attack by $CoAS^-$ at the oxalyl moiety regenerates the aspartate together with oxalyl-CoA [E]. Finally, in the product leaving step, opening of the glycine loop allows release of the acceptor thioester together with formate.

Experimental Methods

Site-Directed Mutagenesis and Protein Production

The Q17A, G259A, G260A, and G261A variants were prepared by QuikChange site-directed mutagenesis (Stratagene) with the FRC gene in the pET-9a vector (Novagen, San Diego, CA) with the following primers: 5'-Q17A 5'-GCT TGA CTT TAC CCA CGT CGC GGC AGG TCC TGC CTG TAC ACA GAT GAT GGG, 3'-Q17A 3'-CCC ATC ATC TGT GTA CAG GCA GGA CCT GCC GCG ACG TGG GTA AAG TCA AGC, 5'-G259A 5'- GGT GCG GGC GGC CAG CCA GGC TGG, 3'-G259A 3'- GCC CGC ACC TGC GTT ACC ACC ACG TGG, 5'-G260A 5'- GGC GCG GGC CAG CCA GGC TGG ATG CTG, 3'-G260A 3'- GCC CGC

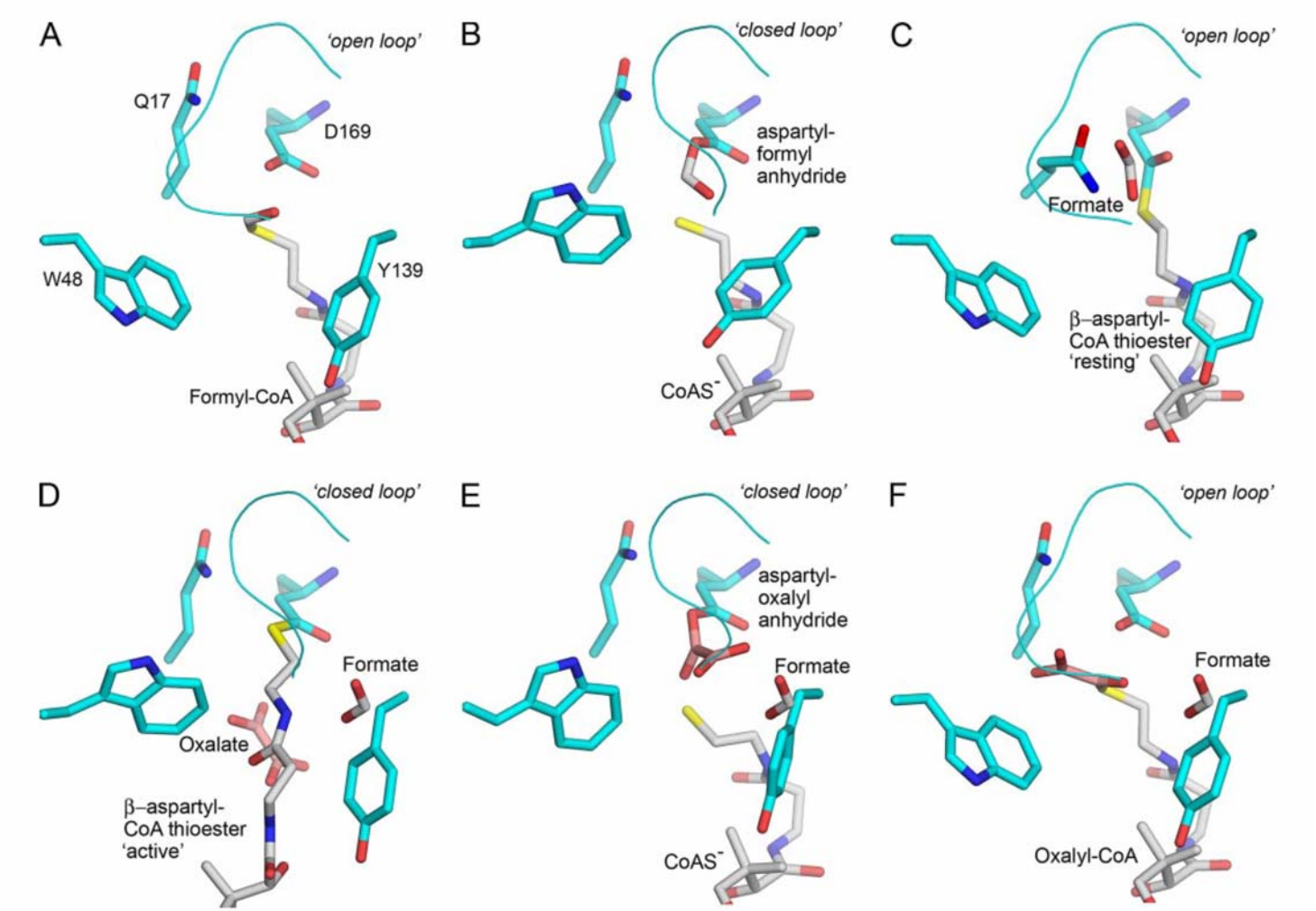

Figure. 2-17. Models and crystal structures showing assumed important features in the active site between the catalytic steps in Figure 2-15. For clarity, the amino acid residues are only labeled in A. Glycine loop is shown as Cα trace. *A*, model of formyl-CoA in the active site. *B*, aspartyl-formyl anhydride formed after step 1; *C*, the enzyme-CoA thioester; *D*, the activated conformation of the enzyme-CoA thioester observed in subunit B of the crystal structure; *E*, the second anhydride; and, *F*, the apoenzyme with both products modeled in the active site. Taken from Berthold 2008 (18).

GCC ACC TGC GTT ACC ACC ACG, 5'-G261A 5'-GGT GGC GGC GCG CAG CCA GGC TGG, and 3'-G261A-3' GCC GCC GCC CGC TGC GTT ACC ACC. PCR primers were obtained from Integrated DNA Technologies, Inc. (Coralville, IA). DNA sequencing was performed by the DNA Sequencing Core of the Interdisciplinary Center for Biotechnology Research at the University of Florida.

Recombinant FRC and variants were produced and purified following the procedure previously described . In short, the plasmids were transformed into the *E. coli* strain BL21(DE3) (Novagen) where the genes were expressed. Purification was then carried out sequentially by four steps of chromatography; DEAE anion exchange, Blue-Sepharose fast flow affinity, Sephadex G-25 size-exclusion, and QHP anion exchange. The final purified enzymes were stored at -80º C in 25 mM sodium phosphate, pH 6.2 with 300 mM NaCl, 1 mM DTT, and 10 % glycerol. Purity was verified by SDS-PAGE and protein concentrations were determined by the Bradford method (27) with Commassie Plus reagent (Pierce) based on a standard curve constructed with known amounts bovine serum albumin or the Edelhoch method (see below).

Determination of Protein Concentration by the Edelhoch Method.

Common spectrometric methods for determining protein concentrations depend heavily on the chosen standard (209). Methods employing the molar absorption coefficient, ε, are more accurate, but are usually based on concentrations determined by dry weight, nitrogen, or amino acid analysis. The Edelhoch method as reported by Gill and von Hippel (89) is based on the data of Edelhoch (70) for the absorbance at 280 nm of tryptophan, tyrosine, and disulfide bonds and is the best way for determining ε for a protein. Based on 116 measurements from 80 proteins (181), the ε^{280} for a protein can be predicted using the following equation:

$$\varepsilon^{280}\ (M^{-1}\ cm^{-1}) = (n^{Trp})(5{,}500) + (n^{Tyr})(1{,}490) + (n^{cystine})(125)$$

where n^{Trp} is the number of tryptophans, n^{Tyr} is the number of tyrsosine residues, and $n^{cystine}$ is the number of disulfide bonds in the protein in question. This method yields values with standard percent deviation of 3.836 when compared to a literature set of concentrations determined by dry weight method, amino acid analysis, Kjeldahl nitrogen determination, or the Edelhoch method for 80 proteins.

While the general equation above does a good job of predicting ε^{280}, the Gill and von Hippel method is slightly more accurate, accounting for the slight change in absorption of buried amino acid residues, and involves measuring A^{280} in denaturing 6 M guanidinium hydrochloride. This $\varepsilon^{280}_{(6MGuHCl)}$ can then be used to calculate the $\varepsilon^{280}_{(buffer)}$, which can then be used to easily and non-destructively determine concentration of samples in storage buffer. The following equation uses values reported by Pace:

$$\varepsilon^{280}\ (M^{-1}\ cm^{-1}) = (n^{Trp})(5{,}685) + (n^{Tyr})(1{,}285) + (n^{cystine})(125)$$

Aliquots of equal volumes of FRC in storage buffer were lyphophilized and subsequently resuspended in either 100 µL of FRC storage buffer (100 mM potassium phosphate, pH 6.5 with 300 mM NaCl) or storage buffer with 6 M GuHCl. The absorbances at 280 and 333 nm were collected. The $\varepsilon^{280}_{(6MGuHCl)}$ was corrected for the effects of light scattering by subtracting 1.929 x A^{333} and used to calculate the concentration in 6 M GuHCl. This concentration was used to calculate the $\varepsilon^{280}_{(buffer)}$ 58, 202 $M^{-1}\ cm^{-1}$.

Assay for Coenyzme A Esters

Concentrations of formyl-, oxalyl-, and succinyl-CoA were determined with the single-point HPLC assay developed by Jónsson (123, 124). CoA ester separation was achieved by C18 reversed-phase HPLC (Dynamax Microsorb 60-8 C18, 250 x 4.6 mm or Varian Pursuit XRs C18 150 x 4.6 mm) with a singlewavelength detector at 260 nm. Varian Galaxie Chromatography Data System software version 1.9.3.2 was used for data analysis.

HPLC gradient methods

Separation methods were optimized for the above C18 columns. Analysis with the Dynamax Microsorb column was achieved with previously described HPLC methods (123, 124). Methods for separation of CoA esters with the Varian Pursuit XRs C18 column and varyied gradients of Buffer A and Buffer B are summarized below. Buffer A was 50 mM sodium acetate, pH 4.7 and Buffer B was 50 mM sodium acetate with 90% CH_3CN, pH 4.5.

Table 2-8. Oxalyl-CoA HPLC method

Time, min	Buffer B, %	Flow, mL/min	
0.00	5	1.0	
0.50			Wait (close)
6.00	9		
6.10	95		
9.00	95		
9.10	5		
11.00	5		

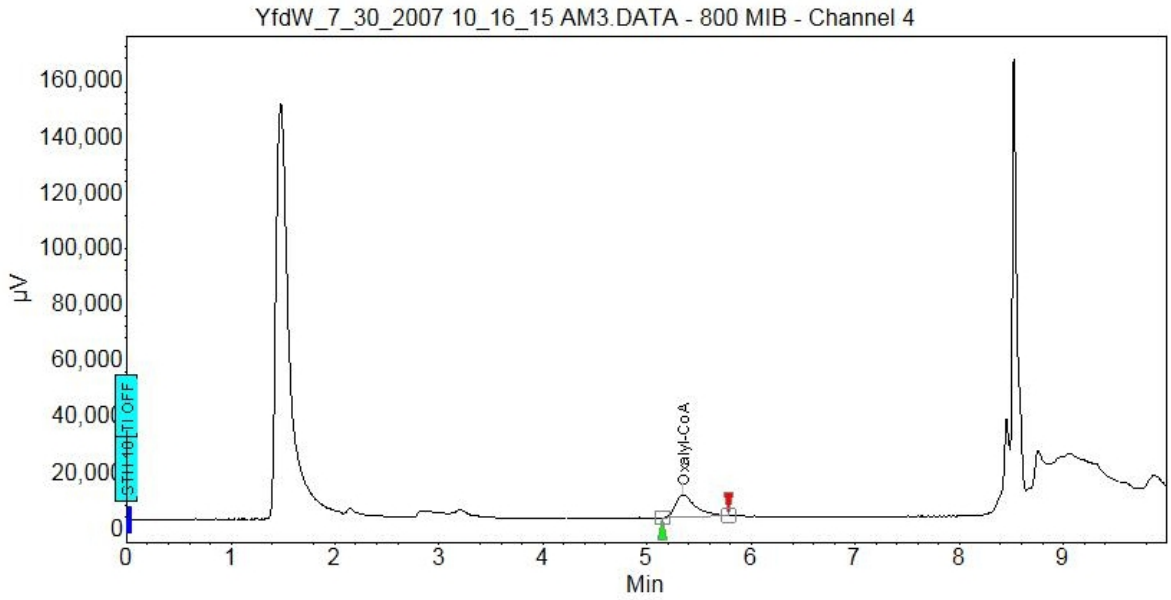

Figure. 2-18. Representative chromatogram for separation of oxalyl-CoA (t_R = 5.2 min).

Table 2-9. Formyl-CoA HPLC method

Time, min	Buffer B, %	Flow, mL/min	
0.00	6	1.0	
0.15			Wait (close)
10.00	11		
10.10	95		
14.00	95		
14.10	6		
16.00	6		

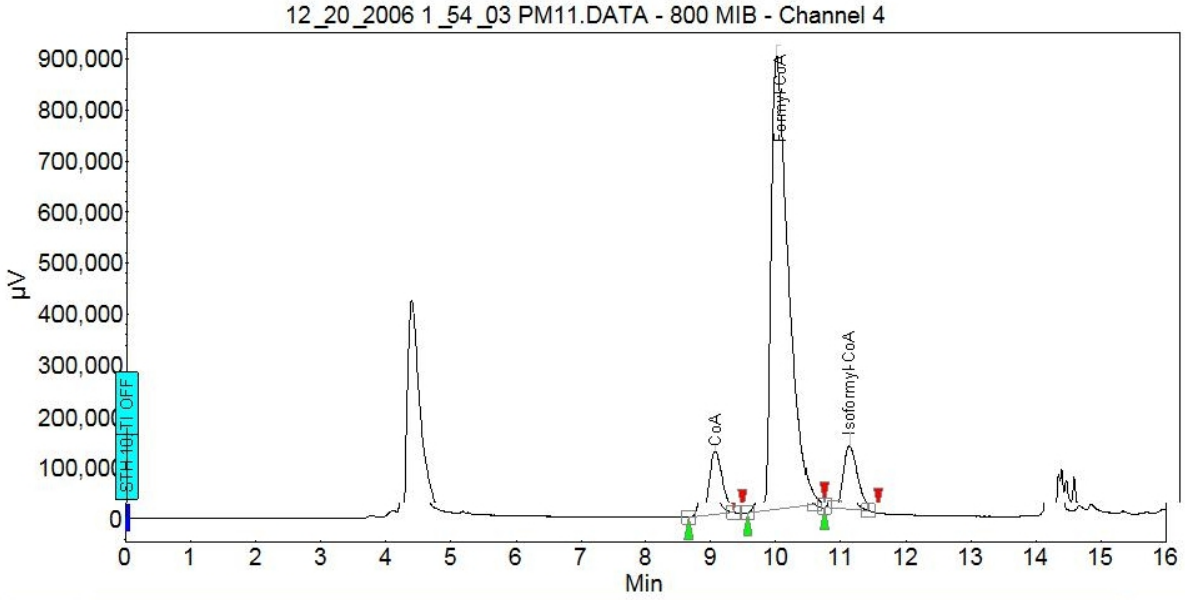

Figure. 2-19. Representative chromatogram for separation of CoA (t_R = 9.10 min) and formyl-CoA (t_R = 10.10 min). Note the 2'-phosphoryalated iso-formyl-CoA at around 11.2 min.

Table 2-10. Succinyl-CoA HPLC method

Time, min	Buffer B, %	Flow, mL/min	
0.00	6	1.0	
0.50			Wait (close)
11.50	14		
11.60	95		
14.00	95		
14.10	6		
18.00	6		

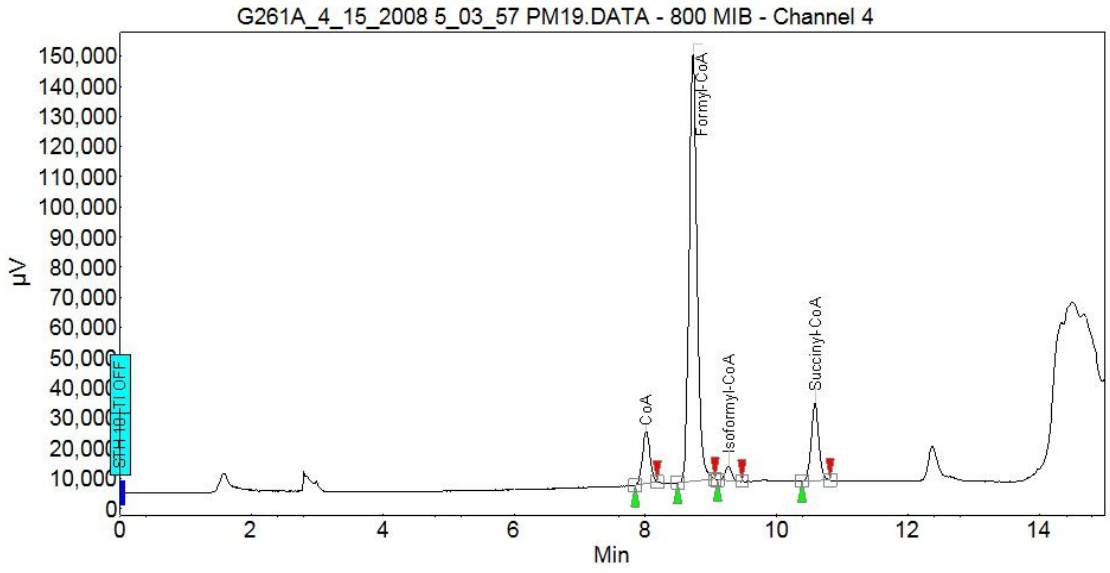

Figure. 2-20. Representative chromatogram for separation of succinyl-CoA (t_R = 10.65 min)

Assay for coenzyme A concentration

Ellman's reagent (5,52-dithio-bis(2-nitrobenzoic acid; DTNB)) was used to accurately assess CoA stock concentrations for inhibition studies. Samples of CoA were allowed to react in 100 mM potassium phosphate, pH 6.7, with 1 mM DTNB in a total volume of 150 μL for 15 minutes at room temperature. Absorbance readings were taken at A^{412} and an extinction coefficient of 14150 $M^{-1}cm^{-1}$ was used to determine CoA concentrations after adjustment to the absorbance of a blank containing DTNB, but no CoA.

Enzyme Kinetic and Inhibition Studies

Formyl-CoA transferase activity was assayed by monitoring the formation of oxalyl-CoA by an HPLC point assay developed by Jónsson (124). Formyl-CoA and oxalyl-CoA were prepared by previously described methods (124). Reaction mixtures containing 60 mM potassium phosphate, pH 6.7, approximately 80 ng of enzyme, and appropriate amounts of formyl-CoA and oxalate were prepared in a total volume of 200 μL. Reactions were started by the addition of formyl-CoA and quenched by the addition of 30% acetic acid. The formation of

oxalyl-CoA was measured by separating the quenched reaction mixtures by reverse-phase chromatography, monitoring the absorbance at 260 nm, and integrating the area under the peak. The effects of contaminating CoA were controlled by first determining the inhibitory effect of CoA against varied concentrations of formyl-CoA. Kinetic constants V_{max}, K_{iCoA}, and $K_{M(formyl-CoA)}$ were then used to fit initial velocity plots of varied oxalate concentration at constant formyl-CoA concentrations to determine the apparent $K_{M(oxalate)}$ and K_{ia}.

The inhibition of FRC by chloride ions was determined at different oxalate concentrations at saturating concentration of formyl-CoA (21.4 μM) and 10 μM CoA with KCl concentrations of 5, 15, and 30 mM.

Hydroxylamine and Sodium Borohydride Trapping Experiments

The experiments were carried out in a reaction volume of 500 μL, containing 6.2 μg of recombinant wild-type FRC in 60 mM potassium phosphate buffer, pH 6.7, and 77 mM oxalate. The reaction was started by the addition of 173 μM formyl-CoA and was allowed to run for 10 seconds before treatment with 15 mM hydroxylamine at pH 7 for 30 seconds at 30 ºC. Small molecules were immediately removed from the reaction solution by size exclusion chromatography (5 mL G-25) after which the residual specific activity of FRC was assayed using the normal HPLC point assay. The trapping experiment was repeated in a reaction mixture in absence of oxalate with FRC or G261A incubated for 30 seconds at 30 ºC with varied concentrations of formyl-CoA (0.14 to 260 μM). As before, the reaction mixture was separated by gel filtration chromatography 30 seconds after the addition of hydroxylamine. Residual activity of the protein treated only with NH_2OH was also assayed.

Borohydride trapping experiments were carried out as above with the exception that the reaction was trapped with the addition of $NaBH_4$ (1M $NaBH_4$ in 1M NaOH) to a final

concentration of 33 mM, immediately followed by addition of an equal volume of 1 M HCl. The reaction mixture was allowed to incubate at room temperature for 30 min prior to gel filtration.

Crystallization and Freeze-Trapping Experiments

Crystallization and analysis of FRC variants was carried out by Dr. Catrine L. Berthold at the Karolinska Institutet, Stockholm, Sweden. FRC was crystallized by the hanging-drop vapor diffusion method using conditions previously optimized for the wild type enzyme (197). 2 μL of the protein solution containing 7.5 mg/mL FRC in 25 mM MES buffer pH 6.2 and 10% glycerol was mixed with 2 μL precipitant solution and set up to equilibrate against 1 mL well solution at 293 K. A precipitant solution of 21-25 % PEG 4000, 0.1 M HEPES buffer pH 7.2-7.5 and 0.5 M $MgCl_2$ resulted in approximately 0.1 x 0.1 x 0.2 mm single crystals that grow to full size within 48 h.

The freeze-trapping experiments were performed by transferring the crystals to a drop containing a modified well solution (30% PEG 4000, 0.5 M $MgCl_2$, 0.1 M HEPES buffer pH 7.2) mixed in a 1:1 ratio with 20 mM formyl-CoA or oxalyl-CoA in 50 mM sodium acetate buffer pH 5.0. The crystals were flash frozen in liquid nitrogen after the desired reaction times. The crystals, diffracting to 2.0 Å resolution, belong to space group I4 with an asymmetric unit containing two 47 kDa FRC monomers, comprising the biological dimer.

Crystals where the aspartyl-formyl anhydride complex was trapped were obtained by a new crystallization condition devoid of chloride ions. An optimized well solution of 1.35 M sodium citrate and 0.1 M HEPES buffer, pH 7.2-7.5, was used when setting up the crystallization experiments using the same protein solution and mixing conditions as above. The crystals belong to the same space group and were isomorphous with the previous ones.

In order to form the anhydride complex 2-3 μL of a formyl-CoA solution was slowly added to the crystals in the drop and crystals were then transferred to an ethylene glycol cryo solution (1 M sodium citrate, 75 mM HEPES buffer, pH 7.2 and 25 % ethylene glycol) after approximately 10 minutes. The formyl-CoA solution was prepared by mixing equal volumes of 20 mM formyl-CoA in 50 mM sodium acetate buffer, pH 5.0, and well solution.

Crystals of the G260A and Q17A mutants of FRC were obtained using the same conditions as for the aspartyl-formyl anhydride complex. Crystals of the G260A mutant were directly frozen in liquid nitrogen after transfer through silicon oil while crystals of Q17A were used for complex formation. For the ternary complex the drops containing the Q17A mutant crystals were supplemented with formyl-CoA as for the wild type aspartyl-formyl anhydride complex, followed by the addition of 1 μL 40 mM potassium oxalate mixed into the well solution. For this complex, the ethylene glycol cryo-solution was supplemented with 40 mM potassium oxalate. Crystals of the Q17A mutant belong to the space group I4 with unit cell dimensions a = b = 153.6 Å and c = 98.1 Å while the G260A mutant crystallized in space group $P4_32_12$ with cell dimensions of a = b = 97.3 Å and c = 193.4 Å.

Data collection, Structure Determination, and Refinement

Data were collected at beamlines ID14 eh1 and ID23 eh2 at the European Synchrotron Research Facility, Grenoble, France and at beamline I911-2 at MAX-lab, Lund, Sweden. Data collection and refinement statistics are summarized in Table 2-1. All images were integrated with MOSFLM (146) and further processed using SCALA (11). Phases from the originally determined apoenzyme (pdb accession code: 1p5h) (197) were used to solve the structures by molecular replacement using MOLREP (248). Refinement by the maximum likelihood method was carried out in REFMAC5 (174) interspersed with manual model building in WinCoot (157)

where water molecules were assigned and checked. The quality of the final structures were validated using PROCHECK (144)and WinCoot (157) and annealed omit maps calculated in CNS (29) were used to confirm the conformations in the active sites. All images of protein molecules were generated using PYMOL (59).

Synthesis of [$^{18}O_4$]-Oxalate

Normalized $H_2{}^{18}O$ (95% enrichment) was obtained from Cambridge Isotopes, Inc. (Andover, MA). The ^{18}O-enriched oxalic acid was prepared by dissolving approximately 6.5 mg of $(COOH)_2 \cdot 2H_2O$ in 500 μL of $H_2{}^{18}O$ in a literature procedure (6). The sample was sealed in an ampule and lyophilized after storage at room temperature for 5 weeks. The ^{18}O content of the oxalic acid (79%) was determined by LC-MS (Mass Spectrometry Laboratory, University of Florida). Oxalate was resuspended in water and the pH brought to 7 with the addition of solid KOH. Oxalate concentration was determined by oxalate decarboxylase enzymatic assay (143).

Isotope (^{18}O)-Labelling Experiment

^{18}O-labelling of FRC Asp-169 was attempted by incubating 12.4 μg of wild-type recombinant FRC with 236 μM formyl-CoA and 19.8 mM 79% enriched [$^{18}O_4$]-oxalate for 1 and 2 minutes at 30° C. The unquenched reaction mixtures were immediately buffer exchanged into 300 mM sodium chloride in 25 mM sodium phosphate, pH 6.2 on Amicon Microcon concentration devices to a final volume of about 50 μL. Half was subsequently reincubated with 236 μM formyl-CoA and 77 mM [$^{16}O_4$]-oxalate for 2 minutes.

Peptide Generation by Proteolysis

The trapped samples (theoretically 12 μg of protein for hydroxylamine experiments or 6.2 μg of FRC each for the ^{18}O-labelling experiments) were buffer exchanged into about 50 μL each of 50 mM NH_4HCO_3, pH 8.5 or 50 mM sodium phosphate, pH 7.5 with Amicon Microcon centrifugal filter devices (Millipore). Concentrators were prepared by storing in 4% Tween 20

overnight at 4° C, rinsed in deionized water, and membranes were washed by centrifuging twice with 500 μL of water to reduce non-specific protein-membrane interactions. The samples were then heated to 60° C for 5 minutes and subsequently digested with 4% (w/w) trypsin or glutamyl endopeptidase for 16 hours at 37° C.

Peptide Generation by Proteolysis (with GuHCl)

The sample (12.4 μg of FRC) was buffer exchanged into 100 μL of 50 mM sodium phosphate, pH 6.7 with 6 M guanidinium HCl and heated for 5 minutes at 60° C. The solution was cooled to room temperature and then diluted to 1 M GuHCl with 50 mM sodium phosphate, pH 7.5. V8 protease (Glu-C) was added (25:1) and the sample was incubated 18 hours at 37° C. Concentrators (Amicon Microcon centrifugal filter devices, Millipore) were prepared by storing in 4% Tween 20 overnight at 4° C, rinsed in deionized water, and washed by centrifuging twice with 500 μL of water to reduce non-specific protein-membrane interactions.

Mass Spectrometric Analysis

Protein digests were submitted for analysis by HPLC/(+)ESI-MS on a ThermoFinnigan (San Jose, CA) LCQ with electrospray ionization (Mass Spectrometry Laboratory, University of Florida). MS and MS/MS data were compared against a database generated from FRC with hydroxylamine and single and double ^{18}O labels allowed on acidic amino acid residues as variable modifications with the MASCOT search engine (185).

Mass spectrometric analysis of whole FRC was carried out by Dr. Gunvor Alvelius at the Karolinska Institutet, Stockholm, Sweden. A sample of formyl-CoA transferase incubated with formyl-CoA in the absence of oxalate was prepared according to an experiment by Lloyd and Shoolingin-Jordan (156). A 125 μL reaction mixture containing 0.153 mM formyl-CoA transferase in 25 mM MES buffer, pH 6.2, with 10% glycerol and 0.596 mM formyl-CoA was incubated for 1 min at room temperature. The reaction mixture was then immediately desalted at

277 K into 1 mM HCl using a prepacked NAP-5 column (Amersham Biosciences). The protein elution of 1 ml was mixed with an equal volume of 98% acetonitrile and 2% formic acid. Data were immediately acquired in positive mode on a QTOF ULTIMA API instrument (Waters Corp., Milford, MA) equipped with the standard Z-spray source with a capillary voltage of 1.5 kV. The instrument was calibrated between 300 and 1400 *m/z* with myoglobin prior to the run. The sample was introduced with a metal-coated borosilicate glass capillary needle (Proxeon Biosystems A/S, Odense, Denmark). Data were collected over a mass range between 300 and 2500 *m/z* and with a scan time of 1 s for about 5 min. The spectra were combined and deconvoluted to zero charged ions with MaxEnt 1 in the Masslynx software (Waters Corp., Milford, MA).

Half-Sites (pET-Duet) Constructs

Wild-type FRC and D169S mutant sequences were cloned from pET-9a constructs (197). Forward primers included a clamp region and restriction site terminating in the start codon for the gene. The reverse primers comprised a clamp region, restriction site, and an in-frame stop codon: 5'-FRC *BamH1* 5'-AGG AGA TAT AGG ATC CGA TGA CTA AAC CAT TAG ATG GAA TTA ATG TGC, 3'-FRC *HindIII* (stop) 5'- ACA GGT AGT TTG AAG CTT AGA CTT, 5'-*Nde1* 5'-AGG AGA TAT ACA TAT GAC TAA ACC ATT AGA TGG AAT TAA TGT GC 3'-D169S *Xho1*(stop) 5'-ACA GGT AGT TTG ACT CGA GAG ACT T. The amplified products were subjected to restriction enzyme digest with *BamH1* and *HindIII* for the D169S PCR product and *Nde1* and *Xho1* restriction enzymes for wt-FRC. The resulting D169S and FRC fragments were isolated and ligated one at a time into the pETDuet-1 multiple cloning sites 1 (with N-terminal His_6 tag) and 2 (no fusion tag) to generate the DuetHisDW and DuetHisWD constructs. JM109 competent cells (Stratagene) were transformed with the resulting plasmids, screened for correct insert size, and confirmed by DNA sequencing.

CHAPTER 3
FORMYL-COA TRANSFERASE (YFDW) FROM *ESCHERICHIA COLI*[2]

Introduction

With the completion of genome sequences for several strains of *Escherichia coli* (23, 101, 186, 256), attention has turned to the annotation of proteins encoded by specific genes of unknown function (244). Deletion studies have shown that the *yfdXWUVE* operon (Figure 3-3), in which the *yfdX* gene is under the control of the EvgAS regulatory system (169), encodes proteins that enhance the ability of *Escherichia coli* MG1655 to survive under acidic conditions (168). Although the molecular mechanisms underlying this phenotypic behaviour remain to be elucidated, the proteins encoded by the *yfdW* and *yfdU* genes in this operon (YfdW and YfdU, respectively) are homologous to the formyl-CoA transferase (FRC) (2, 29, 45) and the oxalyl-CoA decarboxylase (OXC) (10, 15) present in the obligate anaerobe *Oxalobacter formigenes* (237). FRC and OXC are essential for the survival of *Oxalobacter* in that they mediate the conversion of oxalate into formate and CO_2 in a coupled catalytic cycle (Figure 3-1). In combination with an oxalate:formate antiporter (OxlT) (*15*), this cycle is thought to maintain

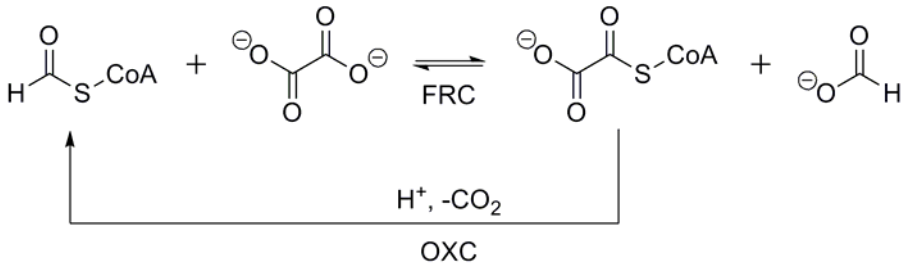

Figure. 3-1. Coupled enzymes of oxalate catabolism in *O. formigenes*.

[2] Reproduced in part with permission from Journal of Bacteriology, Vol. 190 (12), Toyota, C. G., Berthold, C. L., Gruez, A., Jonsson, S., Lindqvist, Y., Cambillau, C., and Richards, N. G. Pages 2556-2564. Copyright 2008 Journal of Bacteriology

the electrochemical and pH gradients needed for ATP synthesis (3, 108, 142). It has therefore been proposed that (i) YfdW catalyzes the conversion of oxalate into oxalyl-CoA using formyl-CoA as a donor, and (ii) the YfdU protein mediates oxalyl-CoA decarboxylation (97). High-resolution X-ray crystallography supports the likely functional similarity of FRC and YfdW in that the two proteins adopt the same unusual interlocked, catalytically active dimer (Figure.3-2) (92, 97, 197) despite having only 61% sequence identity (Figure 1-8). On the other hand, the ability of *Escherichia coli* to metabolize oxalate to formate and CO_2 does not seem to have been reported, and the relevance of such an activity to survival under conditions of low pH remains to be established.

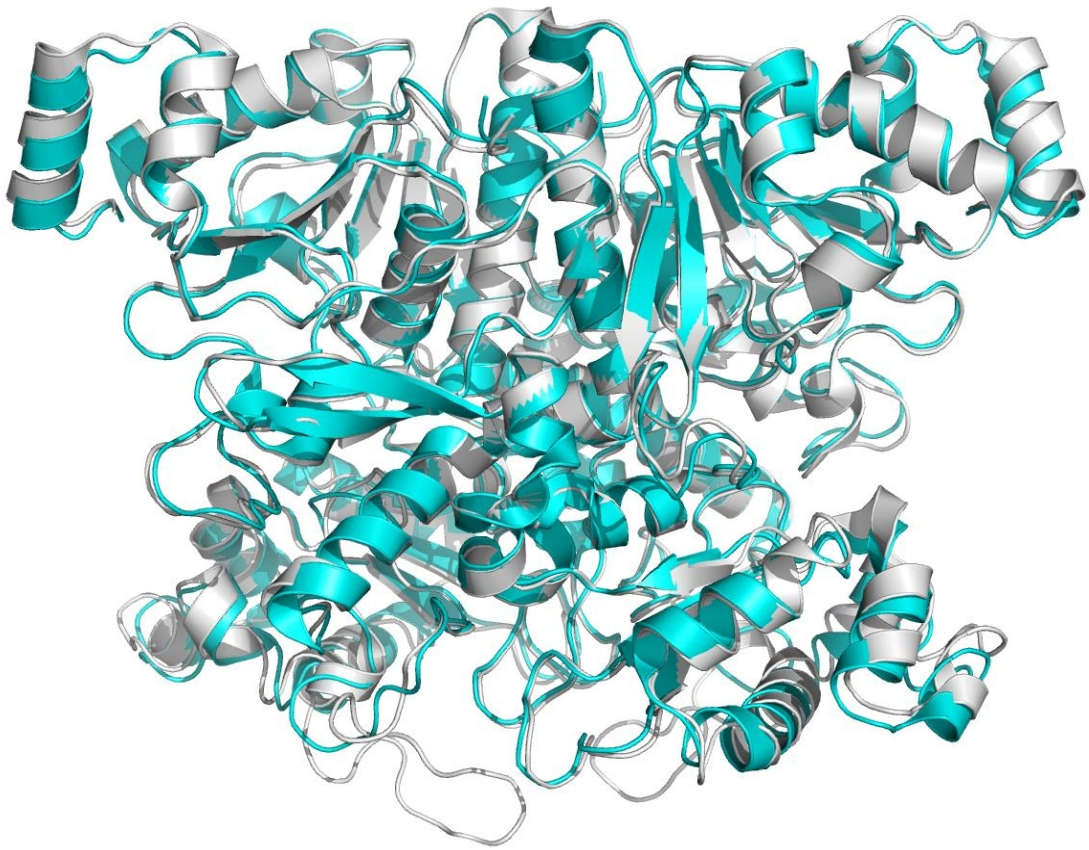

Figure. 3-2. Superimposition of apo-YfdW (cyan) and apo-FRC (white) dimer structures. Coordinates were obtained from the Protein Data Bank files 1pt7 and 1p5h, respectively, and the figure was made using PyMOL (59).

Results

Kinetic Characterization of YfdW

The initial experiments examined whether *Escherichia coli* YfdW could catalyze the synthesis of oxalyl-CoA from formyl-CoA and oxalate, as inferred on the basis of structural genomics (92, 97). Incubating formyl-CoA and oxalate with YfdW in phosphate buffer, pH 6.7, did indeed result in the appearance of oxalyl-CoA, and the amount of this product could be quantified by direct HPLC measurement (Figure 2-17). YfdW differed from FRC in that stronger quenching conditions were required. As seen in Figure 3-4, when attempts were made to stop the YfdW catalyzed reaction with 10% HAc, YfdW continued to form oxalyl-CoA even when incubated on ice. Increasing the concentration of HAc to 20%, however, clearly abolished YfdW activity, but did not increase oxalyl-CoA hydrolysis. In addition, more stringent wash conditions for syringes, the HPLC injection port, and column were necessary to prevent carryover activity.

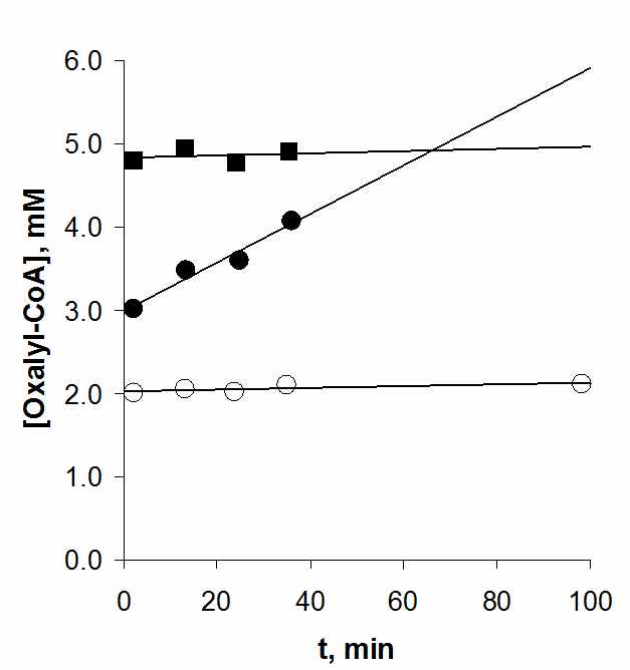

Figure. 3-4. Quench conditions for YfdW. Reactions were quenched and mixtures were inbubated with either FRC or YfdW. Oxalyl-CoA concentration was monitored over time. YfdW with 10% HAc incubated at 0 ºC(●), YfdW with 20% HAc at 32 ºC (○), and FRC with 10% HAc at 32 ºC (■).

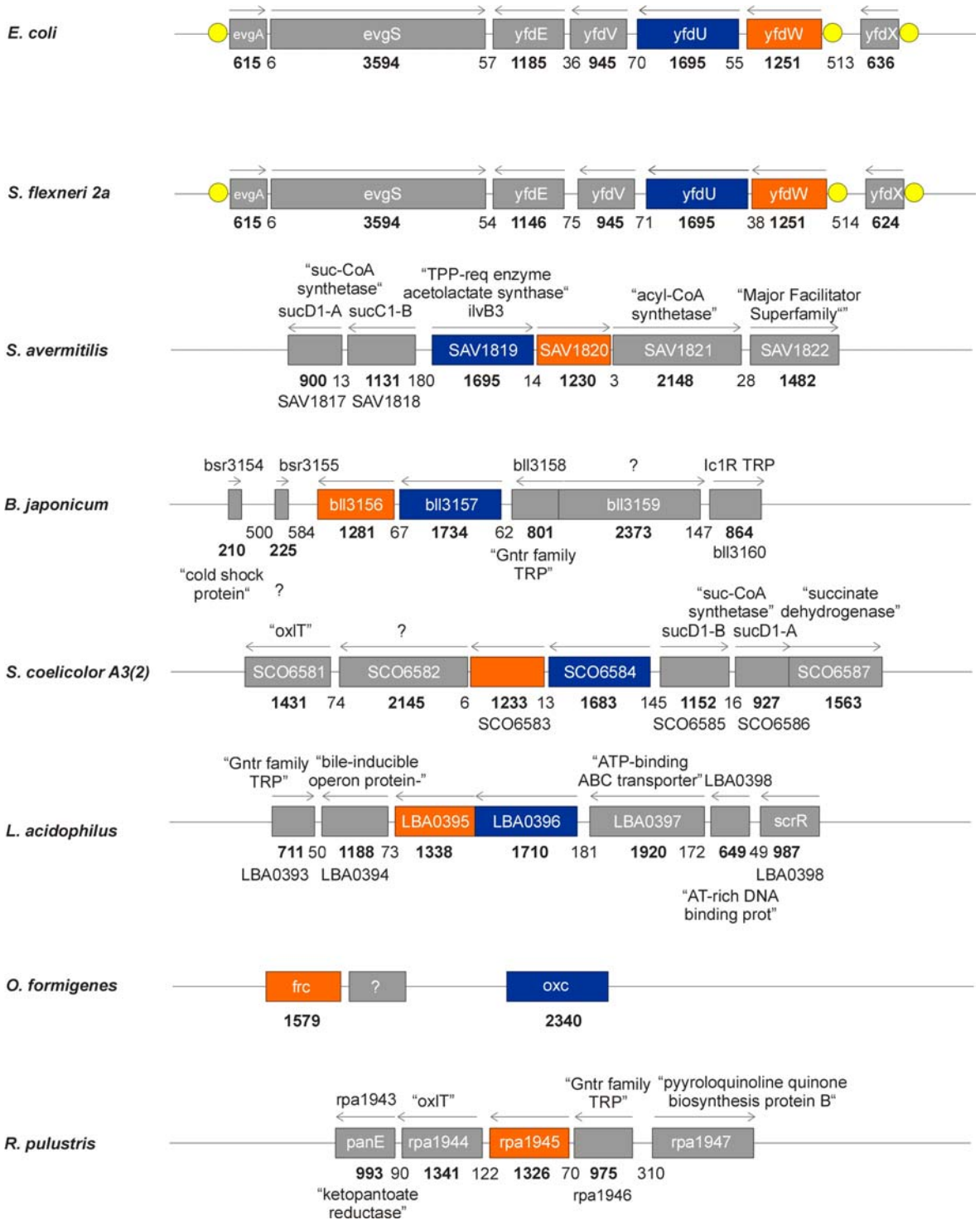

Figure. 3-3. Graphical representation of putative formyl-CoA transferase (*orange*) genes in various organisms for which total genome sequencing data are available. Putative oxalyl-CoA decarboxylase genes are shown in *blue*. Arrows represent the direction of transcription. *Yellow circles* in *E. coli* and *S. flexneri* annotate identified EvgAS regulatory binding motifs in the *yfdXYWUVE* operon. Gene and gap lengths are given (bp).

Thus the wash portion of the HPLC method gradient was increased to 98% Buffer B with 2% Buffer A and run for 3 minutes. The analysis of initial rate data using standard fitting methods (47) gave a value of 510 ± 30 μM for the apparent K_M of oxalate, almost an order of magnitude less than the cognate parameter determined for this substrate in the FRC-catalyzed reaction (3.9 ± 0.3 mM) (197). Variation of oxalate at different fixed concentrations of formyl-CoA gave intersecting lines in the Lineweaver-Burk plot (Figures 3-6 and 3-7), suggesting an ordered bi-bi sequential kinetic mechanism as reported previously for FRC (124) and other Family III CoA

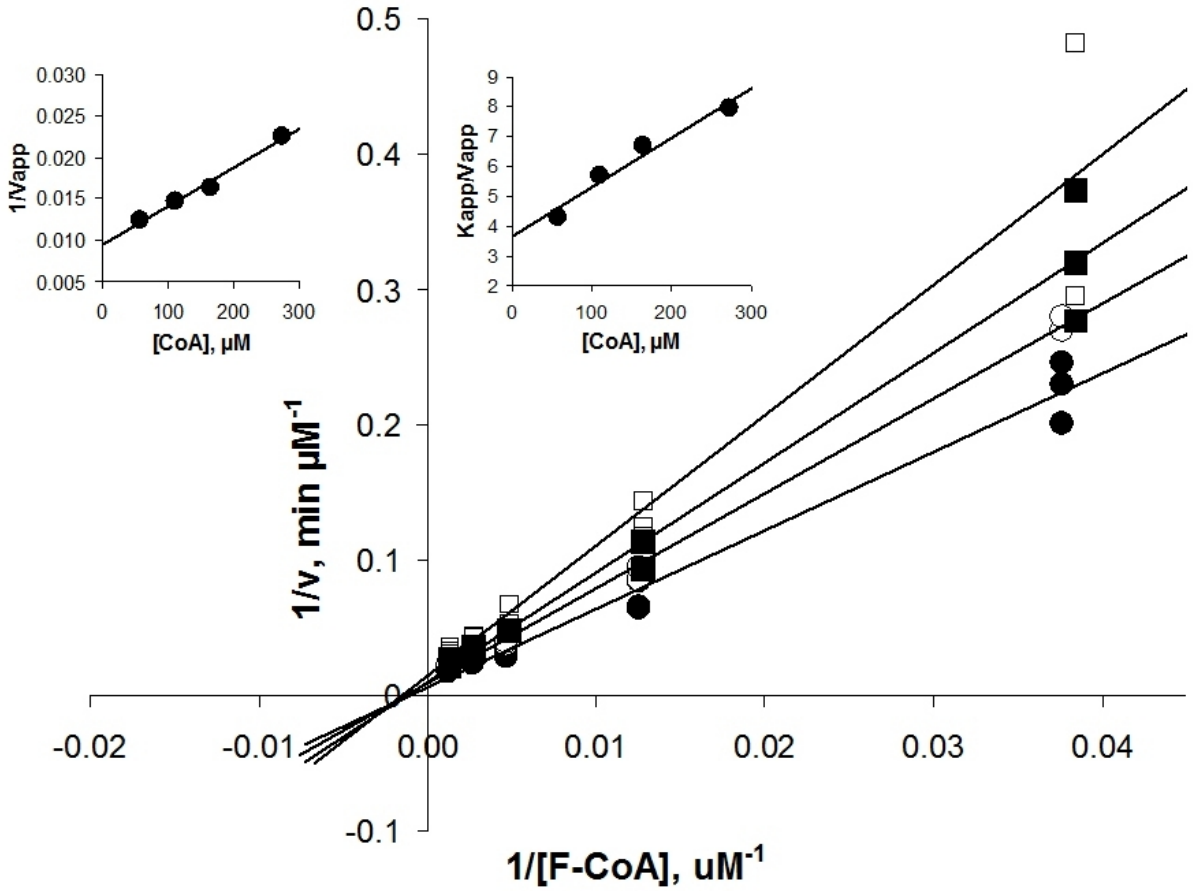

Figure. 3-5. Double-reciprocal plot for the inhibition of YfdW by free CoA against varied [formyl-CoA] at constant saturating [oxalate] = 2.5 mM. Lines are fitted to the data by linear-regression methods. CoA concentrations were 59 μM (●), 111 μM (○), 165 μM (■), and 273 μM (□) K_{ic} and K_{iu}, 218 ± 21 and 213 ± 16 μM, respectively, were determined from the replots of K_{mapp}/V_{app} and $1/V_{app}$ vs. [CoA] (inserts). $K_{M(F\text{-}CoA)}$ of 351 ± 4 μM was determined by fitting the initial velocity plots with the mixed-type inhibition equation with appropriate [CoA].

transferases (60, 77, 84, 102, 137, 149). The finding that oxalate concentrations higher than 2.5 mM inhibit the activity of YfdW (Figure 3-14) is again in sharp contrast to the kinetic behaviour of FRC, which is not inhibited by oxalate at concentrations in excess of 230 mM (124). The evaluation of steady-state kinetic parameters for formyl-CoA in the YfdW- catalyzed reaction was, however, complicated by the presence of free CoA in this substrate as a result of the procedures used to remove a 2'-phosphorylated isomer of this compound, which exhibited a slightly longer retention time than formyl-CoA on reverse-phase HPLC (RP-HPLC) (Figure. 2-18). Contamination of the commercially available CoA used in the synthesis of formyl-CoA

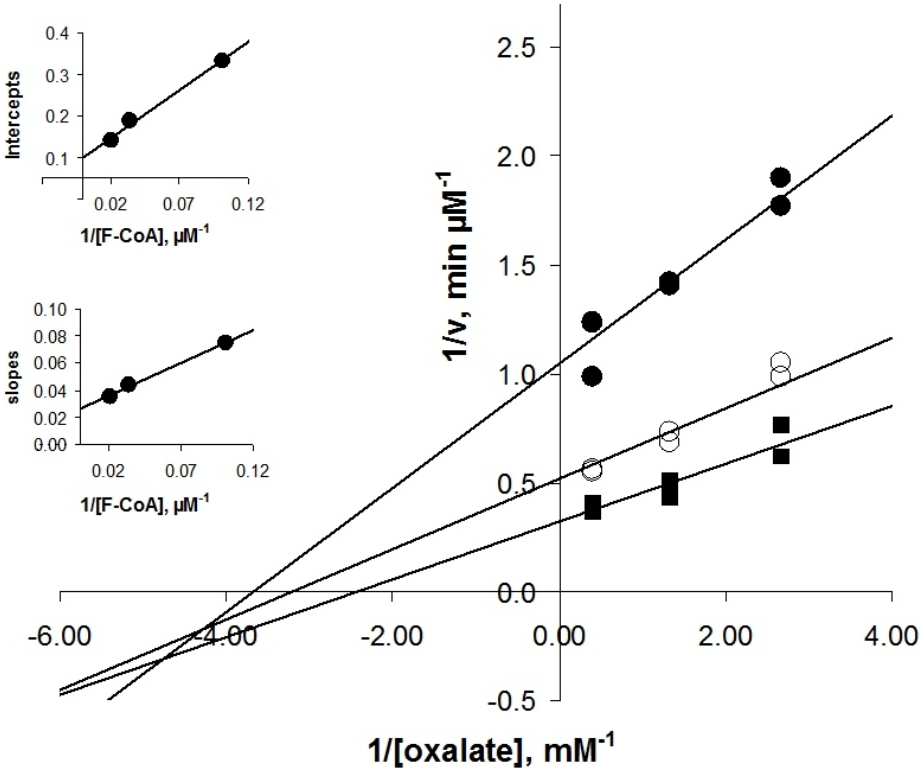

Figure. 3-6. Double reciprocal plot of initial velocities of YfdW with varied [oxalate] (0.125 – 2.5 mM) at 9.9 (●), 29.6 (○), and 49.3 µM (■) [formyl-CoA].

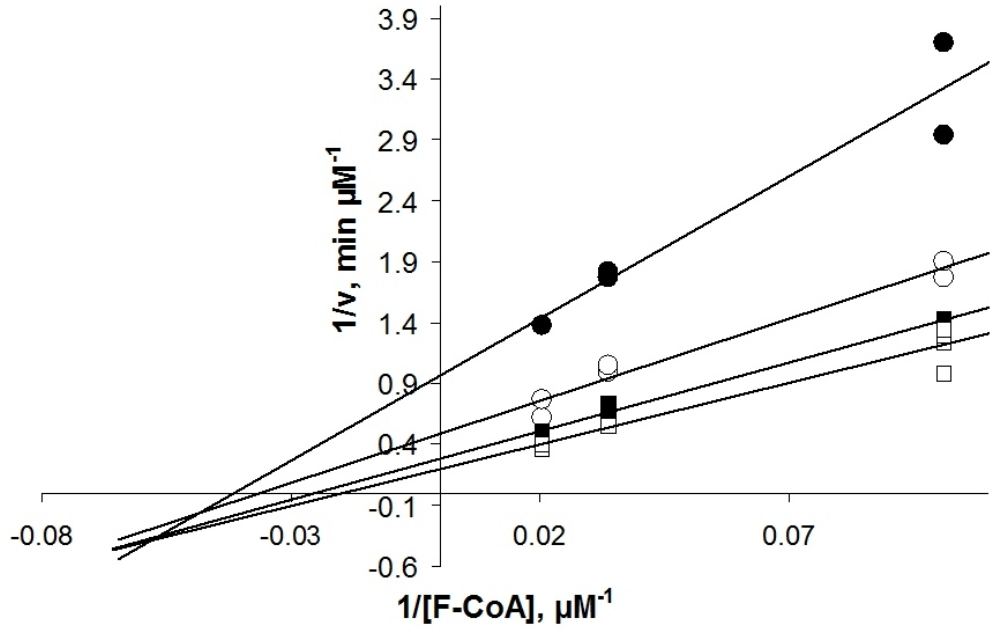

Figure. 3-7. Double reciprocal plot of initial velocities of YfdW with varied [F-CoA] (9.9 – 49.3 µM) at 0.125 (●), 0.375 (○), 0.750 (■), and 2.50 mM (□) [oxalate].

(124) has been reported previously in studies of enzymes for which malonyl-CoA (170) and β-hydroxybutyryl-CoA (36) are substrates. The extent to which free CoA inhibited YfdW activity was assessed using standard kinetic methods, and inspection of the double-reciprocal plot showed a mixed-type inhibition against formyl-CoA (Figure. 3-5). After fitting to the appropriate kinetic equation, values of K_{ic} and K_{iu} values of 220 ± 21 µM and 210 ± 16 µM, respectively, were obtained for inhibition by free CoA, which then permitted the apparent K_M of formyl-CoA to be estimated as 352 ± 4 µM. The turnover number, k_{cat}, under these conditions could then be determined as 130 ± 17 s^{-1}, which is considerably greater than that of FRC for which the cognate value is 5.3 ± 0.1 (Table 3-3). Given the presence of a poly-histidine tag at the N-terminus of YfdW, a similarly tagged variant of FRC was prepared and its steady-state kinetic parameters measured using the HPLC-based end-point assay (Figure 3-8). These experiments showed that

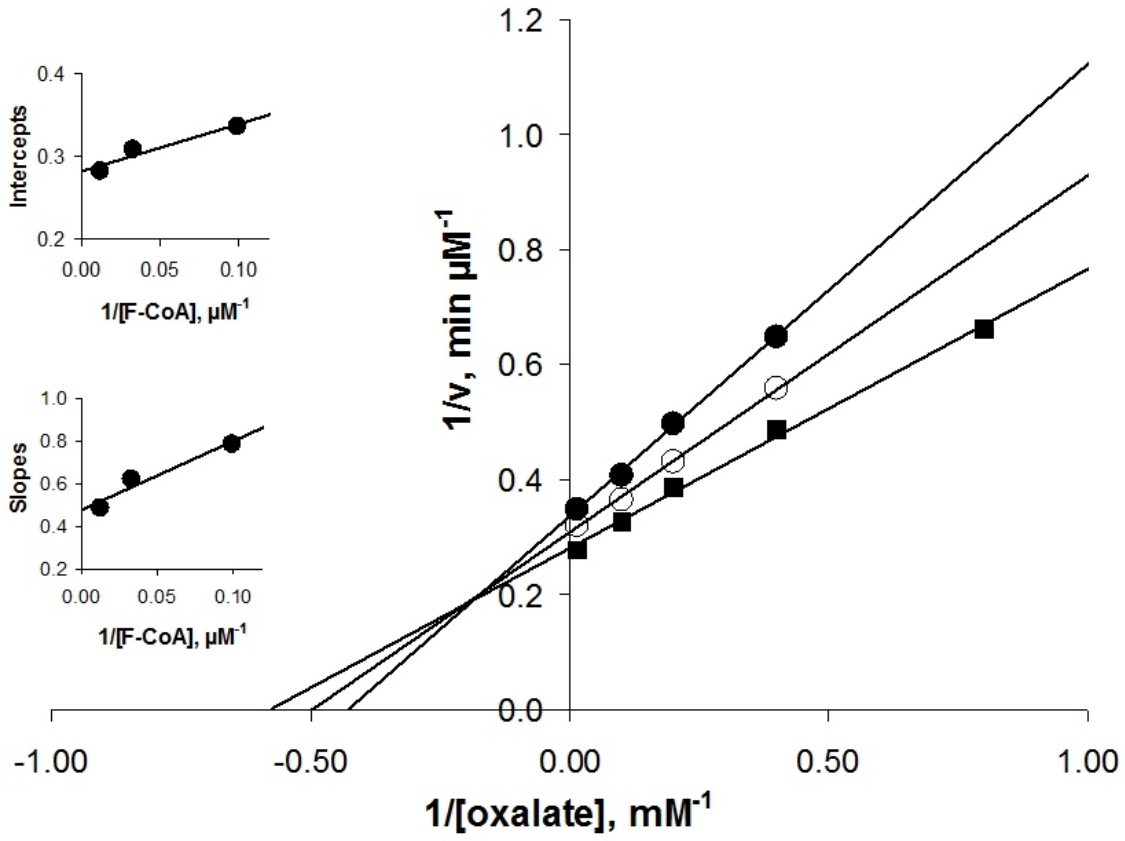

Figure. 3-8: Double reciprocal plot of initial velocities of HisFRC with varied [oxalate] (2.5 – 75 mM) at 10.1 (●), 30.3 (○), and 80.8 μM (■) [formyl-CoA].

the observed difference in k_{cat} values for YfdW and FRC (3-3) cannot be attributed to this structural modification.

The crystallographic observation of a YfdW/acetyl-CoA/oxalate ternary complex (97) suggested that YfdW might be inhibited by acetyl-CoA, and therefore the steady state kinetic behavior of the enzyme in the presence of this compound was assayed (Figure 3-9). As in earlier experiments, the concentration of free CoA was maintained at a fixed value (52 μM) as formyl-CoA was varied. Given that acetyl-CoA binds to the CoA site in the YfdW crystal structure (97), it was assumed that acetyl-CoA and CoA were mutually exclusive inhibitors at a given active site. This permitted the separation of their contributions to the overall rate equation (78), and acetyl-CoA proved to be an uncompetitive inhibitor of formyl-CoA, with a K_{iu} value of

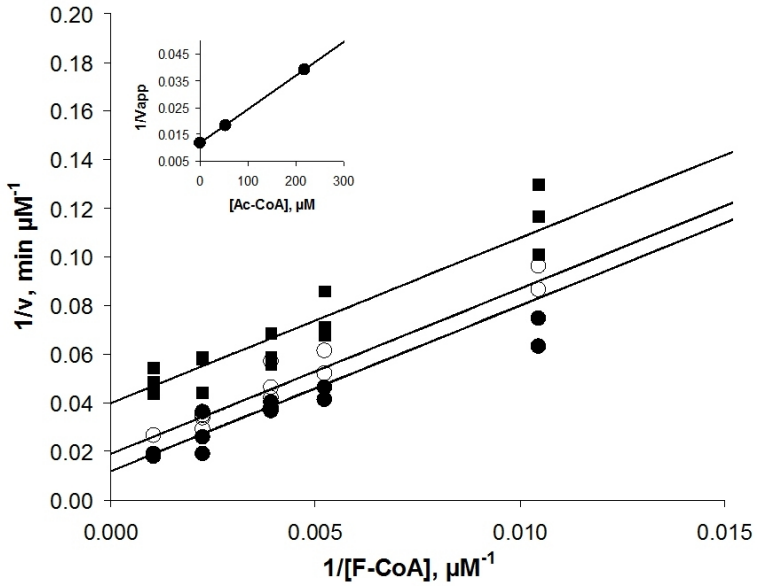

Figure. 3-9. Double-reciprocal plot for the inhibition of YfdW by acetyl-CoA against varied [formyl-CoA] at constant saturating [oxalate] = 2.5 mM and constant [CoA] = 51.6 µM. Ac-CoA concentrations were 0 µM (●), 53.81 µM (○), 217.8 µM (■). K_{iu}, 94 ± 2 µM, was determined from the replot of 1/ V_{app} vs. [CoA] (*insert*). There was no effect on K_{Mapp}/V_{app} within experimental error. Lines were modeled with the Michaelis-Menten equation modified for uncompetitive inhibition.

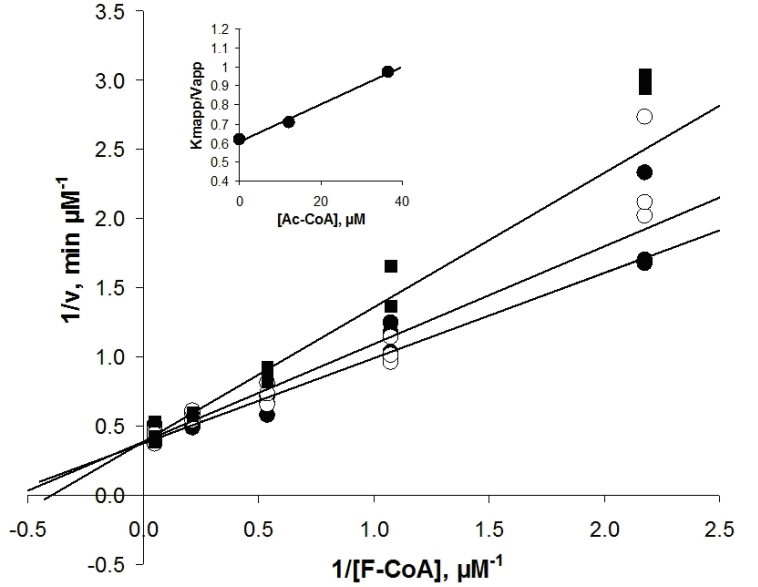

Figure. 3-10. Double-reciprocal plot for the inhibition of FRC by acetyl-CoA against varied [formyl-CoA] at constant saturating [oxalate] = 77 mM and constant [CoA] = 1.5 µM with lines fitted to the data by linear-regression methods. Acetyl-CoA concentrations were 0 µM (●), 12.1 µM (○), and 36.4 µM (■). $K_{i(Ac\text{-}CoA)}$ of 56 ± 6 µM was determined from the replot of K_{mapp}/V_{app} vs. [acetyl-CoA] (*insert*).

94 ± 2 μM. In contrast, acetyl-CoA is a competitive inhibitor of FRC with respect to formyl-CoA, exhibiting a K_{ic} value of 56 ± 6 μM at a fixed CoA concentration of 1.5 μM (Figure 3-10).

Size-Exclusion Chromatography Measurements.

Size exclusion chromatography of YfdW resulted in a MW value of 85.5 kDa (Figure 3-11). Thetheoretical mass of the dimer is 96.6 kDa (monomer 48.3 kDa), suggesting that the active conformation is dimeric, similar to that of FRC and consistent with crystal structure data. The slightly low MW may be a result of a tight overall quaternary structure and is also similar to the results seen for FRC (124).

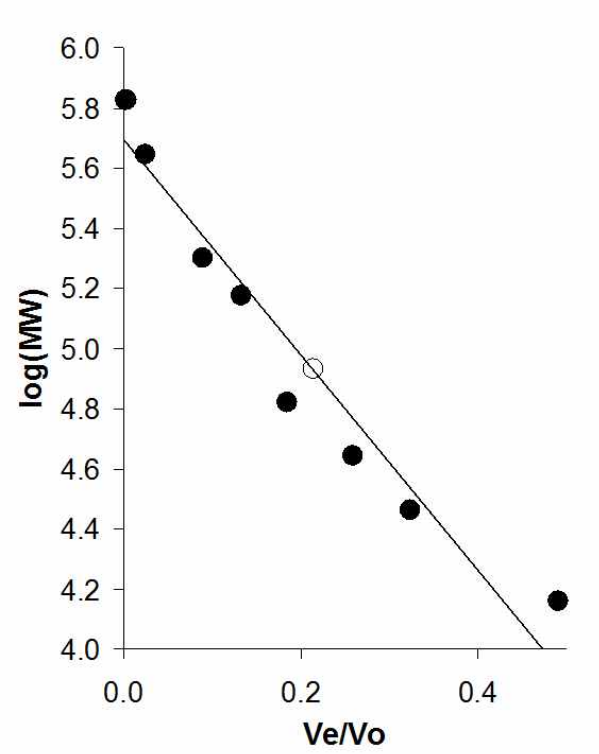

Figure. 3-11. Size-exclusion chromatography data used to estimate the molecular mass of catalytically active YfdW. Retention coefficients (K_D) for the molecular weight standards, used to calibrate the column, are shown by filled circles (●) and the open circle (○) represents the experimentally determined K_D of recombinant YfdW.

Alternate Substrate Studies

A variety of CoA donors and acceptors were incubated with the recombinant, tagged YfdW to elucidate the substrate specificity of the enzyme (Tables 3-1 and 3-2). YfdW showed high levels of substrate specificity, being unable to catalyze CoA transfer from formyl-CoA to acetate, maleate or glutarate. Given that malonyl-CoA and succinyl-CoA are known metabolic intermediates in *Escherichia coli*, however, whether either of these diacids could function as substrates was tested. In the case of malonate, YfdW exhibited very low specific activity (0.01%)

Table 3-1. FRC and YfdW substrate specificity for alternate CoA acceptors. All activities are reported based on the rate of CoA transfer from formyl-CoA to oxalate for each enzyme (n.d. – not determined).

	Formyl-CoA		Oxalyl-CoA	
	FRC	YfdW	FRC	YfdW
Formate	--	--	13	48
Acetate	0	0	0	0
Oxalate	100	100	--	--
Succinate	909	4	n.d.	n.d.
Glutarate	273	0	n.d.	n.d.
Maleate	36	0.2	n.d.	n.d.

Table 3-2. FRC and YfdW substrate specificity for alternate CoA donors with either formate or oxalate as the acceptor. All activities are reported based on the rate of CoA transfer from formyl-CoA to oxalate for each enzyme.

	Formate		Oxalate	
	FRC	YfdW	FRC	YfdW
Formyl-CoA	--	--	100	100
Acetyl-CoA	0	0	0	0
Oxalyl-CoA	13	48	0	0
Succinyl-CoA	727	32	82	0.2
Malonyl-CoA	0	0	0	0
Methylmalonyl-CoA	0	0	0	0
Propionyl-CoA	0	0	0	0

using formyl-CoA as the donor. Control experiments were also performed to ensure that any malonyl-CoA formed did not undergo extensive uncatalyzed decarboxylation under the conditions. Acetyl-CoA formation was also below the detection limits of the HPLC-based assay

when the enzyme was incubated with formyl-CoA and malonate. In contrast, when succinate was used as an acceptor, succinyl-CoA was formed, albeit with a low specific activity (4%) relative to that observed for oxalate with formyl-CoA. A complete determination of the steady-state kinetic parameters for YfdW-catalyzed conversion of succinate to succinyl-CoA was therefore performed to evaluate the substrate specificity of the enzyme (Figure 3-12). These studies gave 80 ± 40 mM for the apparent K_M of succinate, and a turnover number of only 5.3 ± 0.4 s^{-1} when formyl-CoA was employed as a donor. In contrast to observations on YfdW, succinate was an excellent substrate for FRC, the specificity constant being two orders of magnitude greater for

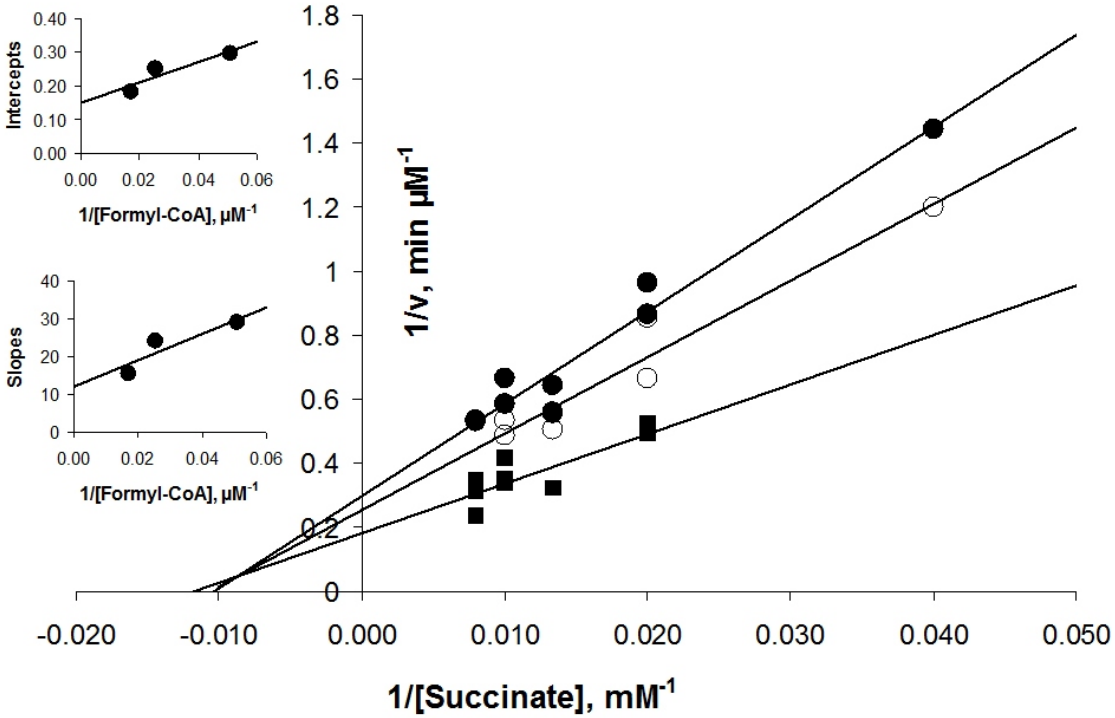

Figure. 3-12. Double reciprocal plot of initial velocities of YfdW with varied [succinate] (50 – 125 mM) at 19.7 (●), 39.8 (○), and 59.3 µM (■) [formyl-CoA]. $K_{M(succinate)}$ = 80 ± 40 mM and K_{ia} = 30 ± 19 µM.

this substrate when compared with that of oxalate using formyl-CoA as a donor (Table 3-4). In a similar manner, it was observed that FRC could employ succinyl-CoA as an alternate CoA donor for the synthesis of formyl- and oxalyl-CoA (Table 3-6). The pattern of the lines in the double

reciprocal plot approached The specific activity of FRC with malonate and formyl-CoA FRC as substrates was also substantially lower (0.1%) than that observed when oxalate was present as the CoA acceptor. No products were detected in the HPLC-based assay when malonyl-CoA was used as a substrate with either formate or oxalate.

Kinetic and Structural Characterization of the W48F and W48Q FRC Variants

The extent to which active site residues must be modified in order to change the substrate specificity of enzymes remains an interesting problem in enzyme evolution (90, 180, 241), and

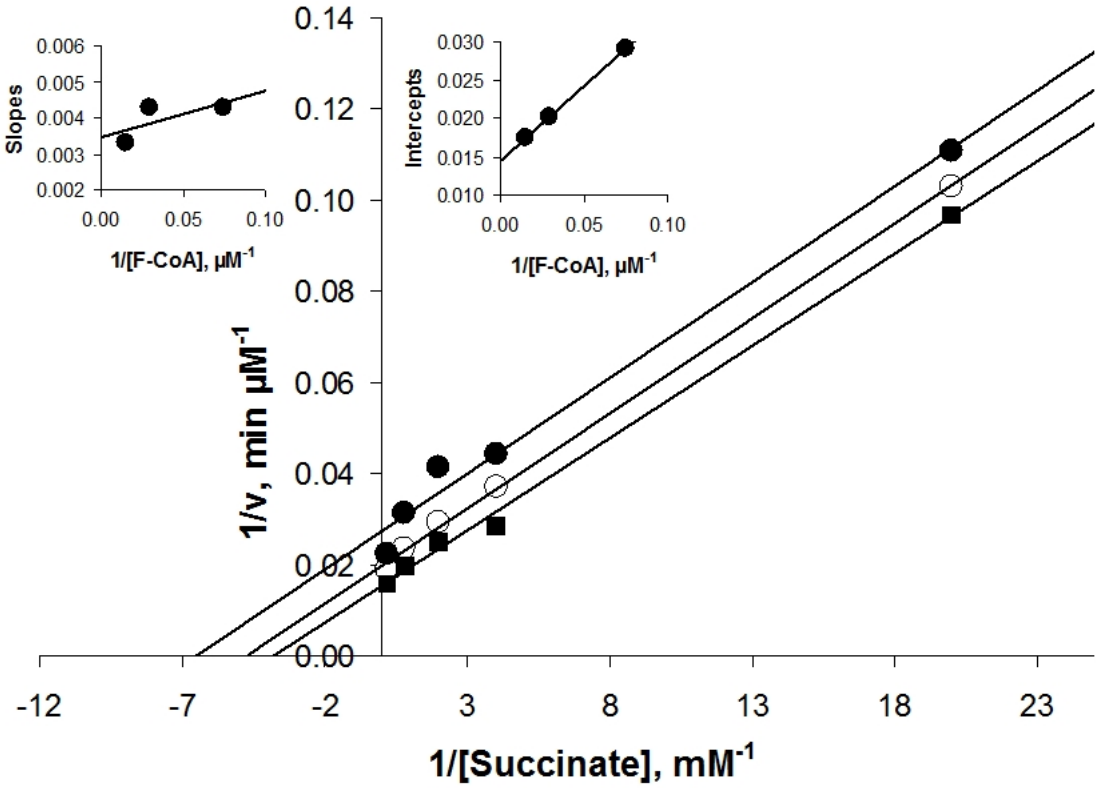

Figure. 3-13. Double reciprocal plot of initial velocities of FRC with varied [succinate] (0.05 – 5.0 mM) at 13.6 (●), 31.4 (○), and 67.2 µM (■) [formyl-CoA]. $K_{M(succinate)}$ = 0.32 ± 0.03 mM and K_{ia} = 0.5 ± 0.4 µM.

its resolution has important implications for efforts to redesign biological catalysts for biotechnological applications (42, 133). The active sites of FRC and YfdW, however, are composed of conserved residues, making it difficult to understand the observed differences in (i)

substrate specificity, and (ii) the ability of oxalate to exhibit substrate inhibition only in the case of YfdW. Structural studies on FRC had, however, revealed the importance of a tetraglycine segment in stabilizing a putative reaction intermediate (124), and conformational changes in this FRC and the Trp-48 FRC mutants. loop appeared correlated with the orientation of the Trp-48 side chain in FRC (197). Super-imposition of the crystal structures for the two CoA transferases

Table 3-3. Steady-state parameters for the formyl-CoA/oxalate transferase activities of YfdW,

Enzyme	Formyl-CoA			Oxalate	
	k_{cat} (s^{-1})	$K_{M(app)}$ (μM)	$k_{cat}/K_{M(app)}$ ($mM^{-1}s^{-1}$)	$K_{M(app)}$ (mM)	$k_{cat}/K_{M(app)}$ ($mM^{-1}s^{-1}$)
His-YfdW	130 ± 17	352 ± 4	370	0.51 ± 0.03	255
WT FRC	5.3 ± 0.1	2.0 ± 0.3	2650	3.9 ± 0.3	1.36
His-FRC	5.5 ± 0.4	4.7 ± 1.6	1200	1.2 ± 0.3	4.58
W48F FRC	17.1 ± 0.2	0.7 ± 0.4	24430	1.5 ± 0.3	11.4
W48Q FRC	5.8 ± 0.3	2.7 ± 0.9	2148	0.43 ± 0.03	13.5

Table 3-4. Summary of the inhibition constants and patterns for His-YfdW, FRC, His-FRC, and and variants.

(μM)	FRC	His-FRC	His-YfdW	W48F	W48Q
CoASH	competitive	competitive	mixed-type	mixed-type	competitive
K_{ic}	16.7 ± 0.7	9 ± 7	218 ± 21	11 ± 5	55 ± 19
K_{iu}	--	--	213 ± 16	35 ± 6	290 ± 5

Table 3-5. Steady-state parameters for the formyl-CoA/succinate transferase activities of YfdW, FRC and the Trp-48 FRC mutants.

Enzyme	Formyl-CoA			Succinate	
	k_{cat} (s^{-1})	$K_{M(app)}$ (μM)	$k_{cat}/K_{M(app)}$ ($mM^{-1}s^{-1}$)	$K_{M(app)}$ (mM)	$k_{cat}/K_{M(app)}$ ($mM^{-1}s^{-1}$)
His-YfdW	5.3 ± 0.4	180 ± 14	29.4	80 ± 40	0.07
WT FRC	149 ± 13	16 ± 2	9312	0.32 ± 0.03	465
W48F FRC	42 ± 6	12 ± 6	3500	0.015 ± 0.005	2800
W48Q FRC	17.9 ± 0.5	6.7 ± 0.9	2672	0.07 ± 0.01	256

showed that this tryptophan residue was replaced by glutamine in YfdW (Figure 3-16). Moreover, for YfdW, an oxalate molecule was seen to bind to a "closed" conformation of this tetraglycine loop (corresponding to residues ^{246}GGGGQ^{250} in YfdW) although the observed glutamine side chain rotamer was the same as seen for Trp-48 in FRC when the cognate loop segment was in its "open" conformation (46). Thus, it was investigated whether site-specific mutagenesis of Trp-48 in FRC might yield variant enzymes exhibiting modified kinetic behavior

that was similar to that determined for YfdW. Two variants were prepared in which Trp-48 was replaced by phenylalanine (W48F) and glutamine (W48Q), and characterized under steady-state conditions. Relatively little change in the specificity constants (k_{cat}/K_M) of the two FRC variant enzymes for formyl-CoA and oxalate was evident when compared with the wild type enzyme (Table 3-3). Perhaps more importantly, the W48Q FRC variant exhibited substrate inhibition with oxalate as observed for YfdW having a K_i value of 74 mM (Figure 3-15). In contrast, the W48F FRC variant was not inhibited by oxalate at concentrations up to 154 mM, suggesting that hydrogen bonding to the Gln-48 side chain is an essential element for the interaction of this substrate with the site, as suggested by the YfdW/acetyl-CoA/oxalate crystal structure (97). So as to understand the structural effects of changing the tryptophan residue in more detail, the crystal structures of the two FRC variants were obtained. Neither the W48Q nor the W48F FRC variant displayed any major structural changes when compared to wild type FRC, with the rmsd of the C_α atoms being 0.2-0.3 $Å^2$ and 0.6-0.7 $Å^2$ relative to subunit A and subunit B of apo-FRC, respectively. In both variant enzymes, the tetraglycine loop (corresponding to residues ^{258}GGGGQ^{262} in FRC) was seen to adopt a "closed" conformation (197). In wild type FRC, a 90^o reorientation of the Trp-48 side chain seems to be important in controlling the tetraglycine loop conformation. This "flipping" of the indole moiety, however, is accompanied by repositioning of Met-44 when the loop adopts its "open" conformation. For YfdW, in which a glutamine residue (Gln-48) replaces tryptophan however, oxalate can bind to the tetraglycine loop in the closed conformation, even though Gln-48 adopts the rotamer conformation corresponding to that of Trp-48 in FRC when the cognate loop is "open". Comparison of the YfdW and W48Q FRC variant structures showed that Gln-48 in W48Q, in the absence of oxalate, does not take the side chain rotamer conformation seen for the cognate residue in YfdW, presumably because of the

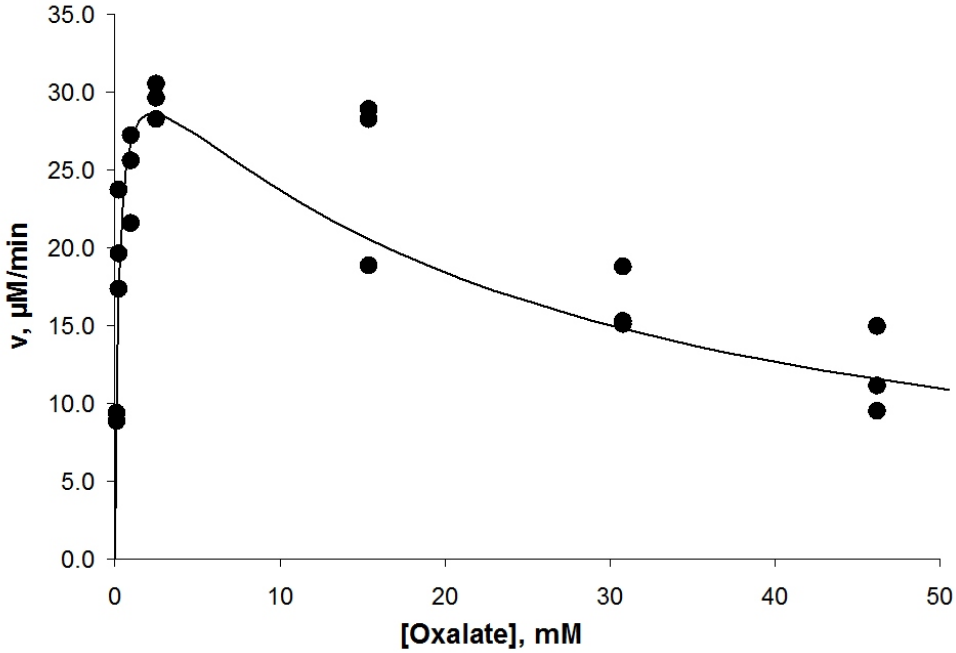

Figure. 3-14. Initial velocities measured for YfdW as function of oxalate concentration at 73.3 µM formyl-CoA. The line is computed from a fit to the Michaelis-Menten equation modified for substrate inhibition (Eqn. 2). The apparent K_i for oxalate inhibition is 23 mM. Taken from Toyota 2008 (245).

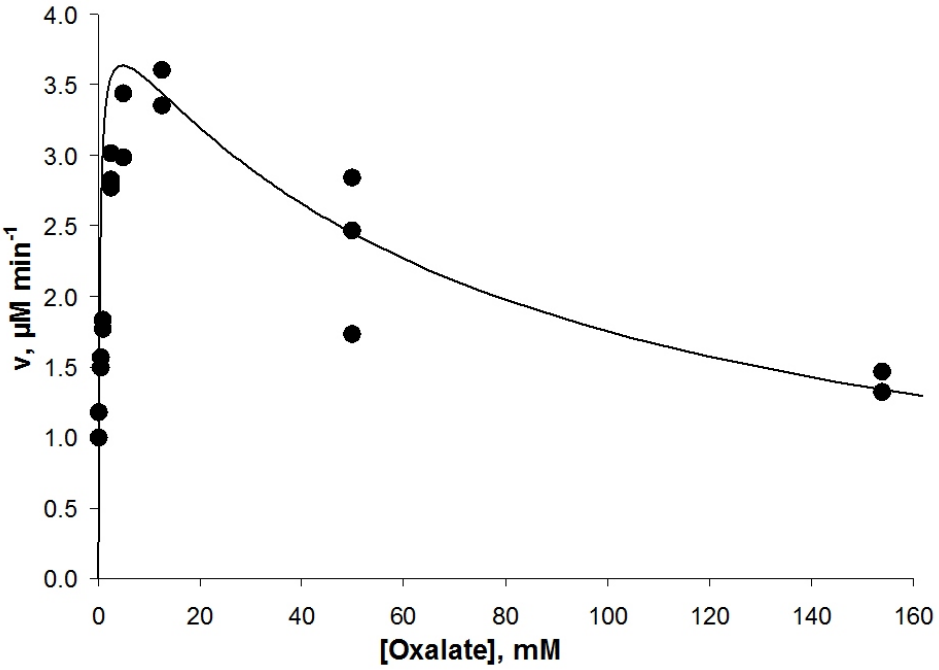

Figure. 3-15. Initial velocities measured for the W48Q FRC mutant as function of oxalate concentration at 70.3 µM formyl-CoA. The line is computed from a fit to the Michaelis-Menten equation modified for substrate inhibition (Eqn. 2). The apparent K_i for oxalate inhibition is 74 mM. Taken from Toyota 2008 (245).

Table 3-6. Data collection and refinement statistics for the W48F and W48Q FRC mutants.

Data Collection	W48Q FRC	W48F FRC
Beamline	ID14eh1 (ESRF)	ID23eh2 (ESRF)
Space Group	C2	I4
Unit cell (Å)	214.2, 98.9, 152.5	152.7, 152.7, 99.45
(°)	90, 135.3, 90	90, 90, 90
Molecules in asymmetric unit	4	2
Resolution (Å)	1.8 (1.9-1.8)[a]	1.95 (2.06-1.95)
R_{sym} (%)	6.3 (40.8)	13.0 (53.2)
Mean (I/σ(I))	12.4 (2.3)	8.8 (2.7)
Completeness (%)	92.0 (68.7)	(97.9) (99.5)
Wilson B-factor	22.6	17.8
Refinement	W48Q FRC	W48F FRC
Resolution range	30-1.8	30-1.95
R factor/ R_{free} (%)	18.2 / 21.1	16.7 / 20.0
Atoms modeled	14725	7608
Number of residues	1708	854
Number of waters	1309	936
Mean B-factor model ($Å^2$)	26.1	20.1
RMS deviation, bonds (Å)	0.008	0.009
RMS deviation, angles (°)	1.08	1.11
Ramachandran zone distribution (%)	92.0 / 7.5 / 0.5 / 0	91.7 / 7.9 / 0.1 / 0.3
PDB deposition ID	2vjq	2vjp

Values given in parentheses represent those of the highest resolution shell.

proximal methionine residue (Met-44) (Figure 3-18). For the W48Q FRC variant to bind oxalate in the site with the tetraglycine loop in a "closed" conformation, Gln-48 and Met-44 would both have to change rotamer conformation. In YfdW, the methionine position is occupied by a smaller valine residue.

Formyl-CoA Hydrolysis in the Presence and Absence of FRC, D169S, and YfdW

In contrast to FRC and the D169A variant of FRC, YfdW does not appear to mediate the hydrolysis of formyl-CoA when pseudo-first order rate constants for the hydrolysis of formyl-CoA were determined. The half-lives for formyl-CoA hydrolysis in the presence of FRC, D169A, and YfdW were 51, 58, and 198 minutes, respectively. Formyl-CoA hydrolysis has been reported with a half-life of 150 minutes at pH 6.7 and 30°C (124).

Table 3-7. Formyl-CoA hydrolysis in the presence of FRC, YfdW, and D169A variant of FRC.

Conditions	$t_{½}$, min
Formyl-CoA	153
Formyl-CoA + FRC (328 nM)	51
Formyl-CoA + YfdW (28 nM)	198
Formyl-CoA + D169A (254 nM)	58

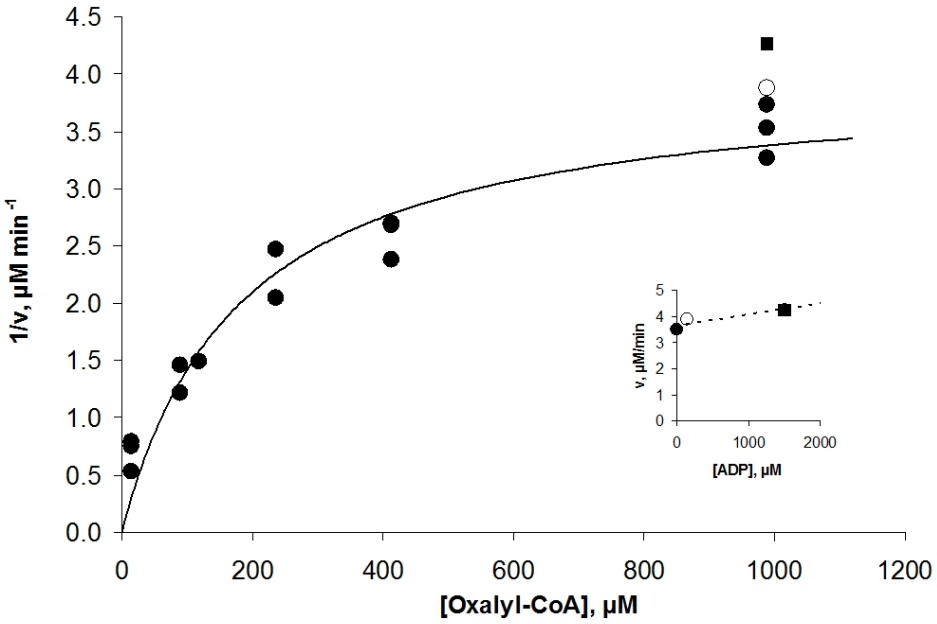

Figure. 3-16. Initial velocity plot of His-YfdU activity with varied oxalyl-CoA in the absence of added ADP (●) and in the presence of 150 µM (○) and 1500 µM ADP (■).

Expression, Purification, and Enzyme Activity of OXC Homologue HisYfdU

The *yfdU* gene in *E. coli* is the homologue of *oxc* in *Oxalobacter formigenes* and the theoretical partner of YfdW. In an attempt to understand the physiological role of the YfdW/YfdU enzyme pair in *E. coli*, a construct containing the *yfdU* gene product cloned from genomic DNA was generated. The protein was expressed, purified by nickel affinity chromatography, and assayed by HPLC. The His-tagged YfdU fusion has a K_M of 180 µM and k_{cat} of 15 s^{-1}, and a turnover number of 8.6 x 10^4 $M^{-1}s^{-1}$. The corresponding values for wild-type

OXC are 23 μM, 88 s^{-1}, and 3.8 x 10^6 $M^{-1}s^{-1}$. Unlike the *Oxalobacter* enzyme, YfdU does not appear to be activated by ADP (see insert in Figure 3-16.)

Discussion

These experiments clearly demonstrate that YfdW is a formyl-CoA:oxalate CoA transferase, as anticipated on the basis of its sequence and structural similarity to *Oxalobacter formigenes* FRC (197). Although this may seem an obvious finding, recent studies have shown that assigning enzyme function on the basis of sequence similarity can often lead to mis-annotation in metabolic databases (203). Moreover, the location of the gene encoding a CoA transferase in an operon that confers resistance to acidic environments seems, at first sight, unexpected. A further interesting outcome of these biochemical studies concerns the high level of substrate specificity that is exhibited by YfdW. Thus, despite considerable efforts to identify other CoA acceptors and donors, only formyl-CoA and oxalate (and equivalently, oxalyl-CoA and formate) seem to be substrates for the enzyme. YfdW can therefore mediate oxalate catabolism in *Escherichia coli* without affecting cellular succinyl-CoA levels. This observation stands in sharp contrast to the kinetic behavior of the *Oxalobacter* enzyme, for which succinate is a better CoA acceptor than oxalate when formyl-CoA is employed as a donor (Table 3-5). In light of the importance of oxalate as an energy source in *Oxalobacter formigenes* (3), the ability of FRC to synthesize succinyl-CoA is unexpected because this enzyme-catalyzed reaction removes a molecule of formyl-CoA thereby breaking the catalytic cycle (Figure 3-1). On the other hand, this side activity of FRC may be one mechanism by which *Oxalobacter* can use oxalate in the biosynthesis of other carbon-containing compounds given that succinyl-CoA is a key component of lysine biosynthesis and other biosynthetic pathways (94, 95). The presence of succinate in the cytoplasm of *Oxalobacter* is suggested by studies that have shown the presence of succinate

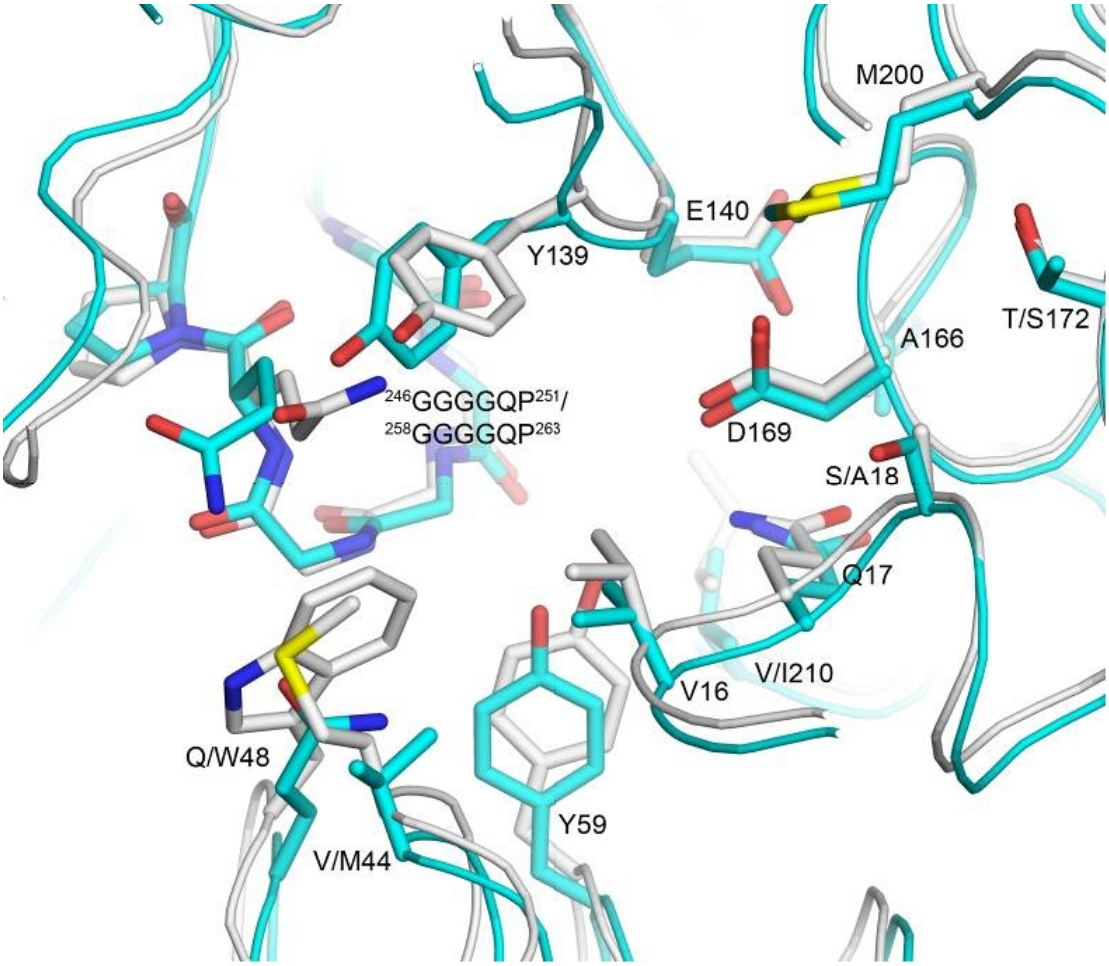

Figure. 3-17. Comparison of the active-site residues in YfdW (*cyan*) and FRC (*white*). Conserved residues are indicated by a one-letter code for amino acids. For positions where amino acids differ, the first letter refers to the residue present in YfdW. Taken from Toyota 2008 (245).

dehydrogenase, fumarase, and malate dehydrogenase, which can be employed to interconvert oxaloacetate and succinate in the latter part of the citric acid cycle (51, 52).

YfdW is inhibited by a variety of components, including acetyl-CoA, free CoA, and oxalate. On the basis of previous work on *Oxalobacter formigenes* (124), it was anticipated that CoA derivatives would compete with formyl-CoA for the free enzyme. Acetyl-CoA and free CoA are uncompetitive and mixed-type inhibitors, however, with respect to both formyl-CoA and oxalate. Hence it seems that these compounds can both bind to YfdW/substrate complexes that are formed during catalytic turnover. The simplest explanation for such kinetic behavior is

that the two active sites in the YfdW dimer can "communicate" so that only a single active site can catalyze the reaction at a given time ("half-sites" reactivity) (141). As a result, if CoA-derivatives bind to a free CoA site in a YfdW/substrate complex (or catalytic intermediate), then the enzyme undergoes a conformational change that precludes the formation of critical intermediates (18, 124) or product release at the other site. A more interesting observation was that YfdW is inhibited by elevated levels of oxalate, a kinetic behavior that is not seen for the *Oxalobacter* formyl-CoA transferase. This inhibition was hypothesized to arise from oxalate binding at a second "non-productive" site defined (in part) by the Gln-48 side chain in YfdW. Such binding is precluded by the presence of a tryptophan residue in FRC, and replacement of Trp-48 by glutamine to give the W48Q FRC variant yields an enzyme for which oxalate inhibition is observed. Hence, it seems that replacing the indole side chain by that of glutamine "opens" a hole in the FRC active site into which oxalate can bind in a non-productive conformation. This mutation also results in altered conformational preferences of a tetraglycine loop that is known to be important for catalytic function (18, 123, 124, 197), implying that altered active site dynamical motions may play a role in modulating kinetic properties (24, 72). The high K_i determined for oxalate in YfdW inhibition seems to preclude any physiological importance for this behavior. With the identification of YfdW as a formyl-CoA:oxalate CoA transferase, questions are raised concerning the extent and importance of oxalate-related metabolism in *Escherichia coli*, especially because this work demonstrates that YfdU is a ThDP-dependent oxalyl-CoA decarboxylase. Although *Escherichia coli* has been implicated in the biomineralization processes leading to formation of calcium oxalate crystals (41), recent measurements suggest that *Escherichia coli* does not degrade oxalate in media containing this compound at 5 mM concentration (247). The experiments, however, did not systematically vary

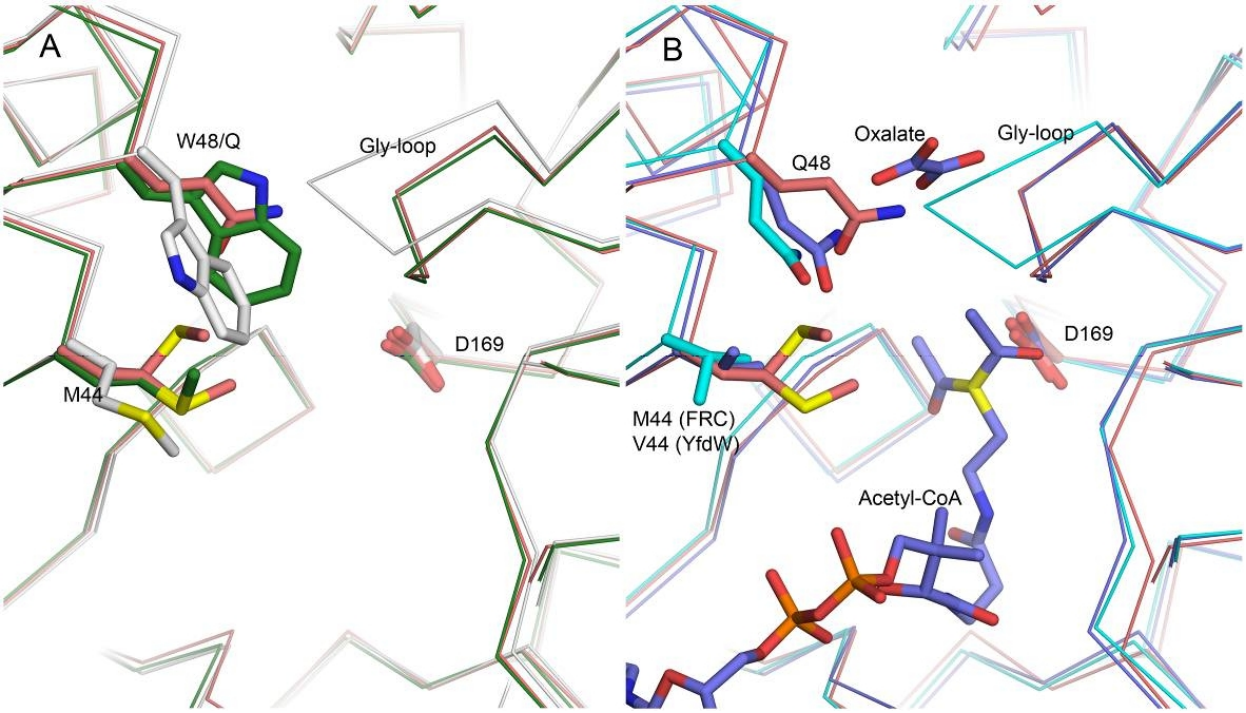

Figure. 3.18. Active-site structure in the W48Q FRC variant. *A*, superimposition of apo-FRC with the tetraglycine loop in its open (*white*) and closed (*green*) conformations and the W48Q FRC variant (*pink*). *B*, superimposition of apo-YfdW (*cyan*) with the open conformation of the tetraglycine loop, the YfdW–acetyl-CoA–oxalate ternary complex with the tetraglycine loop in its closed conformation (*blue*), and the W48Q FRC variant with the tetraglycine loop in its closed conformation (*pink*). In both panels, the catalytic residue, Asp-169, and side chains important in controlling the conformational properties of the tetraglycine loop are displayed as *stick models*. Met-44 in the W48Q FRC variant is modeled in two conformations, and the carbonyl group of acetyl-CoA also adopts two conformations in the structure of the YfdW–acetyl-CoA–oxalate ternary complex (97). Taken from Toyota 2008 (245).

the incubation conditions and so it is possible that conditions exist under which *Escherichia coli* can metabolize exogenous oxalate. On this point, it should be noted that the YhjX gene product has been annotated as a possible formate:oxalate antiporter based on 25% sequence identity to *Oxalobacter formigenes* OxlT, which has been extensively characterized (108, 255). In a recent transcriptomic profiling study, YhjX has been identified as a transporter upregulated by rapid cellular acidification (pH 5.5) in *Escherichia coli* (129). Work is therefore needed to establish if *Escherichia coli* can mediate oxalate degradation, especially when in low pH environments. It is therefore interesting that the coupled action of YfdW and YfdU results in the consumption of a

proton, as employed in the AR2 and AR3 mechanisms of acid resistance mediated by the PLP-dependent enzymes, glutamate decarboxylase and arginine decarboxylase (87). It appears that *Escherichia coli* has the required cellular machinery for either oxalate dependent AR and/or oxalate metabolism analogous to that in *Oxalobacter formigenes*. YfdU, in contrast to OXC, does not appear to be activated by ADP; thus, YfdU imay not be involved in metabolism. However the question of whether oxalate catabolism can take place in *Escherichia coli* upon up-regulation of the *yfdXWUVE* operon and YhjX expression under conditions of low pH remains.

Experimental Methods

Materials

Unless otherwise stated, all chemicals and reagents were purchased from Sigma-Aldrich (St. Louis, MO) or Fisher Scientific (Pittsburgh, PA), and were of the highest available purity. Recombinant, wild type FRC was expressed and purified following literature procedures (197). Protein concentrations were determined using a modified Bradford assay (Pierce, Rockford, IL) (27) for which standard curves were constructed with bovine serum albumin as previously reported (124)), or the Edelhoch method (89). PCR primers were obtained from Integrated DNA Technologies, Inc. (Coralville, IA), and DNA sequencing was performed by the DNA Sequencing Core of the Interdisciplinary Center for Biotechnology Research at the University of Florida. Formyl-CoA and oxalyl-CoA were prepared as described elsewhere (124).

Expression and Purification of His-Tagged YfdW

The subcloning and expression of the *yfdW* gene have been described in detail elsewhere (240, 251). Briefly, the *yfdW* gene was PCR amplified from the genomic DNA of *Escherichia coli* K12 and subcloned into the pDest17 vector using Gateway technology (Invitrogen, Carlsbad, CA). Protein production was carried out in the Tuner(DE3)pLysS strain of *Escherichia coli*, and the His-tagged YfdW protein purified by metal-affinity chromatography

and subsequent gel filtration on a Superdex 200 column eluting with 5 mM HEPES buffer containing 150 mM NaCl, pH 7.5.

Expression and Purification of His-Tagged FRC

The gene encoding *Oxalobacter formigenes* FRC (225) was cloned into the pET-28b vector (Novagen, San Diego, CA) so as to introduce a His-tag with 10-amino acid linker at the N-terminus of the recombinant protein. Primers used were as follows: 5'-*Nde1* 5'-AGG AGA TAT ACA TAT GAC TAA ACC ATT AGA TGG AAT TAA TGT GC and 3'-*BamH1*(stop) 5'-AAG TCT GGA TCC TCA AAC TAC CTG T . BL21(DE3) competent cells were transformed with the resulting construct and protein expression was induced by the addition of IPTG at an OD^{600} of 0.6. After harvesting and pelleting by centrifugation at 5000 *g* for 15 min, the cells were re-suspended in lysis buffer (50 mM potassium phosphate, pH 7.2, containing 300 mM NaCl, 10 mM imidazole and 1 mM β-mercaptoethanol) and sonicated. Cell debris was removed by centrifugation at 10,000 *g* for 15 min, and the supernatant was loaded on to an 0.5 mL Ni-NTA column (Novagen) equilibrated with lysis buffer at 4 ^{o}C. The column was washed with lysis buffer containing 50 mM imidazole, and His-FRC was eluted (5 x 0.5 mL) with elution buffer (50 mM potassium phosphate, pH 7.2, containing 300 mM NaCl and 250 mM imidazole). Size-exclusion chromatography on a Sephadex G-25 column (30 mL) equilibrated with storage buffer (25 mM sodium phosphate, pH 6.7, 300 mM NaCl, and 1 mM DTT) removed the imidazole, and the purified protein was stored at -80 ^{o}C in 10% glycerol.

Expression and Purification of FRC Variants

The expression and purification of wild-type FRC and the W48F and W48Q FRC variants lacking the N-terminal histidine fusion tag were performed by following procedures described in the literature (124, 197).

Size-Exclusion Chromatography Measurements.

A BIOSEP SEC-S2000 column (300 x 7.8 mm with 75 x 7.8-mm guard column) was calibrated using lysozyme (14.4 kDa), carbonic anhydrase (29.0 kDa), peroxidase (44.0 kDa), bovine serum albumin (66.0 kDa), alcohol dehydrogenase (150 kDa), amylase (200 kDa), apoferritin (443 kDa), and thyroglobulin (669 kDa) in 100 mM potassium phosphate buffer, pH 7, with 100 mM KCl at a flow rate of 1 mL/min. A 75 μL aliquot of 53.8 μg/μL YfdW in 100 mM potassium phosphate, pH 6.7 was injected to give a single peak with retention time corresponding to a molecular mass of 85 kDa. K_D is calculated as $(V_{elution} - V_{void})/(V_{column} - V_{void})$.

Confirmation of Quench Conditions

Kinetic assays of CoA transferase activity in FRC were quenched in 10% acetic acid (124). Conditions for stopping the transferase reaction with YfdW were examined. Reactions were run as below: 90 μL of reaction mixture were quenched in 10 μL of either 10% or 20% HAc, followed by incubation at either 0 ^{o}C or 32 ^{o}C. Aliquots were removed at times of up to 100 minutes and oxalyl-CoA concentration was ascertained by measurement of absorbance at A^{260} (*vida infra*).

Steady-State Kinetic Assays

All kinetic measurements were performed using an HPLC-based assay, as reported in previous studies on FRC (124, 197). For measurements of YfdW-catalyzed CoA transfer, assay mixtures consisted of YfdW (54 ng) and the carboxylic acid acceptor in 100 mM potassium phosphate, pH 6.7 (total volume 100 μL). The concentration of free CoA in all samples was normalized to that present as a contaminant in the assay mixtures containing the largest amount of formyl-CoA. After incubating this solution at 30 ^{o}C, reaction was initiated by the addition of formyl-CoA. An aliquot (90 μL) was taken after 60 seconds, and quenched by addition to 20%

aq. HAc (10 μL). The amount of the appropriate thioester product was then quantitated by injection of these samples onto a C_{18} analytical column (Dynamax Microsorb 60–8 C_{18}, 250 x 4.6 mm reverse-phase analytical column equilibrated with 86% Buffer A (25 mM NaOAc, pH 4.5) and 14% Buffer B (Buffer A containing 20% CH_3CN)) at a flow rate of 1 mL/min. Immediately after injection the proportion of Buffer B was increased to 6% over 210 s, then to 100% for 90 s before the wash using 98% Buffer A and 2% Buffer B. CoA-containing species were observed by monitoring absorbance at 260 nm, and their concentrations were determined by integrating the peak areas and comparison with those for known amounts of authentic material. These measurements were calibrated using independent determinations of formyl-CoA concentration using (i) a hydroxylamine-based colorimetric assay (227) and (ii) the oxalate concentration in hydrolyzed and nonhydrolyzed samples of oxalyl-CoA as measured with a standard detection kit (Sigma). No formation of CoA ester products was observed in control experiments when the enzyme or either substrate was omitted from the mixture.

In kinetic assays of FRC, His-tagged FRC and the two FRC variant enzymes, a similar HPLC-based procedure was followed except that assays contained either FRC (41 ng), His-tagged FRC (46 ng), W48F (41 ng) or W48Q (43 ng). Reactions were quenched in 10% aq. HAc (10 μL) and aliquots were eluted initially with 96% Buffer A (25 mM NaOAc, pH 4.5) and 4% Buffer B (Buffer A containing 40% CH_3CN) at a flow rate of 1 mL/min. The amount of buffer B was then increased to 11% over 210 s and then to 100% Buffer B for 90 s, after which it was returned to 4%.

Determination of Steady-State Kinetic Constants

Kinetic constants were obtained by curve-fitting to the following equations for sequential bi-bi kinetics (Eqn. 1), substrate inhibition (Eqn. 2), competitive inhibition (Eqn. 3) and mixed-type inhibition (Eqn. 4) (47)):

$$\nu = \frac{V_{\max}[B]}{K_{MB}\left(1+\frac{K_{ia}}{[A]}\right)+[B]\left(1+\frac{K_{MA}}{[A]}\right)} \qquad \text{(Eqn. 1)}$$

$$\nu = \frac{V_{\max}[S]}{K_M+[S]+\left(\frac{[S]^2}{K_{iS}}\right)} \qquad \text{(Eqn. 2)}$$

$$\nu = \frac{V_{\max}[S]}{K_M\left(\frac{[I]}{K_{ic}}\right)+[S]} \qquad \text{(Eqn. 3)}$$

$$\nu = \frac{V_{\max}[S]}{K_M\left(1+\frac{[I]}{K_{ic}}\right)+[S]\left(\frac{[I]}{K_{iu}}\right)} \qquad \text{(Eqn. 4)}$$

In these equations, K_{ia}, K_{MA} and K_{MB} represent the dissociation of the first substrate to bind to the enzyme (formyl-CoA) and the K_M values for formyl-CoA and oxalate, respectively, K_{iS} is the substrate inhibition constant of oxalate against varied formyl-CoA concentration, and K_{ic} and K_{iu} are the inhibition constants for competitive and uncompetitive mechanisms, respectively. Patterns of intersecting lines in double-reciprocal plots (supporting information) were used to ascertain the mode of inhibition, and hence the correct equations for use in evaluating the inhibition constants (47, 216) K_{ic} and K_{iu}, and the formyl-CoA K_M were determined by fitting initial velocity plots of CoA inhibition directly with the Michaelis-Menten equation for mixed-type (Eqn. 3) or competitive inhibition (Eqn. 4). K_M values for oxalate and succinate and K_{ia} could then be determined by fitting initial velocity plots using an ordered bi-bi equation when the second substrate (oxalate or succinate) was varied (Eqn. 1). In the case of YfdW, attaining saturating formyl-CoA concentrations proved to be impractical. In this case, apparent K_M and V_{max} values for either oxalate or succinate were obtained by fitting to the initial velocity plots at

fixed, varied formyl-CoA concentrations and various concentrations of the appropriate acid acceptor. Linear fits to the replots of $(K_M/V_{max})_{app}$ and $(1/V_{max})_{app}$ against [formyl-CoA] were then used to estimate K_M and K_{ia} (216). All curve fitting was performed with KaleidaGraph 3.5 (Synergy Software, Reading, PA).

Determination of the Specific Activity of FRC and YfdW with Alternate Substrates

The specific activities of FRC with alternate substrates were determined by incubating 8.8 nM enzyme (83 ng FRC in 200 µL) in 60 mM potassium phosphate, pH 6.7, 125 mM in the CoA acceptor, and 80 µM in the CoA donor at 30º C. In the case of YfdW, 11.2 nM (108 ng YfdW in 200 µL) was used with 75 mM acceptor and 350 µM CoA donor. Specific activities for YfdW with succinate or oxalate were determined from initial velocity experiments. Substrates were regarded as having no activity when no products were detected in reactions that were run for 60 min.

Crystallization and Structure Determination of the W48F and W48Q FRC Variants

Crystallization and analysis of FRC variants was carried out by Dr. Catrine L. Berthold at the Karolinska Institutet, Stockholm, Sweden. Crystallization of the FRC mutants was performed by the vapor diffusion method in 24-well plates where hanging drops of 2 µL protein solution and 2 µL well solution were set up to equilibrate against 1 mL well solution at 293 K. A protein solution containing 7.5 mg/mL of the desired mutant in 50 mM MES buffer, pH 6.2 with additional 10% glycerol was used when screening for optimal conditions for crystallization. The W48Q variant of FRC was crystallized against a well solution of 1.35 M sodium citrate and 0.1 M HEPES buffer, pH 7.2-7.4, resulting in crystals of the tetragonal space group I4. These crystals were protected in a cryosolution of three parts well solution mixed with one part 100% ethylene glycol before being flash-frozen in liquid nitrogen. For the W48F FRC mutant a well

solution of 1.9 M malic acid, pH 7.0, gave crystals belonging to the monoclinic space group C2. The crystallization drops containing the W48F mutant were covered in silicon oil, through which the crystals were dragged before being flash-frozen. X-ray data were collected in a nitrogen stream at the beamlines ID14 eh1 and ID23 eh2 at the European Synchrotron Research Facility, Grenoble. All crystallographic data were processed with MOSFLM (147) followed by SCALA of the CCP4 program suit (11). The structure of the apoenzyme (pdb code: 1p5h) (197) was used to retrieve the phases by molecular replacement using the program MOLREP (248). Refinement was carried out with REFMAC (174) and manual model building was performed in COOT (76) where water molecules were assigned and the structures were validated. The stereochemistry of the structures was checked with PROCHECK (144).

Formyl-CoA Hydrolysis in the Presence and Absence of FRC, D169S, and YfdW

Pseudo-first order rate constants for the hydrolysis of formyl-CoA at pH 6.7 and 30°C were determined by standard fitting procedures. Half-lives for hydrolysis in the presence of FRC, D169A, and YfdW were 51, 58, and 198 minutes, respectively. Formyl-CoA hydrolysis has been reported with a half-life of 150 minutes at pH 6.7 and 30°C (124).

Cloning, Expression, and Purification of HisYfdU and HisYfdW

The *E. coli* genes *yfdW* and *yfdU* were cloned from genomic DNA isolated from BL21(DE3) by nested PCR. DNA was purified by phenol-chloroform extraction (208). The first PCR primers were 5'- CGC CTG GCC GGT GTT GGC GTA ATG G and 3'-5'- CCC TGT TTG CCC GAG TAA TAG ATA CAA ATA GAG CCG C. Nested primers were designed to include upstream *Nde1* and downstream *HindIII* restriction endonuclease sites: HisYfdW 5'- A GGT ATT CAT ATG TCA ACT CCA CTT CAA GGA ATT AAA GTT CTC GAT TTC, His YfdW 3'-5'- GGG AGC AAG CTT CCC CCG TTA ATA TCA GAT GGC G, HisYfdU 5'- CGA GGT TAT TAC ATA TGT CAG ATC AAC TTC AAA TGA CAG ATG G , and HisYfdU

3'-5'-CTC ACC ATC GCA TAA TGA GTT AAG CTT AGG AGA CGA TGT CAG. The second PCR products were digested with *Nde1* and *HindIII* and inserted into gel-purified pET-28b (Novagen) linearized with the same restriction enzymes. PCR primers were obtained from Integrated DNA Technologies, Inc. (Coralville, IA). Constructs were confirmed by DNA sequencing by the DNA Sequencing Core of the Interdisciplinary Center for Biotechnology Research at the University of Florida.

A single BL21(DE3) cell transformed with either the HisYfdU or HisYfdW construct was used to inoculate a culture of LB with 50 μg/mL kanamycin. The culture was allowed to grow all day at 37 ºC and shaken at 215 rpm. At 4 pm, 1 mL of the culture was used to inoculate 500 mL of ZYM 5052 autoinducing media (239). The culture, shaken overnight at 37 ºC and 215 rpm, was harvested by centrifugation at 5000 xg for 10 minutes (OD^{600} of ~6). The His-tagged protein was purified as described previously in this chapter.

Activity of HisYfdU

The activity of HisYfdU was assayed as previously described (15). Prior to analysis, HisYfdU was incubated with 60 μM ThDP on ice for at least 30 minutes. In a total volume of 100 μL, 3.4 nM HisYfdU was combined with 60 μM ThDP and 6 mM $MgCl_2$, in 60 mM potassium phosphate, pH 6.7. The reaction was started with the addition of the appropriate amount of oxalyl-CoA. The reaction was quenched with 30% HAc and the formyl-CoA produced was measured by single point HPLC assay.

CHAPTER 4
OXALYL-COA DECARBOXYLASE[3]

Introduction

Oxalyl-coenzyme A (CoA) decarboxylase (OXC) is one of two enzymes in the oxalate degradation pathway in the gastrointestinal bacterium *Oxalobacter formigenes* (10). OXC is a typical thiamine diphosphate (ThDP)-dependent nonoxidative decarboxylase, converting oxalyl-CoA to formyl-CoA and CO_2. In the catalytic cycle (Figure 4-1) that is almost certainly common to all ThDP-dependent enzymes in this family (67), turnover is initiated by activation of ThDP through deprotonation of C2 in the thiazolium ring to give the ylide [1]. This is facilitated by a conserved glutamate, which donates a hydrogen bond to N1' of ThDP and stabilizes the 1',4'-imino-pyrimidine tautomer enabling the 4'-NH to abstract a proton from C2 (134, 151). Nucleophilic attack by the cofactor ylide on the α-carbonyl of the substrate [2] and protonation of the oxygen atom of the carbonyl then gives rise to a covalent substrate-ThDP adduct [3]. The positively charged thiazolium ring then facilitates decarboxylation to form an α-carbanion/enamine [4] complex that is protonated at the α-carbon [5] before C-C bond cleavage takes place to yield the product [6] and the ylide, completing the catalytic cycle. Previously, it was reported that the first crystal structure of the OXC holoenzyme, a homotetramer with each of the 60 kDa subunits contained one tightly bound ThDP, Mg^{2+}, and ADP (15). The presence of ADP is required for maximal decarboxylase activity, presumably because it stabilizes the functional conformation of the enzyme. On the basis of this structure, a catalytic mechanism for the formation of formyl-CoA was proposed. In addition, it was speculated that the 4'-amino group of the pyrimidine ring of ThDP might be involved in stabilizing the developing negative

[3] Reproduced in part with permission from Structure, Vol.15, Berthold, C. L., Toyota, C. G., Moussatche, P., Wood, M., Leeper, F., Richards, N. G., and Lindqvist, Y. Pages 853-861. Copyright 2007 Cell Press.

charge on the oxygen bound to the α-carbon atom as the substrate reacts with the ylide intermediate and that a water molecule, anchored by hydrogen bonds to the side chains of Tyr-120, Glu-121, and the main chain carbonyl oxygen atom of Ile-34, protonates the α-carbanion/enamine intermediate formed after decarboxylation. Here, the structures of OXC in complex with its substrate oxalyl-CoA [2], with its product formyl-CoA [6], and with a trapped covalent reaction intermediate [5] are presented (numbering from Figure 4-1). In the substrate complex [2], a ThDP analogue, 3-deazathiamine diphosphate (dzThDP), was used in place of ThDP to prevent turnover. In order to further substantiate these findings, two additional X-ray crystal structures are presented: a reference structure containing only dzThDP as well as a structure of active OXC in complex with CoA. Combining the structural data with kinetic data from several active-site variants has allowed profound insight into the catalytic mechanism of OXC.

Results

Structure of OXC with dzThDP

The thiamine-analogue dzThDP is an extremely efficient inhibitor of ThDP-dependent enzymes (145, 167). As a substrate analogue, dzThDP is almost identical to ThDP, but with the nitrogen atom of the thiazolium ring exchanged for a carbon atom; the lack of positive charge prevents formation of the activated ylide and no attack on the substrate can take place. The charge state of dzThDP, however, mimics the ylide with an overall neutral thiazolium ring and has been shown to bind more tightly than ThDP to several of the enzymes utilizing the cofactor (145). To be able to draw conclusions from the structure of a nonreactive substrate complex containing dzThDP, it was desirable to study structural changes that resulted from exchanging ThDP with dzThDP.

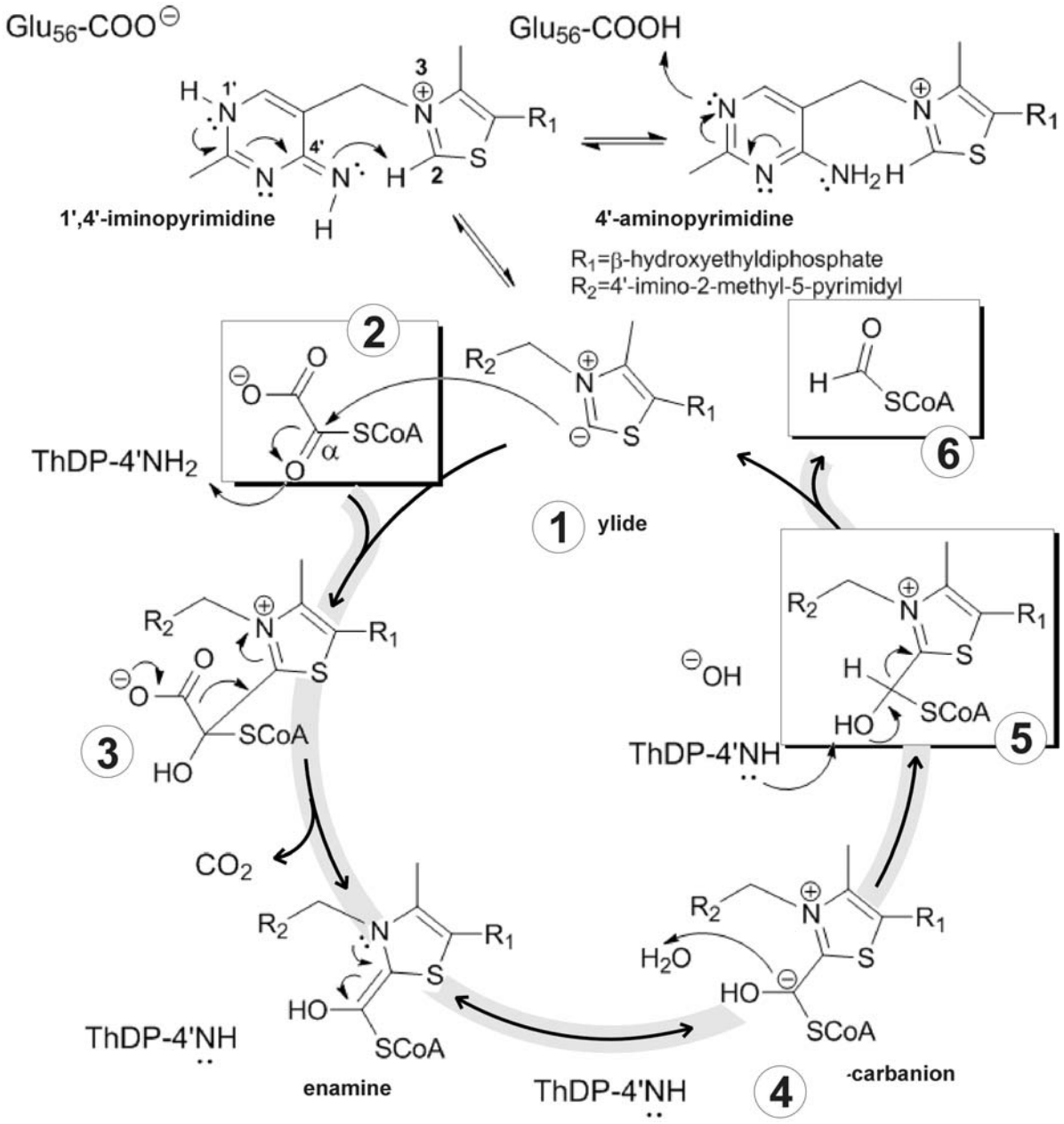

Figure. 4-1. Scheme of OXC mechanism for ThDP-dependent oxalyl-CoA decarboxylation. 1, ThDP-ylide; 2, oxalyl-CoA; 3, pre-decarboxylation intermediate; 4, α-carbanion/ enamine intermediate; 5, formyl-CoA-ThDP covalent complex; and 6, formyl-CoA. Crystal structures of OXC with oxalyl-CoA bound, OXC with formyl-CoA, and covalent intermediate are highlighted.

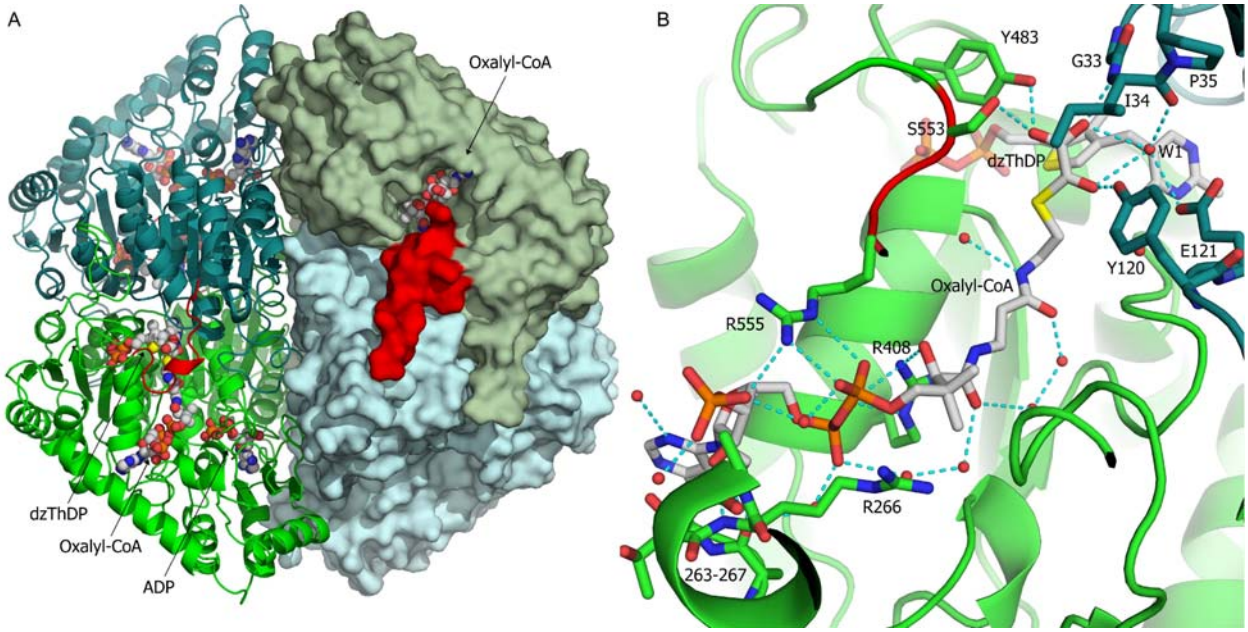

Figure. 4-2. OXC tetramer and active site. *A*, the OXC tetramer represented with one of the catalytic dimers in a surface mode. ADP, dzThDP, and oxalyl-CoA are represented as *balls-and-sticks*. The C-terminal region that undergoes organization upon substrate binding is shown in *red*. *B*, the substrate binding site with side chains interacting with oxalyl-CoA shown as *sticks*. The C-terminal residues after Arg-555 have been omitted for clarity. The main chain of two residues in the newly organized C-terminus is shown coloured in *red*. Taken from Berthold 2007 (17).

The structure of OXC with bound dzThDP, refined to 2.2 Å resolution (Table 4-1), is virtually identical to the holoenzyme structure solved previously (rmsd, 0.24 Å for 546 Cα atoms) (15).

Structure of the Oxalyl-CoA Complex and the CoA Complex

The substrate binding site in OXC was identified by crystallizing OXC inhibited with dzThDP and then soaking oxalyl-CoA into the crystals. The structure was refined to 2.0 Å resolution. The substrate is bound with the CoA carrier in the cleft between the regulatory (R)- and pyrophosphate (PP)-domain of one subunit, and, with a length of approximately 30 Å, it reaches all the way into the active site where the oxalyl group is well positioned for attack by the cofactor (Figure 4-2). No significant reorganization of the active site takes place upon substrate binding and superposition of the holostructure to the substrate complex results in an rmsd of 0.286 Å for 546 Cα atoms. The only significant structural changes upon substrate binding are

seen at the C-terminus of OXC. The C-terminal residues 553–565, which, in the structure of the holoenzyme, are flexible and without interpretable density (15), organize upon substrate binding and fold down over the active site (Figure 4-2A). Of the 1,070 $Å^2$ total accessible surface of the substrate, 920 $Å^2$ are buried upon binding to the enzyme; the C-terminal residues contribute approximately 200 $Å^2$. The side chain of Arg-555 forms intimate contact with the substrate by a hydrogen bond network bridging the diphosphate and the 3'-phosphate of the ribose in the CoA moiety (Figure 4-2B). The main chain of residues 263–267 form a loop on the other side of the ribose ring and keep it in place by three direct hydrogen bonds and one linked by a water molecule. The diphosphate is positioned between the three arginine residues, 266, 408, and 555. Most of the interactions between the substrate and protein are formed between the ribose and diphosphate part of the substrate. There are only a few hydrogen bonds linked by water molecules to the rest of CoA. The oxalyl group of the substrate is precisely positioned by hydrogen bonds to all three substrate oxygen atoms. One of the carboxylate oxygen atoms is held by Tyr-483 and Ser-553 and the other by the main chain amino group of Ile-34 (Figures 4-3A

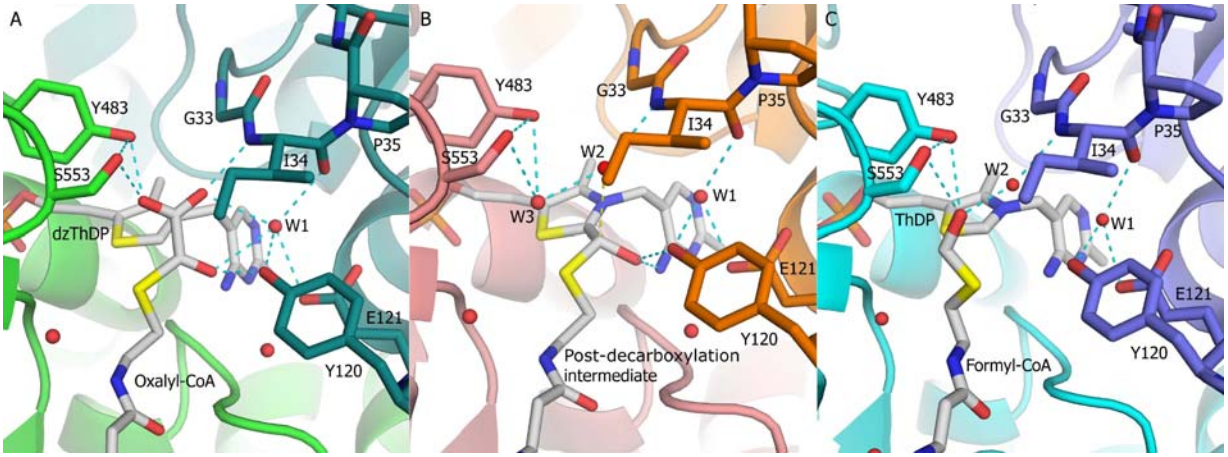

Figure. 4-3. Three snapshots of OXC intermediates. *A*, close-up of oxalyl-CoA binding [2]. *B*, structure of the postdecarboxylation intermediate [5]. *C*, structure of the product complex [6]. For all images, the C-terminus after residue Arg-555 has been omitted for clarity. Residues from different subunits are coloured *differently* and *red spheres* represent water molecules. Taken from Berthold 2007 (17).

and 4-4A). Tyr- 483 is in a strained conformation in the disallowed part of the Ramachandran plot and Ile-34 is followed by the conserved Pro-35, the amide of which adopts a cis conformation (98). Consistently, in all determined structures of OXC, a water molecule (W1) is observed, bound between the side chains of Tyr-120 and Glu-121 and the carbonyl oxygen atom of Ile-34. The substrate Cα-carbonyl oxygen atom makes hydrogen bonds to Tyr-120 and W1, bridging to Glu-121 and the cis-Pro-35 loop. The substrate is thus perfectly positioned for attack by the activated cofactor with a distance of approximately 3 Å between the substrate Cα atom and C2 of the ThDP thiazolium ring. The structure of the CoA complex containing ThDP, solved to 2.2 Å resolution, is virtually identical (rmsd, 0.181 Å for 559 Cα atoms) to the substrate complex; the structured C-terminus also folds over CoA.

Structure of a Trapped Covalent Intermediate

A transiently accumulated covalent intermediate [5], formed after attack of the C2 of the ThDP thiazolium ring on the substrate Cα atom and after decarboxylation, was trapped in

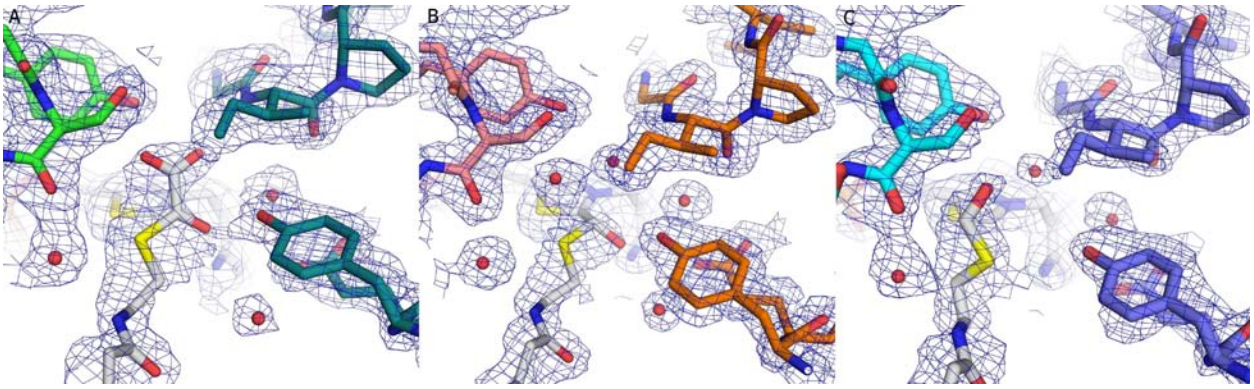

Figure. 4-4. Annealed composite omit maps calculated for the structures shown around the active site: in *A*, the oxalyl-CoA complex [2]; *B*, the postdecarboxylation intermediate complex [5]; and *C*, the product complex [6]. The contour level is 1σ. Residue labels can be seen in Figure 4-3. Taken from Berthold 2007 (17).

Table 4-1. Data collection and refinement statistics for OXC structures

Ligand Complex	Substrate [2]	Intermediate [5]	Product [6]		CoA
Cofactor	dzThDP	ThDP	ThDP	dzThDP	ThDP
Data collection statistics					
Resolution (Å)	152-2.06 (2.17-2.06)	76.0-1.82 (1.92-1.82)	51.92-2.15 (2.27-2.15)	63.89-2.20 (2.32-2.20)	63.89-2.20 (2.32-2.20)
Cell axis a = b, c (Å)	127.0, 151.8	126.2, 151.9	127.6, 152.0	127.7, 152.4	127.7, 152.1
R_{merge}	0.104 (0.503)	0.090 (0.480)	0.100 (0.246)	0.137 (0.430)	0.008 (0.172)
Mean ((I)/ σ(I))	11.8 (2.5)	10.2 (2.0)	9.8 (2.8)	14.5 (2.4)	10.1 (3.8)
Completeness (%)	96.2 (74.2)	99.2 (99.9)	98.8 (96.9)	97.8 (87.8)	99.2 (99.4)
Wilson B-factor ($Å^2$)	25.4	18.7	26.7	35.0	27.7
Refinements Statistics					
Resolution (Å)	30.0-2.06	30.0-1.82	25.0-2.15	30.0-2.2	30.0-2.2
Reflections work/test set	76,781/3,994	112,438/5,831	69,803/3,658	64,803/3,413	65,382/3,439
Number of residues	1,118	1,118	1,115	1,094	1,118
Number of waters	908	1185	615	618	666
R_{fact}/R_{free} (%)	17.4/21.2	15.0/17.6	18.9/23.1	17.7/21.5	19.9/23.8
Rmsd from ideal					
Bonds (Å)/Angles (º)	0.009/1.34	0.008/1.43	0.009/1.30	0.08/1.26	0.008/1.18
Ramachandran residues in region (%)					
Most favoured	88.9	89.7	89.5	89.8	89.4
Additional allowed	10.7	9.9	10.1	9.7	10.1
Generously allowed	0.2	0.1	0.2	0.2	0.2
Disallowed	0.2	0.2	0.2	0.2	0.2
Occupancy of ligands	1.0/1.0	0.8/1.0	0.6/0.8	--	1.0/1.0
PDB deposition ID	2ji6	2ji7	2ji8	2ji9	2jib

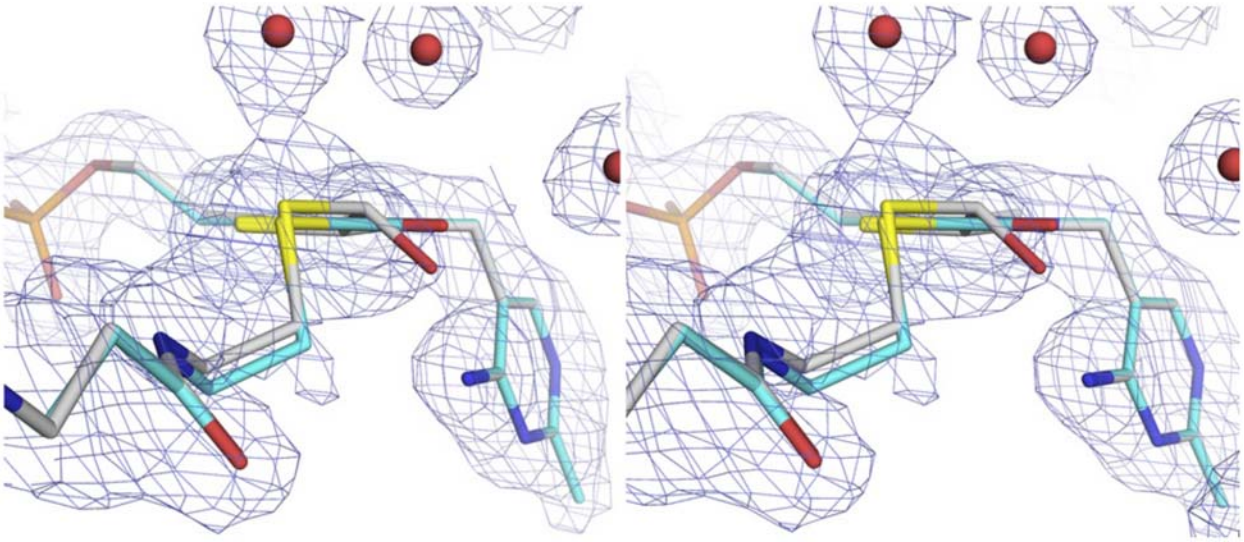

Figure. 4-5. Stereoview of postdecarboxylation intermediate complex data refined with both the enamine form [4] and protonated intermediate [5]. The nonplanar protonated intermediate [5] is shown with *grey* carbons and the enamine carbanion form [4] is shown with carbons in *cyan*. Both are viewed along the thiazolium plane. The annealed composite omit map is contoured at 1σ and shows a better fit for the protonated intermediate. Taken from Berthold 2007 (17).

crystallographic freeze-trapping experiments and refined to 1.8 Å resolution (Figures 4-3B and 4-4B). No structural changes are observed when compared to the holoenzyme (rmsd, 0.216 Å for 546 Cα atoms) except the ordering of the C terminus. The OXC intermediate was best modeled into the electron density with a nonplanar Cα conformation (Figure 4-5), and not as the stabilized enamine previously seen in postdecarboxylation intermediate complexes of transketolase, the dehydrogenase of the *Thermus thermophilus* HB8 branched chain α-ketoacid dehydrogenase complex (178), and pyruvate oxidase (POX) (262). The Cα is best modeled as lying slightly out of the thiazolium plane, although this observation is at the limit of the error at this resolution. Whether the density in the calculated omit map (Figures 4-4B and 4-5) corresponds to a single homogenous intermediate or a mixture of intermediates at different states can not be certain, but modeling other intermediate conformations with varying occupancy does not improve the model and results in increased amounts of negative electron density in the difference map. In the

intermediate structure, the Cα-OH and 4'-NH of ThDP form a close contact, with a hydrogen bond distance of 2.55 Å. The Cα-OH also makes a hydrogen bond to Tyr-120 (Figure 4-3B). At the approximate positions of the substrate carboxyl oxygen atoms in the oxalyl-CoA complex, two water molecules (W2 and W3 in Figure 4-3B) are bound. W3 also interacts with Ser-553 and Tyr-483. W2 makes a hydrogen bond to the main chain nitrogen of Ile-34 and is ideally positioned (2.7 Å) to have donated a proton to the Cα atom, and further, proton transfer to the α-carbanion is likely to have occurred. Thus, the structure represents the covalently bound product (*vida infra*).

Structure of the Formyl-CoA Complex

The product complex [6] was formed by soaking crystals of ThDP-bound OXC in a solution of formyl-CoA (Figures 4-3C and 4-4C). No structural changes in the protein framework are observed in OXC complexed with formyl-CoA when compared with the

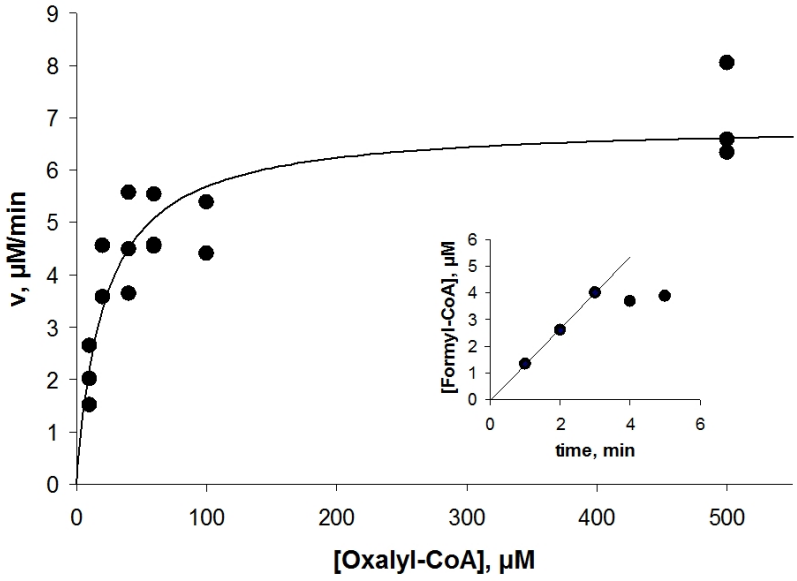

Figure. 4-6. Initial velocity plot of S553A OXC variant. Oxalyl-CoA concentration was varied form 10 – 500 µM and enzyme concentration was 9 nM. *Inset*, progress curve for the formation of formyl-CoA over time.

holoenzyme with the exception of the ordering of the C-terminus (rmsd, 0.237 Å for 546 Cα atoms). In the product complex structure, there are some rearrangements compared with the substrate complex around the CoA sulfur atom (Figure 4-6). The carbonyl group of formyl-CoA forms a hydrogen bond via a water molecule (W2) to the main chain nitrogen of Ile-34.

Kinetic Validation of Active Site Residues Deduced from the OXC Crystal Structures

Several site-directed OXC mutants and a variant containing a truncated C-terminal region were expressed and kinetically characterized by standard methods (Table 4-2) (15). Catalytic activity was abolished in the C-terminal truncation mutant and the OXC variant in which Glu-56 was replaced by alanine. This glutamate residue is strictly conserved in the POX family, and is needed for ThDP activation by promoting formation of the 1',4'-iminopyrimidine tautomer of the cofactor, which then facilitates deprotonation at C2. Mutation of this glutamate persistently results in severely reduced activity in all ThDP-dependent enzymes studied with the exception of glyoxylate carboligase which has a valine in place of the otherwise conserved glutamate (130). As expected, size exclusion experiments showed that all the prepared variants eluted as tetramers, but interestingly that the E56A mutant eluted with a retention time corresponding to that of a dimer. This disruption to the quaternary structure of OXC might be a consequence of impaired cofactor binding due to the loss of the important hydrogen bond between Glu-56 and the N1' of ThDP.

While truncation of the C-terminus, disordered in the holoenzyme, abolished activity, mutation of Arg-555 gave a significant rise in K_M without affecting k_{cat}. Replacement of Tyr-120, Glu-121, Tyr-483, or Ser-553 with alanine resulted in significantly reduced activity of the enzyme (Table 4-2) without greatly affecting the K_M, showing that all four are important for

Table 4-2. Summary of kinetic data for OXC, OXC variants, and HisYfdU.

Enzyme	K_M, μM	k_{cat}, s^{-1}	%WT	k_{cat}/K_M, $s^{-1}M^{-1}$
OXC (15)	23 ± 3.5	88 ± 4	100	3.8×10^6
E56A	--	--	0	--
Y120F	43 ± 9	7.2 ± 0.6	8.2	1.7×10^5
Y120A	60 ± 14	0.26 ± 0.03	0.3	4.1×10^3
E121Q	18 ± 4	3.3 ± 0.3	3.8	1.8×10^5
E121A	41 ± 8	0.1 ± 0.01	0.1	2.4×10^3
Y483F	40 ± 11	1.7 ± 0.2	1.9	4.1×10^4
Y483A	24 ± 7	1.4 ± 0.1	1.6	5.6×10^4
S553A	21 ± 5	13 ± 1.5	15	6.2×10^5
R555A	66 ± 8	85 ± 4	96	1.3×10^6
553-565	--	--	0.001	--
HisYfdU	180 ± 39	15 ± 1	--	8.6×10^4

efficient catalysis. However, the fact that activity is not abolished in any of these mutants suggests that none of them participate directly in the proton transfer reactions.

Discussion

C-Terminal Organization Upon Substrate Binding

The structure of OXC in complex with CoA reveals that binding of the carrier CoA is what induces the structural organization of the C-terminal 13 residues. The presence of the dzThDP analogue, with no net charge and thus an excellent mimic of the ylide state of ThDP, does not have this effect in the absence of CoA, suggesting that deprotonation of ThDP alone is not inducing this conformational change. Formation of the ylide was previously suggested to trigger a loop to close down over the pyruvate dehydrogenase E1 subunit from *Escherichia coli* (PDH-E1) active site (145). The C-terminal segment closes down over the substrate and thus provides much of the binding energy, which explains why none of the single mutations have drastic effects on the K_M. There are still sufficient interactions such that the tight binding of the CoA carrier remains. On the other hand, the OXC mutant with a truncated C-terminus can no longer bind the substrate and is inactive. It has previously been suggested for both acetohydroxyacid synthase (AHAS) and *Zymomonas mobilis* pyruvate decarboxylase (zPDC) that the C-terminus

might play an important role in the catalytic cycle by moving aside to let the substrate access the active site and then closing down during catalysis (40, 136). These structural data provide evidence for this hypothesis by showing that substrate binding in OXC clearly induces C-terminal folding.

Substrate Alignment for Ylide Attack

The oxalyl-CoA binding site is organized to perfectly position the substrate for nucleophilic attack by the ThDP-ylide. For the attack to occur, the negative charge developing on the Cα-carbonyl oxygen of the oxalyl-moiety must be stabilized. The cofactor 4'-NH_2 was suggested for this task (15), and here the structural data show this to be probable. Jordan *et al*. (160) have also concluded that the predecarboxylation intermediate exists in its 1',4'-iminopyrimidine form in agreement with the postulated mechanism in which the 4'-NH_2 is responsible for proton donation. The carboxyl group of the substrate is perpendicular to the positively charged thiazolium ring, which promotes decarboxylation by permitting overlap of the s- and p*-orbitals (68, 246). Tyr-120, Tyr-483, and Ser-553 participate in positioning the oxalyl group in the active site. Although mutating these residues only has a minor effect on K_M, the specificity constant is severely reduced, demonstrating their importance in aligning the substrate favorably for cofactor attack.

Postdecarboxylation Intermediate

A postdecarboxylation intermediate complex [5] could be observed in crystals soaked with oxalyl-CoA at 4 ºC for 8–10 min; shorter soaks showed no or low occupancy complexes, and longer soak times resulted in a heterogeneous composition of complexes in the crystal where some of the substrate molecules had turned over to formyl-CoA. From this, it can be concluded that the decarboxylation proceeds rapidly, in agreement with existing proposals for other ThDP-decarboxylases (126). A water molecule, W2, is at 2.7 Å distance from the Cα atom of the

intermediate, ideally positioned for transfer of a proton to a Cα-carbanion intermediate, and provides an explanation for the observation that no single mutation of active site residues (except Glu-56) abolishes catalysis. Replacement of residues Tyr-120 or Glu-121 with alanine has an effect on k_{cat} due to the importance in firmly positioning the water molecule, W1. W1 also makes a hydrogen bond to the Ile-34 carbonyl oxygen with the adjacent Pro-35 in the cis-conformation, an interaction that is crucial for positioning the Ile-34 NH group (Figure 4-3). The Ile-34 NH group is involved in binding substrate, and most importantly, the water molecule W2, involved in transfer to the α-carbanion intermediate. Tyr-483 and Ser-553 also participate in positioning W2 via W3, and there is also a significant reduction in the turnover number when these residues are replaced by site-directed mutagenesis. The short distance between water molecules W2 and W3 (2.5 Å) suggests that W2 might have some hydroxide ion character, which would be consistent with a proton having been transferred to the α-carbanion. Thus it appears that the covalently bound product is present, indicating that, in the catalytic cycle, product release from the cofactor is the slowest step of the reaction catalyzed by OXC. There is also a close contact between Cα-OH and 4'-NH_2, 2.55 Å, which confirms participation of the 4'-amino group of ThDP in proton transfers to and from the substrate carbonyl oxygen and stabilization of the intermediate. In OXC, the enamine/α-carbanion before protonation may be nonplanar and thus has more α-carbanion character than would a planar enamine. A planar enamine would not have the proton donor, W2, optimally positioned for proton transfer, and the Cα carbon would be less basic. The difference from other enzymes in which a planar enamine state has been observed (82, 178, 262) may be explained by the fact that the latter oxidative enzymes require a second "acceptor" substrate. To allow the intermediate to proceed via the energetically more stable enamine might then be a way for these enzymes to protect the intermediate from protonation of

Cα during binding of the second substrate. For OXC, on the other hand, relaxation into the planar enamine structure would only impede the subsequent Cα protonation step in the proposed mechanism. The complete removal of the strain and relaxation would then occur only upon product dissociation, and would further drive this process.

Until 2006, a planar enamine-like structure was consistently seen in all post-decarboxylation intermediate structures (82, 178, 262). A crystallographic study was then published in which the decarboxylase subunit of the human α-ketoacid dehydrogenase complex (BCKDC-E1b), in complex with several substrate analog intermediates, consistently showed a nonplanar (and therefore more α-carbanion-like) structure (161). Common for the BCKDC-E1b analog complexes and the OXC natural intermediate structure is the fact that the Cα is best modeled as lying slightly out of the thiazolium plane. This out-of-plane distortion, as discussed by (161), might force the intermediate into its most active state. When the orbitals are not

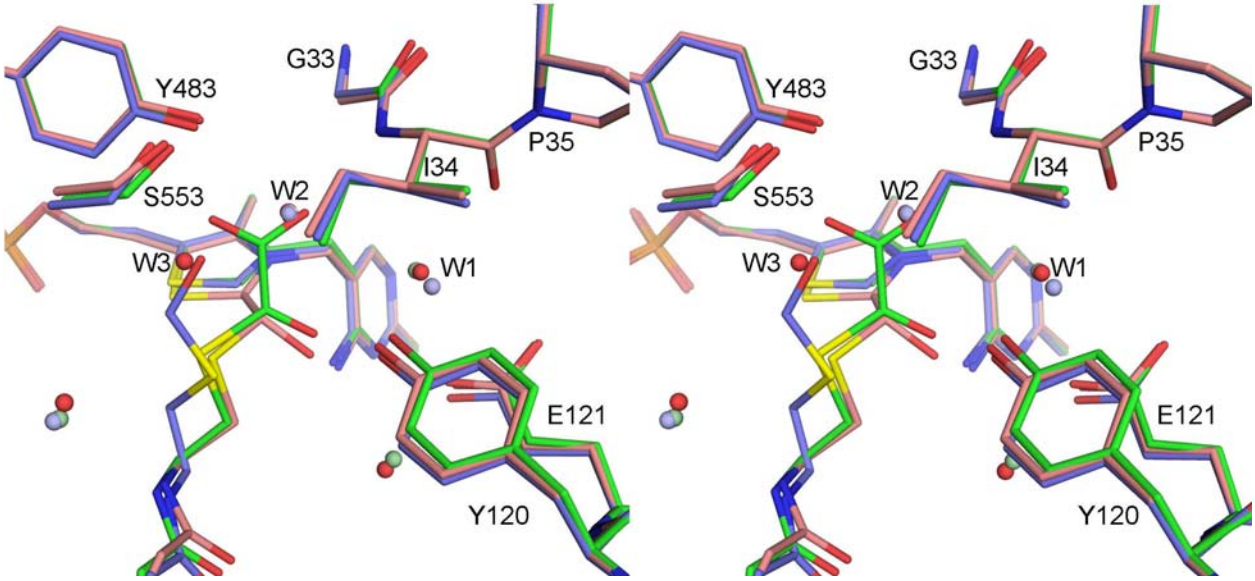

Figure. 4-7. Stereoview of the aligned OXC structures. The substrate (*green*), intermediate (*pink*), and product complexes (*blue*) are overlayed. Water molecules of three structures are shown in the same colours, but in a lighter shade. The C-terminus after residue Arg-555 has been omitted for clarity. Taken from Berthold 2007 (17).

completely aligned, the negative Cα charge cannot be as effectively delocalized into the thiazolium ring, the basicity of Cα is increased, and the subsequent step of the reaction when Cα is protonated is enhanced. This is likely to be true in this case as well, because it allows the proton donor (W2) to come close to Cα (2.7 Å). The close Cα-OH-to-4'-NH_2 contact and out-of-plane distortion was observed in the predecarboxylation intermediates of PDH-E1 (5) and POX (262). The authors of these studies claimed that the strain was a contributing force for the decarboxylation step and that it would be relaxed upon enamine formation. The strained out-of-plane distortion might persist also in the postdecarboxylation intermediate of OXC, and could therefore act as a contributing force throughout the reaction.

Formyl-CoA Release

The reason for the relative stability of the covalent product intermediate might be the close contact to the 4'-amino group of ThDP. The strained conformation, with the Cα out of plane with the thiazolium ring and the positive charge on the thiazolium ring, might be the factors leading to cleavage of the C2-Cα bond and product release from the cofactor.

Conclusions on Catalysis in Simple Decarboxylating ThDP Enzymes

Common to OXC and many other ThDP-dependent enzymes catalyzing a decarboxylation, mutations of active site residues, other than the conserved glutamate needed for activation of the cofactor, hardly ever lead to abolished activity (Table 4-2) (88, 125) showing that only the cofactor itself is essential for catalysis. In agreement with the postulated mechanism for OXC in Figure 4-1 and the structure of the intermediate complex presented here, it has been shown by CD data on several ThDP enzymes (126, 176), and directly observed by NMR (134), that the 4'-N atom of the pyrimidine moiety performs most of the acid-base reactions involving the substrate Cα-carbonyl oxygen atom in the reaction sequence by conversion between the 4'-amino and the 1',4'-imino form of the cofactor. OXC and other related simple decarboxylating

ThDP enzymes achieve a significant fraction of their catalytic power from setting up the central α-carbanion intermediate for proton transfer to Cα (269). In the case of OXC, the proton is derived from a bound water molecule in the active site. The cis-Pro loop containing Ile-34 has a central role in the OXC active site by positioning the substrate, the product, and the water molecule, W2, donating the proton to the α-carbanion intermediate. The conformation of the loop is maintained by a hydrogen bond network involving the invariant water molecule, W1, in the active site. There have been several studies reporting on communication between the active sites through a proton-conducting channel resulting in alternating site reactivity (66, 86, 125, 127). In OXC, there is no proton conduction channel and no evidence for alternating site reactivity in the structures of OXC. Although the electron density of ligands is often better defined in one subunit than in the other due to different occupancies, in no case are different species visible in the active sites. Transketolase has also been reported to lack alternating site reactivity (82).

Experimental Methods

Protein Expression, Mutagenesis, and Purification

OXC was produced recombinantly in *E. coli* as described previously (15, 16). Site-specific OXC variants were produced by the QuikChange site-directed mutagenesis method (Stratagene) or the overlap extension method (109), and were expressed and purified according to protocols used for the wild-type enzyme (15, 16). Briefly, this procedure includes affinity chromatography on a Blue-sepharose fast flow affinity column followed by desalting on Sephadex G-25 size-exclusion column, and further purification by QHP anion-exchange chromatography. The C-terminal truncation variant lost the capacity to bind to the affinity column, but could be retained and purified to homogeneity by ion-exchange chromatography. The OXC apoenzyme was prepared by dialysis overnight against 50 mM Tris (2-amino-2-

(hydroxymethyl)propane-1,3-diol) buffer, pH 8.5, containing 1 mM dithiothreitol and 1 mM EDTA, followed by buffer exchange into 50 mM MES (4-morpholine-ethanesulphonic acid) buffer, pH 6.5. No activity was observed for the OXC apoenzyme, or for apoenzyme incubated with dzThDP and Mg^{2+}, although full activity was regained when ThDP and Mg^{2+} were added to the apoenzyme. Samples of oxalyl-CoA and formyl-CoA were prepared and purified as described previously (124).

Enzyme Assay

The OXC variant enzymes were assayed by the previously described high-performance liquid chromatography point assay monitoring the formation of formyl-CoA (15). Typically, the enzyme was diluted with 25 mM sodium phosphate buffer, pH 6.5, containing 300 mM NaCl, to a final concentration of about 0.7 mg/ml, and initial velocities were recorded as a function of oxalyl-CoA concentration (10–500 mM).

Crystallization and Complex Formation

Crystallizations were performed Dr. Catrine Berthold by the hanging drop vapor-diffusion method under conditions very similar to those described previously for the holoenzyme structure (16). Well diffracting crystals were produced with a precipitating solution containing 0.5 M $CaCl_2$, 0.1 M BisTris propane (2-[bis(2-hydroxyethyl)amino]-2-(hydroxymethyl) propane-1,3-diol), pH 6.5, and 26% polyethylene glycol 550 monomethyl ether. In contrast to the holoenzyme crystals (16), no twinning was detected among the complexes. The dzThDP-inhibited (5 mM) OXC crystals were produced at 20ºC, while active OXC containing ThDP was crystallized at 4º C through streak seeding after 2 hr equilibration with the well solution. The lower temperature facilitated the freeze-trapping experiments by reducing the reaction rate. The CoA complex was produced by cocrystallization of wild-type OXC with 1 mM CoA. The soaking experiments were performed by transferring the crystals to a new drop containing 2 ml of 0.2 M BisTris

propane, pH 6.5, and 52% polyethylene glycol 550 monomethyl ether mixed with 2 ml of 50 mM sodium acetate, pH 5.0, containing either 20 mM oxalyl-CoA or formyl-CoA. Crystals soaked in this mixture remained unaffected more than 12 hr without reduced diffraction quality. The crystals were flash frozen in liquid nitrogen after desired soaking times, and the soaking solution was sufficient as cryoprotectant. Soaking times for the substrate, covalent intermediate, and product complexes were 5 min, 8 min, and 12 min, respectively. Crystals inhibited by dzThDP were used to obtain the substrate complex by soaking rather than cocrystallization due to the instability of oxalyl-CoA.

Data Collection and Structure Determination

Data were collected at beamline I711 at MAX-lab in Lund, Sweden, and at ID14 eh1, eh3, and eh4 at the European Synchrotron Research Facility in Grenoble, France and analysed by Catrine Berthold. A summary of all data sets can be found in Table 4-1. All data were processed with Mosflm (146) and then scaled and further processed with programs in the CCP4 suite (11). Due to slight shifts in length of cell axes, molecular replacement with the previously solved holostructure as a search model (PDB code: 2c31) was used for phasing. The R_{free} set was imported from the holoenzyme structure for all data sets. REFMAC5 (175) was used for refinement and model building as well as water assignment were performed in COOT (76). Atomic displacement parameters were refined in REFMAC by the TLS (translation, libration, screw) method, with each of the two monomers in the asymmetric unit treated as a single TLS group. The soaked ligands were not included until the end of the refinements. Libraries were created with the Dundee PRODRG2 server (http://davapc1.bioch.dundee.ac.uk/programs/prodrg/). Refinement of the covalent intermediate was performed in parallel with restrains for a planar and tetrahedral conformation around Cα. The geometric restrains were then loosened toward the end of refinement. Annealed omit maps calculated in CNS (29) were used to confirm

the conformations at the active site (Figure 4-4), and the geometry of the refined structures were checked with PROCHECK (144). All Figures of protein molecules were produced with PyMol (59).

CHAPTER 5
SUMMARY

Kinetic Mechanism of Family III CoA Transferases

Family III CoA transferases differ from Family I transferases both in sequence similarity and in kinetic mechanism. Hydroxylamine and borohydride trapping experiments, as well as more direct evidence from MS and crystallographic data, have demonstrated that, despite their divergent kinetic mechanisms, both Families mediate the transferase reaction through a covalent enzyme CoA thioester intermediate. The formyl-CoA transferases, a subgroup of Family III CoA transferases, rely on a conserved flexible loop comprising four glycine residues to protect labile reaction intermediates and contribute to substrate specificity. Analysis of two formyl-CoA transferase homologs from *E. coli* and *O. formigenes* demonstrates that modification of the residues near the glycine loop, but outside of the active site, confers 100-fold increase for oxalate affinity and replacement of these residues with alanine severely impairs the ability of the enzyme to catalyze the formation of oxalyl-CoA from formyl-CoA

FRC and OXC from *E. coli*

This work has clearly demonstrated that YfdW and YfdU from *E. coli* are a formyl-CoA transferase and an oxalyl-CoA decarboxylase, respectively; these enzymes are functionally homologous to FRC and OXC from *O. formigenes*. The submillimolar K_M values for formyl-CoA and oxalyl-CoA are an order of magnitude larger than for the *O. formigenes'* enzymes, but are similar to each other as is expected with a complementary enzyme pair. The turnover number for oxalate with YfdW is 100 times higher than for the *O. formigenes* enzyme. Thus, despite the critical nature of the FRC reaction, YfdW is more stringent for using formyl-CoA and oxalate than is FRC. In an X-ray structure (1pt8), oxalate is seen bound outside of the active site

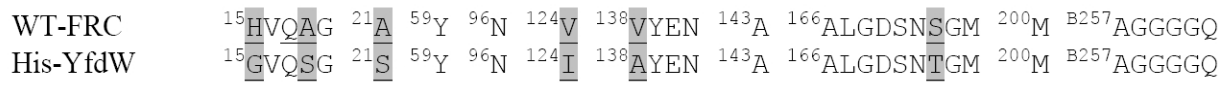

Figure.5-1. Pair-wise sequence alignment 10 Å around the active sites of FRC and YfdW. Residues that differ are highlighted in *grey*.

in YfdW. This binding pocket, blocked by Trp-48 in FRC, has been identified as the basis for substrate inhibition of YfdW by oxalate. Due to the exceptional similarity in active site residues (Figure 5-1) differences in catalytic specificity are likely the result of altered motion seen in the mobile tetraglycine loops in the two enzymes.

The physiological role of YfdW and YfdU in *E. coli* remains unclear. It appears that YfdW was derived from FRC (Figure 5-2; bootstrap values in Appendix C). Sequence similarity remains high and, rather than losing specificity for oxalate, YfdW has evolved tighter specificity. Both the *yfdXWUVE* operon and *yhjX* gene are induced by low pH and, in contrast to OXC, YfdU is not stimulated by ADP. Thus it seems that the *yfdW* and *yfdU* genes continue to be physiologically relevant in *E. coli* and evidence suggests a role in acid resistance rather than metabolism.

Future Work

Folding

If the complete tertiary structure is considered, knots in proteins are not uncommon. Disulfide bridges and links through metal centers can lead to knotted or closed loops (150). There are examples of proteins with true knots in their peptide backbone structure: trefoil knots in members of the α/β-knot superfamily of methyltransferases (MTases) including TrmH from *Auifex aeolicus* (189), AviRb from *Streptomyces viridochromogenes* (173), TrmH from *Thermus thermophilus* (179), and YibK from *Haemophilus influenzae* (165), and in the chromophore-

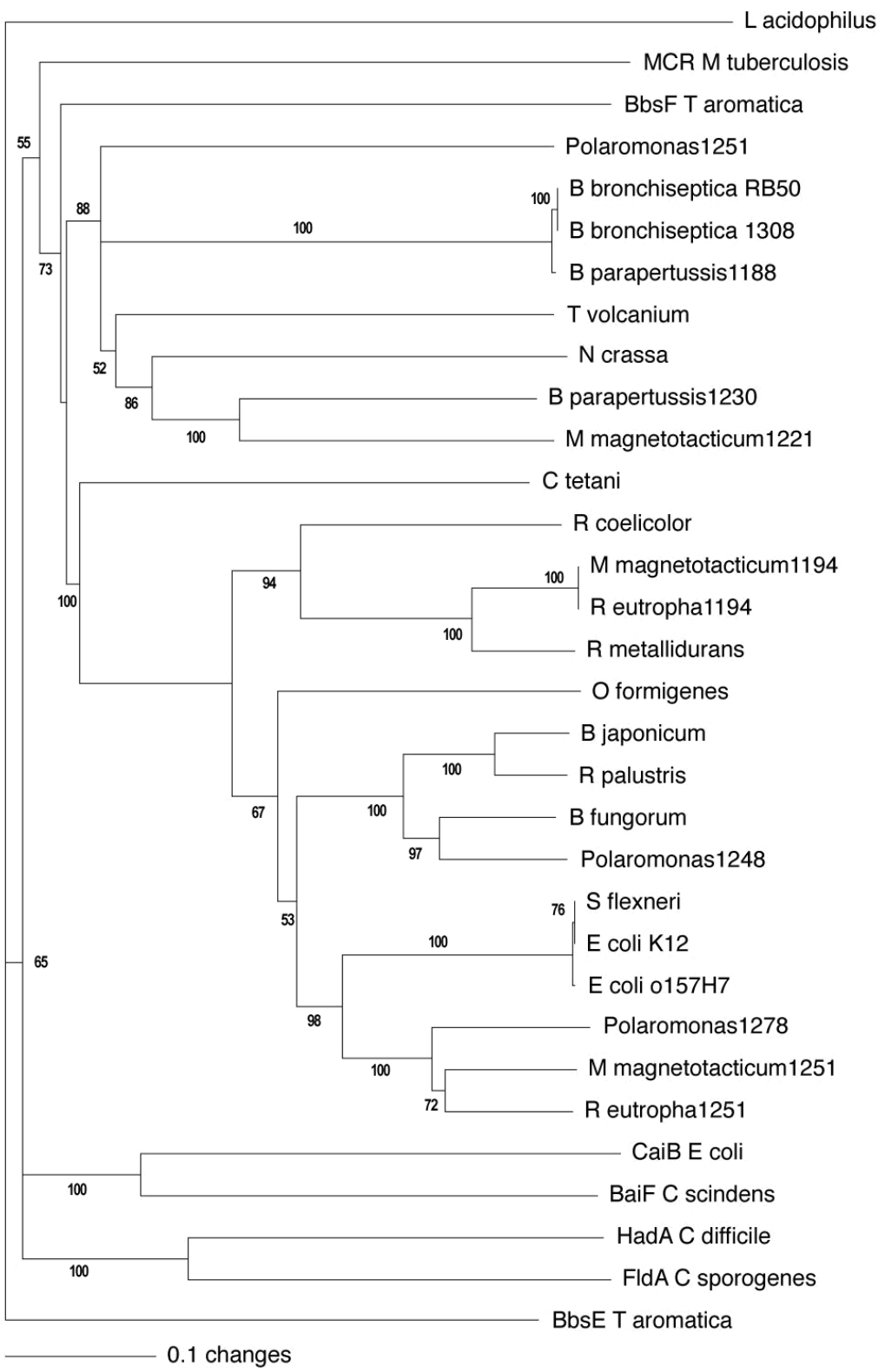

Figure. 5-2. Phylogram of FRC, putative formyl-CoA transferases, and known Family III CoA transferases from pair-wise sequence alignment of polypeptide sequences.

binding domain of *Deinococcus radiodurnas* phytochrome (254); and figure-of-eight knots in the crystal structure of the plant protein acetohydroxy acid isomeroreductase (243).

FRC is similar to the disulfide-linked examples above with the exception that its two monomers are non-covalently linked through each other. A preliminary melting curve monitored by CD and fluorescence shows that the dimer denatures at 57 ºC (Figure 5-3) in a process that appears to be irreversible (data not shown). Proteolytic MS data (Figure 2-14) suggest that the central dimer interface which includes α-helix-9 from both monomers is exceptionally resistant to enzymatic digestion. An FRC heterodimer, comprising an active monomer and an inactive monomer where Asp-169 has been replaced with alanine, was successfully overexpressed in *E. coli*. The mechanism by which *E. coli* and *O. formigenes* (and all other organisms that employ this interlocked dimer scaffold) form the active dimer *in vivo* is an interesting problem and deserves careful study.

Monitoring of the fluorescence of native tryptophan residues is a method that can be used to examine FRC folding(204). Trp-109 is found on α-helix-6 in the large domain of FRC. It is located 10 Å and 24 Å from surface residues Ser-389 and Glu-394, respectively, both found on the linker region near the C-terminus of FRC. These residues are candidates for mutation to cysteine residues for labelling with IAEDANS; they should provide excellent reporters on unfolding FRC. Another good experiment will use ANS, or 8-anilino-1-naphthalenesulfonic acid (see Figure 5-4), an environment-sensitive fluorophore which is virtually nonfluorescent in water, but can be used as a probe for hydrophobicity—in nonpolar environments it emits a blue fluorescence with quantum yield ~0.70 (238). Thus, as FRC is treated with increasing concentrations of chaotropic agents, increased binding of ANS with exposed hydrophobic

regions can be monitored fluorescently to characterize folding intermediate populations as seen in experiments on β-lactamase (96) and the *trp* repressor (166).

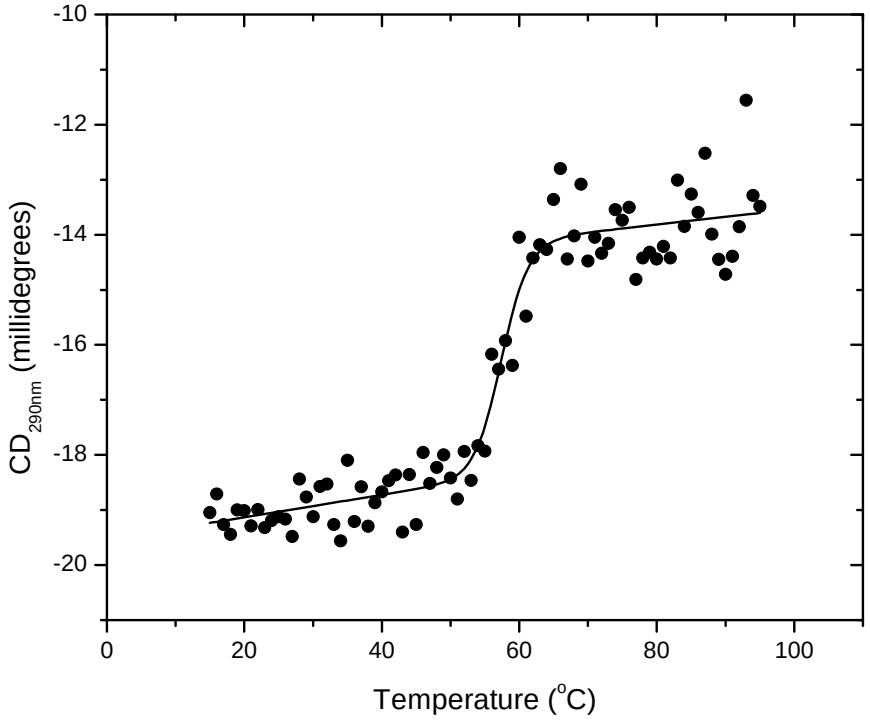

Figure. 5-3. Melting curve for FRC monitored by CD at 290 nm.

Due to the irreversible nature of FRC dimerization, it seems likely that chaperones play an important in the expression of the active enzyme. If this is true, both *E. coli* and *O. formigenes*, must both express this chaperone. A simple immuniprecipitation experiment in conjuction with proteolytic MS will likely identify this theoretical protein. As both FRC and YfdW can be expressed with polyhistidine fusion tags, commercially available anti-His antibodies can be used to coprecipitate the transferases with any proteins associated in their synthesis.

Dynamics

Clearly the tetraglycine loop (Gly-258-261) in FRC and the flexible C-terminus of OXC are important for efficient catalysis. Despite the vast amount of crystallographic data on the FRC structure, there are no data that confirm the catalytic competence of the glycine loop movement. Protein folding studies monitor global changes in protein structure using spectroscopic methods like UV/vis absorption, fluorescence detection, and circular dichroism. Protein dynamics seek to report on conformational changes on catalytic time scales which are on the order of micro- to milliseconds (81). NMR methods have been used successfully to follow fluctuations near protein active sites (135). However, NMR analysis of proteins are extremely rare above 30 KDa (260), and thus complete assignment of the FRC monomer (47.2 kDa) backbone is not likely. Site-directed spin labelling (SDSL) experiments are also able to monitor structural changes in the millisecond timescale (116) and are therefore appropriate for dynamics studies. FRET has been used to monitor the catalysis-linked reduction of the flavoenzyme *p*-hydroxybenzoate hydroxylase (PHBH)(257).

Both SDSL and FRET methods require labelling the protein by chemically bonding fluorophores or spin labelling reagents to specific amino acids (253). Lysine groups can be derivatized with succinimidyl active ester, isothiocyanate, or sulfonyl chloride activated fluorophores. Sulfonyl chlorides and isocyanates are reactive species that can be used to label hydroxyl groups. Labelling of cysteine residues is a common approach because they are reactive at physiological pH (6.5 – 8.0). One criterion for a target protein is that there are no cysteines, or other target groups, accessible to labelling reagents. Table 5-1 summarizes the 6 cysteine residues per monomer in recombinant wild-type FRC. Cysteine titration experiments can be run to prove that some residues are not reactive towards labelling reagent. One method is to label the

Table 5-1: Cysteine residues in wild type FRC. The MS column indicates whether the cysteine residue-containing peptides have been identified in MS expreriments.

	Conservation	Location	Interacts	MS	Environment	Mutant
Cys-^{22}	Conserved in "true FRCs": A, G, T	Helix α6	Helix α9	V8DE	Large domain; buried, hydrophobic	A
Cys^{65}	R, S(YfdW), H or C	Loop (β5- α7)	possible H-bond with His^{379} (β11)	no	Large domain; partially buried	S
Cys^{145}	C, A, S, or G	Helix α7	Sheet β7	no	Large domain; buried, hydrophobic	A
Cys^{269}	Highly conserved: F or Y	Sheet β7	Near Helix α16	no	Small domain; near surface, but buried, hydrophobic	A
Cys^{293}	Conserved in "true FRCs": A, S, R, M, L, or V	Helix α12	Helix α13	V8DE	Small domain, buried, hydrophobic	A
Cys^{347}	Conserved: A, V, or Y	Sheet β9	Helix α16	Trypsin	Small domain, buried, hydrophobic	A

protein, proteolyse, and analyse by mass spectrometric methods. Table 5-1 also summarizes the total sequence coverage of mass spectrometric analysis of digests of FRC to date.

Tryptophan has been used as a FRET donor in conjunction with ANS or IAEDANS acceptors (R_0 = 22 Å)(219). IAEDANS, 5-((((2-iodoacetyl)amino)ethyl)amino) naphthalene-1-sulfonic acid, covalently attached to engineered cysteine residues has been used for FRET studies (93). FRC has 8 native tryptophan residues: Trp-48, 109, 156, 265, 272, 289, 301, and

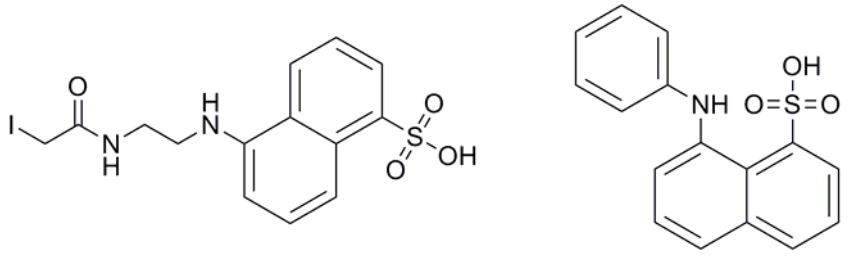

Figure. 5-4. IAEDANS and ANS.

339. Trp-48 is located in a flexible loop near the active site. The native fluorescence of Trp-48 may act as a reporter on gross conformational changes in the enzyme or AEDANS-labelled cysteine mutants could be used to monitor changes in the environment of Trp-48. Trp-48 is found on a loop connecting helices α2 and α3 and is located near both the tetraglycine loop and catalytic Asp-169. Trp-48 is found packed against the glycine loop residues when in the closed position (124), and if these environments differ enough to cause discernable changes in the FRET donor characteristics of Trp-48, it may be useful as a reporter on conformational changes linked to catalysis.

APPENDIX A
PRIMERS USED FOR MUTAGENESIS AND CLONING

Primers for pET-28b constructs

5'-Nde1 FRC	5'-AGG AGA TAT ACA TAT GAC TAA ACC ATT AGA TGG AAT TAA TGT GC
3'-FRC BamH1(stop)	5'-AAG TCT GGA TCC TCA AAC TAC CTG T
5'-Nco1 FRC	5'-AAG GAG CCA TGG AGA TGA CTA AAC CGT TAG ATG
3'-FRC Xho1(stop)	5'-CTG ACC TCG AGA ACT ACC TGC TTG C
5'-BamH1FRC	5'-AGG AGA TAT AGG ATC CGA TGA CTA AAC CAT TAG ATG GAA TTA ATG TGC
3'-FRC Xho1	5'-CCC AGA AAG TCT GAC CTC GAG AAC TAC CTG TTT TGC ATG C

Primers for Duet constructs

5'-FRC BamH1	5'-AGG AGA TAT AGG ATC CGA TGA CTA AAC CAT TAG ATG GAA TTA ATG TGC
3'-FRC HindIII(stop)	5'- ACA GGT AGT TTG AAG CTT AGA CTT
3'-FRC Xho1(stop)	5'- ACA GGT AGT TTG ACT CGA GAG ACT T

QUICKCHANGE primers for FRC variants

5'-Q17I	5'-GTC ATT GCA GGT CCT GCC TGT ACA CAG-3'
3'-Q17I	5'-TGC AAT GAC GTG GGT AAA GTC AAG CAC-3'
5'-Q17A	5'-GCT TGA CTT TAC CCA CGT CGC GGC AGG TCC TGC CTG TAC ACA GAT GAT GGG-3'
3'-Q17A	5'-CCC ATC ATC TGT GTA CAG GCA GGA CCT GCC GCG ACG TGG GTA AAG TCA AGC-3'
5'-W48F	5'-GAT ATG ACT CGT GGA TTC CTG CAG GAC AAA CC-3'
3'-W48F	5'-GGT TTG TCC TGC AGG AAT CCA CGA GTC ATA TC-3'
5'-W48Q	5'-GAT ATG ACT CGT GGA CAG CTG CAG GAC AAA CC-3'
3'-W48Q	5'-GGT TTG TCC TGC AGC TGT CCA CGA GTC ATA TC-3'
5'-P159R	5'-CCG GTT TCT GGG ATG GTC GTC CAA CCG TTT CCG GC-3'
3'-P159R	5'-GCC GGA AAC GGT TGG ACG ACC ATC CCA GAA ACC GG-3'
5'-G258A	5'-GGT GGT AAC GCA GCG GGC GGC GGC C-3'
3'-G258A	5'-GGC CGC CGC CCG CTG CGT TAC CAC C-3'
5'-G259A	5'-GGT GCG GGC GGC CAG CCA GGC TGG-3'
3'-G259A	5'-GCC CGC ACC TGC GTT ACC ACC ACG TGG-3'
5'-G260A	5'-GGC GCG GGC CAG CCA GGC TGG ATG CTG-3'
3'-G260A	5'-GCC CGC GCC ACC TGC GTT ACC ACC ACG-3'
5'-G261A	5' GGT GGC GGC GCG CAG CCA GGC TGG
3'-G261A	5' GCC GCC GCC CGC TGC GTT ACC ACC

Nest primers for YfdW and YfdU

5'-YfdVUW	5'-CGC CTG GCC GGT GTT GGC GTA ATG G-3'
3'-YfdVUW	5'-CCC TGT TTG CCC GAG TAA TAG ATA CAA ATA GAG CCG C
5'-YfdW	5'-AGG TAT TCA TAT GTC AAC TCC ACT TCA AGG AAT TAA AGT TCT CGA TTT C-3'
3'-YfdW	5'-GGG AGC AAG CTT CCC CCG TTA ATA TCA GAT GGC G -3'
5'-YfdU	5'-CGA GGT TAT TAC ATA TGT CAG ATC AAC TTC AAA TGA CAG ATG G-3'
3'-YfdU	5'-CTC ACC ATC GCA TAA TGA GTT AAG CTT AGG AGA CGA TGT CAG-3'

Nested primers for YhjX

5'-YhjX nest	5'-GCC GTT TTT CCC CAG GCA TAA AGT GC-3'
3'-YhjX nest	5'-GCC CAG TAG CTC GCG GC-3'
5'-YhjX	5'-GCA GGA ATA CTC ATA TGA CAC CTT CAA ATT ATC AGC GTA CCC GC-3'
3'-YhjX	5'-CCA GTA GCT CGA AGC TTA GCA TTA AAG GGA GCC-3'

APPENDIX B
SUMMARY OF KINETIC CONSTANTS

Table B-1. Summary of all kinetic constants for wild-type FRC and variants

	k_{cat} (s^{-1})	$K_{M(F\text{-}CoA)}$ (μM)	$k_{cat}/K_{M(F\text{-}CoA)}$ ($s^{-1}mM^{-1}$)	$K_{M(oxalate)}$ (mM)	$k_{cat}/K_{M(oxalate)}$ ($s^{-1}mM^{-1}$)	K_{ia} (μM)
WT-FRC	5.3 ± 0.1	2.0 ± 0.3	2700	3.9 ± 0.3	1.4	16 ± 2
G259A	1.9 ± 0.1	4.7 ± 0.8	410	12.1 ± 0.5	0.16	0.9 ± 0.6
G260A	0.23 ± 0.02	18 ± 3	13	18.0 ± 1.6	0.012	3 ± 3
G261A	1.65 ± 0.01	26.6 ± 0.9	62	0.47 ± 0.08	3.5	3 ± 2
Q17A	0.12 ± 0.1	3.3 ± 0.5	36	13.2 ± 0.6	0.009	79 ± 3
His-YfdW	130 ± 17	352 ± 4	370	0.51 ± 0.03	255	18 ± 0.1
His-FRC	5.5 ± 0.4	4.7 ± 1.6	1200	1.2 ± 0.3	4.58	22 ± 6
W48F FRC	17.1 ± 0.2	0.7 ± 0.4	24430	1.5 ± 0.3	11.4	10 ± 7
W48Q FRC	5.8 ± 0.3	2.7 ± 0.9	2148	0.43 ± 0.03	13.5	4 ± 1

Table B-2. Summary of all inhibition constants and patterns for wild-type FRC and variants.

(μM)	WT-FRC	Q17A	G258A	G259A	G260A	G261A
CoASH	competitive	mixed-type		mixed-type	mixed-type	mixed-type
K_{ic}	16.7 ± 0.7	16.0 ± 0.6		6.0 ± 1.0	55 ± 19	2 ± 1
K_{iu}	--	100 ± 14		460 ± 129	290 ± 5	41 ± 1

(μM)	WT-FRC	His-FRC	His-YfdW	W48F	W48Q
CoASH	competitive	competitive	mixed-type	mixed-type	competitive
K_{ic}	16.7 ± 0.7	9 ± 7	218 ± 21	11 ± 5	55 ± 19
K_{iu}	--	--	213 ± 16	35 ± 6	290 ± 5

Table B-3. Steady-state parameters for the formyl-CoA/succinate transferase activities of YfdW, FRC and the Trp-48 FRC mutants.

Enzyme		Formyl-CoA		Succinate		
	k_{cat} (s^{-1})	$K_{M(app)}$ (μM)	$k_{cat}/K_{M(app)}$ ($mM^{-1}s^{-1}$)	$K_{M(app)}$ (mM)	$k_{cat}/K_{M(app)}$ ($mM^{-1}s^{-1}$)	K_{ia} (μM)
His-YfdW	5.3 ± 0.4	180 ± 14	29.4	80 ± 40	0.07	30 ± 19
WT FRC	149 ± 13	16 ± 2	9312	0.32 ± 0.03	465	0.5 ± 0.4
W48F FRC	42 ± 6	12 ± 6	3500	0.015 ± 0.005	2800	12 ± 8
W48Q FRC	17.9 ± 0.5	6.7 ± 0.9	2672	0.07 ± 0.01	256	9 ± 4

Table B-4. Steady-state parameters for OXC

Enzyme	K_M, μM	k_{cat}, s^{-1}	%WT	k_{cat}/K_M, $s^{-1}M^{-1}$
OXC (15)	23 ± 3.5	88 ± 4	100	3.8×10^6
E56A	--	--	0	--
Y120F	43 ± 9	7.2 ± 0.6	8.2	1.7×10^5
Y120A	60 ± 14	0.26 ± 0.03	0.3	4.1×10^3
E121Q	18 ± 4	3.3 ± 0.3	3.8	1.8×10^5
E121A	41 ± 8	0.1 ± 0.01	0.1	2.4×10^3
Y483F	40 ± 11	1.7 ± 0.2	1.9	4.1×10^4
Y483A	24 ± 7	1.4 ± 0.1	1.6	5.6×10^4
S553A	21 ± 5	13 ± 1.5	15	6.2×10^5
R555A	66 ± 8	85 ± 4	96	1.3×10^6
553-565	--	--	0.001	--
HisYfdU	180 ± 39	15 ± 1	--	8.6×10^4

APPENDIX C
DENDOGRAMS

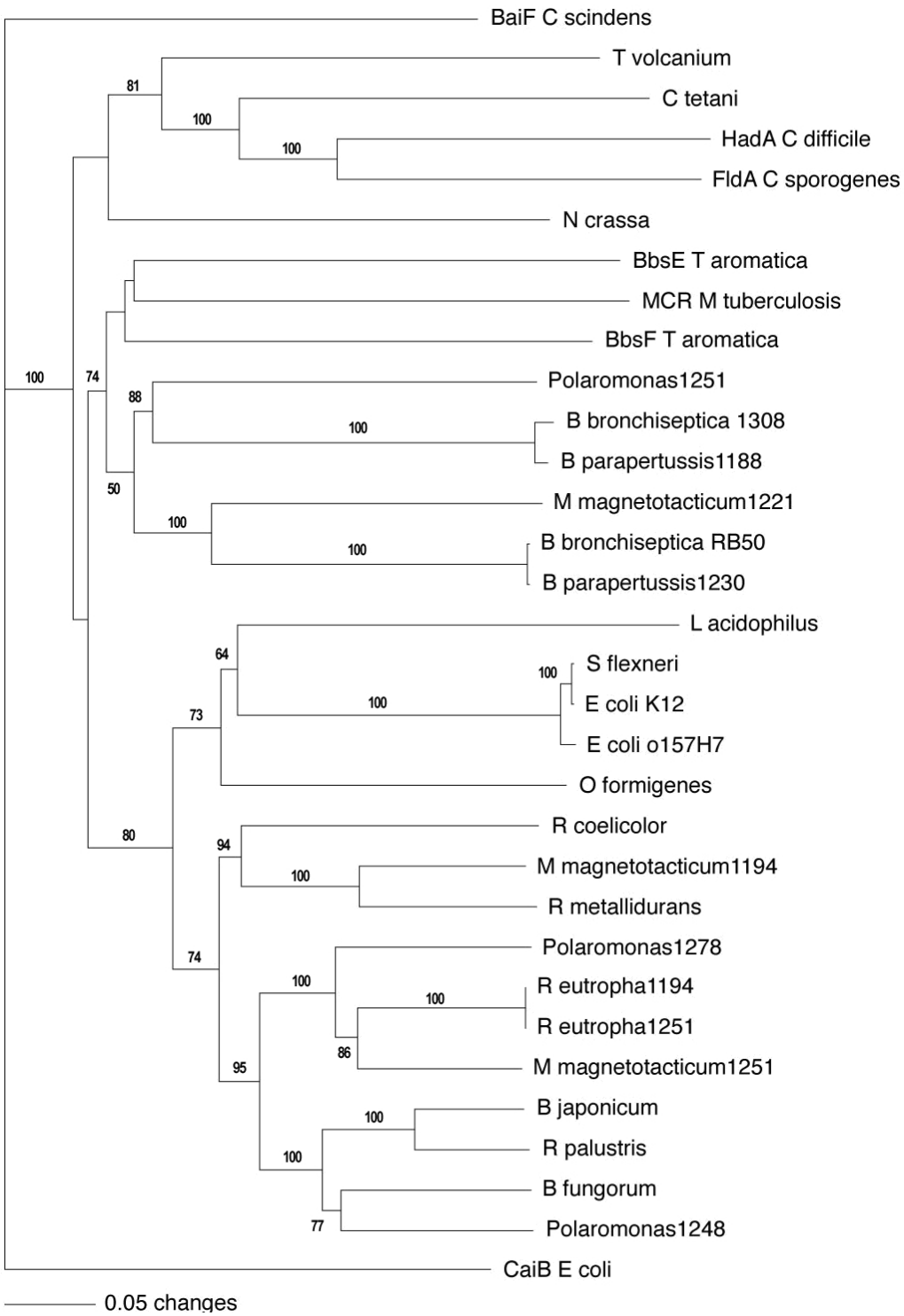

Figure.C-1. Phylogram of Family III CoA transferases from pair-wise sequence alignment of nucleotide sequences.

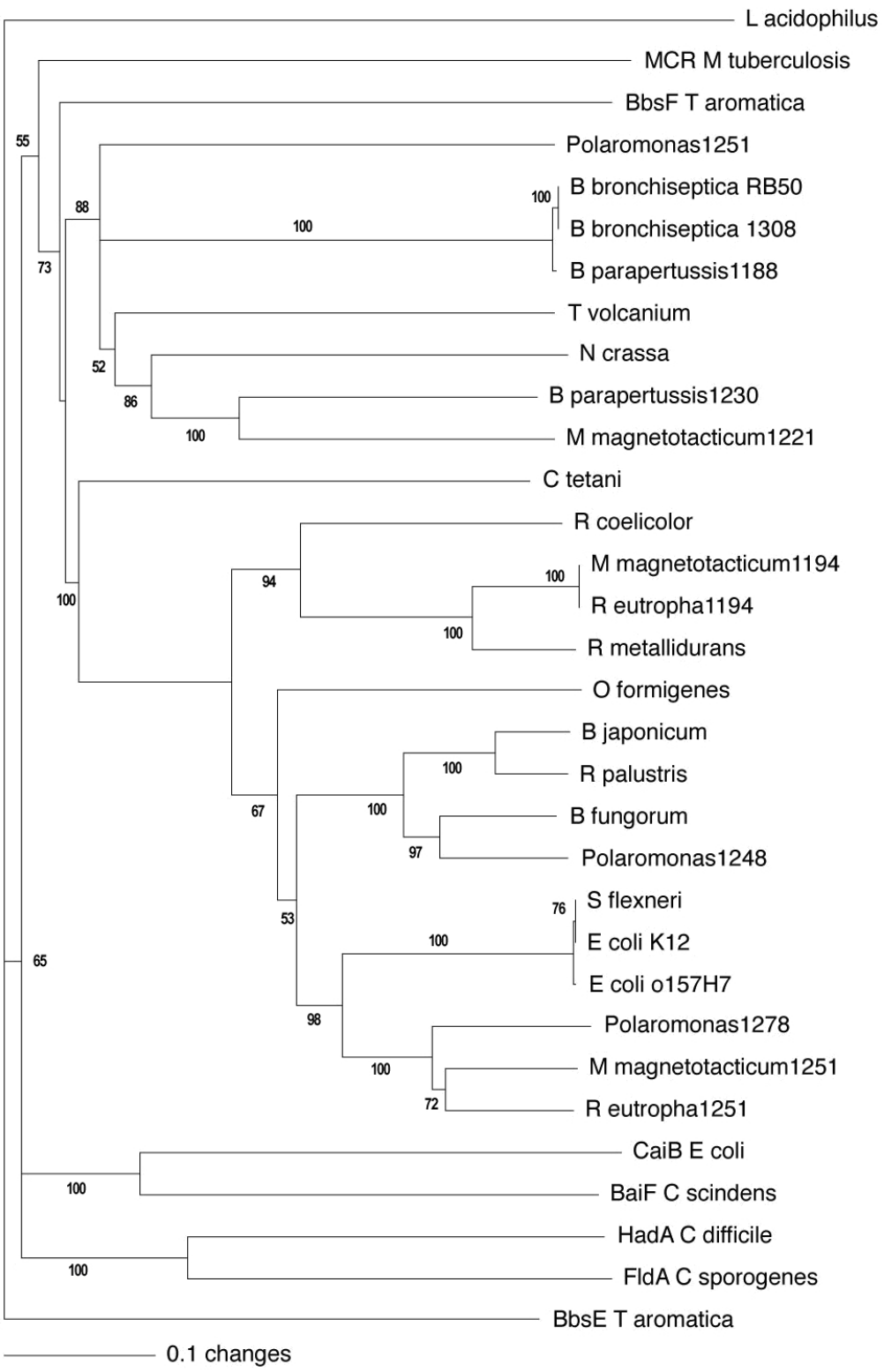

Figure.C-2. Phylogram of Family III CoA transferases from pair-wise sequence alignment of amino acid sequences.

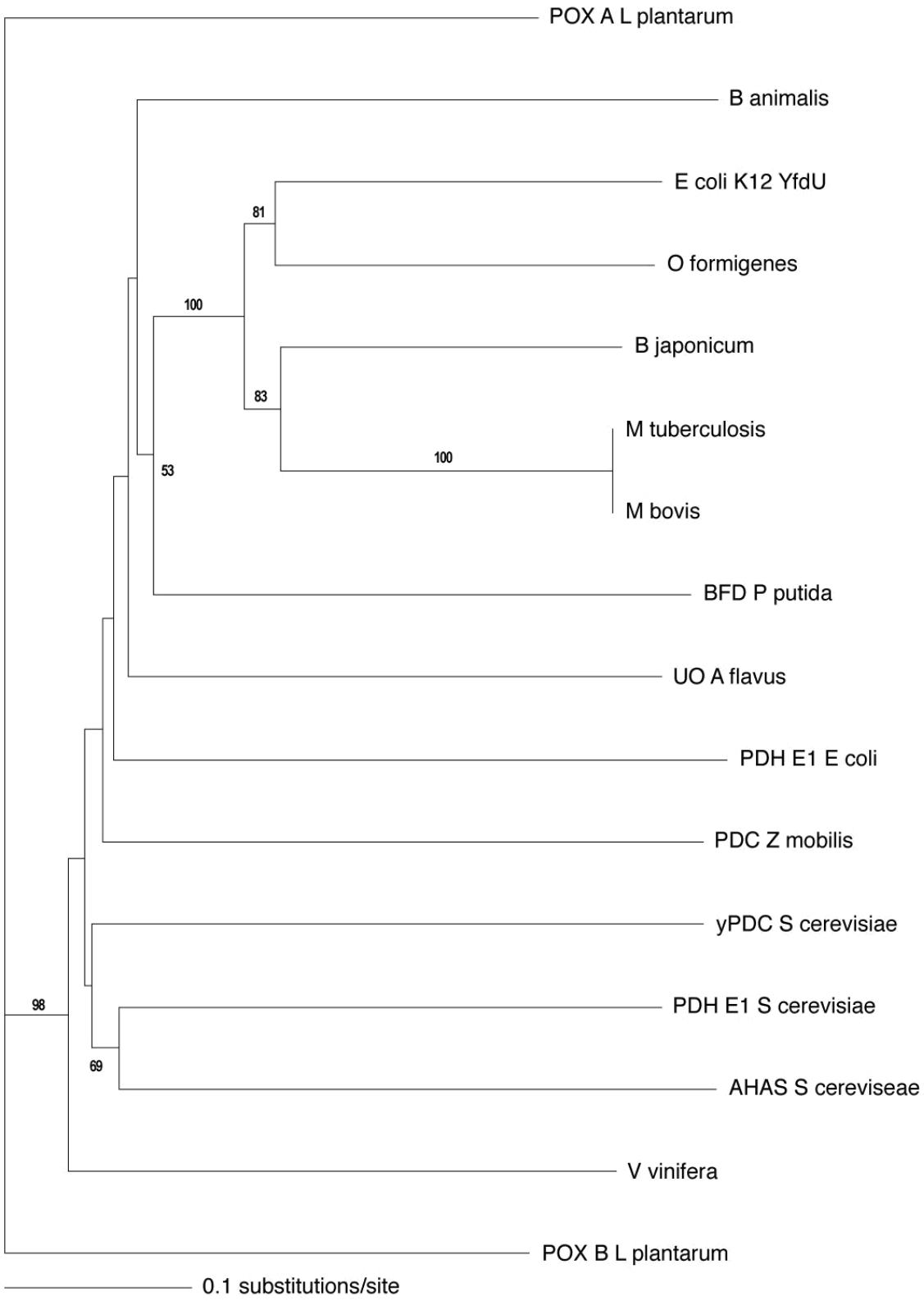

Figure.C-3. Phylogram of ThDP-dependent decarboxylases from pair-wise sequence alignment of nucleotide sequences.

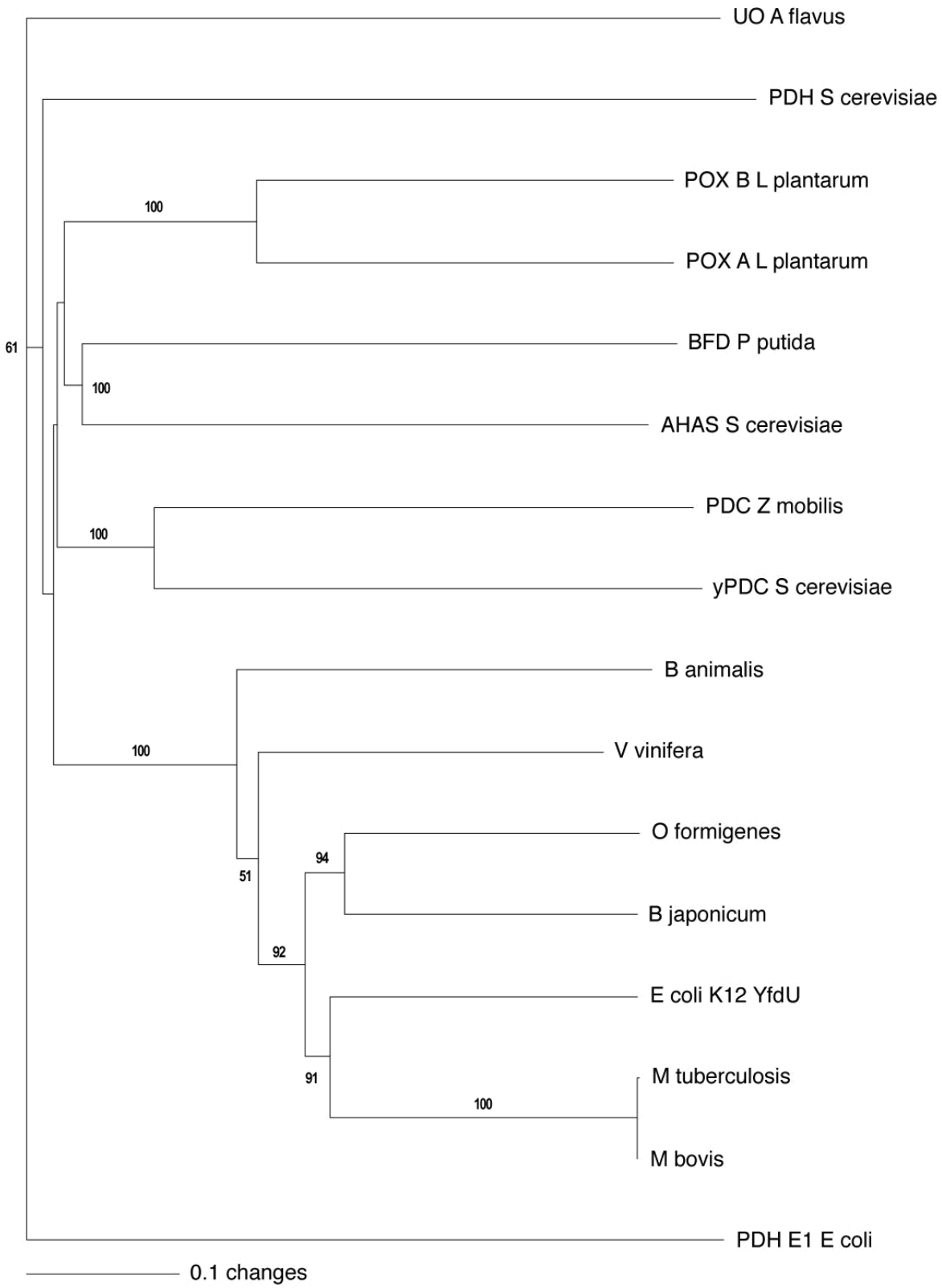

Figure.C-4 Phylogram of ThDP-dependent decarboxylases from pair-wise sequence alignment of amino acid sequences.

LIST OF REFERENCES

1. **Allison, M. J., K. A. Dawson, W. R. Mayberry, and J. G. Foss.** 1985. Oxalobacter formigenes gen. nov., sp. nov.: oxalate-degrading anaerobes that inhabit the gastrointestinal tract. Arch Microbiol **141:**1-7.

2. **Allison, M. J., E. T. Littledike, and L. F. James.** 1977. Changes in ruminal oxalate degradation rates associated with adaptation to oxalate ingestion. J Anim Sci **45:**1173-9.

3. **Anantharam, V., M. J. Allison, and P. C. Maloney.** 1989. Oxalate - Formate Exchange - the Basis for Energy Coupling in Oxalobacter. Journal of Biological Chemistry **264:**7244-7250.

4. **Andersch, W., H. Bahl, and G. Gottschalk.** 1983. Level of Enzymes Involved in Acetate, Butyrate, Acetone and Butanol Formation by *Clostridium-Acetobutylicum.* European Journal of Applied Microbiology and Biotechnology **18:**327-332.

5. **Arjunan, P., M. Sax, A. Brunskill, K. Chandrasekhar, N. Nemeria, S. Zhang, F. Jordan, and W. Furey.** 2006. A thiamin-bound, pre-decarboxylation reaction intermediate analogue in the pyruvate dehydrogenase E1 subunit induces large scale disorder-to-order transformations in the enzyme and reveals novel structural features in the covalently bound adduct. J Biol Chem **281:**15296-303.

6. **Ash, D. E.** 1982. Ph.D. Thesis. University of Pennsylvania.

7. **Azcarate-Peril, M. A., J. M. Bruno-Barcena, H. M. Hassan, and T. R. Klaenhammer.** 2006. Transcriptional and functional analysis of oxalyl-coenzyme A (CoA) decarboxylase and formyl-CoA transferase genes from *Lactobacillus acidophilus*. Applied and Environmental Microbiology **72:**1891-1899.

8. **Baddiley, J., and E. M. Thain.** 1951. Coenzyme-A .2. Evidence for Its Formulation as a Derivative of Pantothenic Acid-4' Phosphate. Journal of the Chemical Society**:**2253-2258.

9. **Baetz, A. L., and M. J. Allison.** 1990. Purification and characterization of formyl-coenzyme A transferase from *Oxalobacter formigenes*. J Bacteriol **172:**3537-40.

10. **Baetz, A. L., and M. J. Allison.** 1989. Purification and characterization of oxalyl-coenzyme A decarboxylase from *Oxalobacter formigenes.* J Bacteriol **171:**2605-8.

11. **Bailey, S.** 1994. The CCP4 Suite - Programs for Protein Crystallography, p. 760-763, Acta Crystallographica Section D-Biological Crystallography, vol. 50.

12. **Barker, H. A., I. M. Jeng, N. Neff, J. M. Robertson, F. K. Tam, and S. Hosaka.** 1978. Butyryl-CoA:acetoacetate CoA-transferase from a lysine-fermenting *Clostridium*. J Biol Chem **253:**1219-25.

13. **Bateman, K. S., E. R. Brownie, W. T. Wolodko, and M. E. Fraser.** 2002. Structure of the mammalian CoA transferase from pig heart. Biochemistry **41:**14455-62.

14. **Benson, R. W., and P. D. Boyer.** 1969. The participation of an enzyme-bound oxygen group in a coenzyme A transferase reaction. J Biol Chem **244:**2366-71.

15. **Berthold, C. L., P. Moussatche, N. G. Richards, and Y. Lindqvist.** 2005. Structural basis for activation of the thiamin diphosphate-dependent enzyme oxalyl-CoA decarboxylase by adenosine diphosphate. J Biol Chem **280:**41645-54.

16. **Berthold, C. L., H. Sidhu, S. Ricagno, N. G. Richards, and Y. Lindqvist.** 2006. Detection and characterization of merohedral twinning in crystals of oxalyl-coenzyme A decarboxylase from *Oxalobacter formigenes.* Biochim Biophys Acta **1764:**122-8.

17. **Berthold, C. L., C. G. Toyota, P. Moussatche, M. D. Wood, F. Leeper, N. G. Richards, and Y. Lindqvist.** 2007. Crystallographic snapshots of oxalyl-CoA decarboxylase give insights into catalysis by nonoxidative ThDP-dependent decarboxylases. Structure **15:**853-61.

18. **Berthold, C. L., C. G. Toyota, N. G. Richards, and Y. Lindqvist.** 2008. Reinvestigation of the Catalytic Mechanism of Formyl-CoA Transferase, a Class III CoA-transferase. J Biol Chem **283:**6519-29.

19. **Beyreuther, K., H. Bohmer, and P. Dimroth.** 1978. Amino-acid sequence of citrate-lyase acyl-carrier protein from *Klebsiella aerogenes*. Eur J Biochem **87:**101-10.

20. **Bhaumik, P., W. Schmitz, A. Hassinen, J. K. Hiltunen, E. Conzelmann, and R. K. Wierenga.** 2007. The catalysis of the 1,1-proton transfer by α-methyl-acyl-CoA racemase is coupled to a movement of the fatty acyl moiety over a hydrophobic, methionine-rich surface. J Mol Biol **367:**1145-61.

21. **Bieber, L. L.** 1988. Carnitine. Annu Rev Biochem **57:**261-83.

22. **Blair, J. B.** 1969. Skeletal muscle coenzyme A transferase. Purification and properties. J Biol Chem **244:**951-4.

23. **Blattner, F. R., G. Plunkett, 3rd, C. A. Bloch, N. T. Perna, V. Burland, M. Riley, J. Collado-Vides, J. D. Glasner, C. K. Rode, G. F. Mayhew, J. Gregor, N. W. Davis, H. A. Kirkpatrick, M. A. Goeden, D. J. Rose, B. Mau, and Y. Shao.** 1997. The complete genome sequence of *Escherichia coli* K-12. Science **277:**1453-74.

24. **Boehr, D. D., D. McElheny, H. J. Dyson, and P. E. Wright.** 2006. The dynamic energy landscape of dihydrofolate reductase catalysis. Science **313:**1638-1642.

25. **Borriello, S. P., and M. H. Wilcox.** 1998. *Clostridium difficile* infections of the gut: the unanswered questions. J Antimicrob Chemother **41 Suppl C:**67-9.

26. **Boynton, Z. L., G. N. Bennett, and F. B. Rudolph.** 1994. Intracellular Concentrations of Coenzyme A and Its Derivatives from *Clostridium acetobutylicum* ATCC 824 and Their Roles in Enzyme Regulation. Appl Environ Microbiol **60:**39-44.

27. **Bradford, M. M.** 1976. A rapid and sensitive method for the quantitation of microgram quantities of protein utilizing the principle of protein-dye binding. Anal Biochem **72:**248-54.

28. **Britz, M. L., and R. G. Wilkinson.** 1982. Leucine dissimilation to isovaleric and isocaproic acids by cell suspensions of amino acid fermenting anaerobes: the Stickland reaction revisited. Can J Microbiol **28:**291-300.

29. **Brunger, A. T., P. D. Adams, G. M. Clore, W. L. DeLano, P. Gros, R. W. Grosse-Kunstleve, J. S. Jiang, J. Kuszewski, M. Nilges, N. S. Pannu, R. J. Read, L. M. Rice, T. Simonson, and G. L. Warren.** 1998. Crystallography & NMR system: A new software suite for macromolecular structure determination. Acta Crystallographica Section D-Biological Crystallography **54:**905-921.

30. **Buckel, W.** 1976. Acetic anhydride: an intermediate analogue in the acyl-exchange reaction of citramalate lyase. Eur J Biochem **64:**263-7.

31. **Buckel, W.** 1992. Unusual Dehydrations in Anaerobic-Bacteria. Fems Microbiology Reviews **88:**211-231.

32. **Buckel, W., and H. A. Barker.** 1974. 2 Pathways of Glutamate Fermentation by Anaerobic Bacteria. Journal of Bacteriology **117:**1248-1260.

33. **Buckel, W., and A. Bobi.** 1976. The enzyme complex citramalate lyase from *Clostridium tetanomorphum*. Eur J Biochem **64:**255-62.

34. **Buckel, W., V. Buschmeier, and H. Eggerer.** 1971. [The action mechanism of citrate lyase from *Klebsiella aerogenes*]. Hoppe Seylers Z Physiol Chem **352:**1195-205.

35. **Buckel, W., U. Dorn, and R. Semmler.** 1981. Glutaconate CoA-transferase from *Acidaminococcus fermentans*. Eur J Biochem **118:**315-21.

36. **Burns, K. L., L. T. Gelbaum, M. C. Sullards, D. E. Bostwick, and S. W. May.** 2005. Iso-coenzyme A. J Biol Chem **280:**16550-8.

37. **Caldwell, J., A. J. Hutt, and S. Fournelgigleux.** 1988. The Metabolic Chiral Inversion and Dispositional Enantioselectivity of the 2-Arylpropionic Acids and Their Biological Consequences. Biochemical Pharmacology **37:**105-114.

38. **Campieri, C., M. Campieri, V. Bertuzzi, E. Swennen, D. Matteuzzi, S. Stefoni, F. Pirovano, C. Centi, S. Ulisse, G. Famularo, and C. De Simone.** 2001. Reduction of oxaluria after an oral course of lactic acid bacteria at high concentration. Kidney Int **60:**1097-105.

39. **Cardon, B. P., and H. A. Barker.** 1946. Two New Amino-Acid-Fermenting Bacteria, *Clostridium propionicum* and *Diplococcus glycinophilus*. J Bacteriol **52:**629-634.

40. **Chang, A. K., P. F. Nixon, and R. G. Duggleby.** 2000. Effects of deletions at the carboxyl terminus of *Zymomonas mobilis* pyruvate decarboxylase on the kinetic properties and substrate specificity. Biochemistry **39:**9430-7.

41. **Chen, L., Y. H. Shen, R. Jia, A. J. Xie, B. Huang, X. B. Cheng, Q. F. Zhang, and R. Y. Guo.** 2007. The role of *Escherichia* coliform in the biomineralization of calcium oxalate crystals. European Journal of Inorganic Chemistry**:**3201-3207.

42. **Chica, R. A., N. Doucet, and J. N. Pelletier.** 2005. Semi-rational approaches to engineering enzyme activity: combining the benefits of directed evolution and rational design. Current Opinion in Biotechnology **16:**378-384.

43. **Chohnan, S., K. Akagi, and Y. Takamura.** 2003. Functions of malonate decarboxylase subunits from *Pseudomonas putida*. Biosci Biotechnol Biochem **67:**214-7.

44. **Chohnan, S., T. Fujio, T. Takaki, M. Yonekura, H. Nishihara, and Y. Takamura.** 1998. Malonate decarboxylase of *Pseudomonas putida* is composed of five subunits. FEMS Microbiol Lett **169:**37-43.

45. **Chohnan, S., H. Furukawa, T. Fujio, H. Nishihara, and Y. Takamura.** 1997. Changes in the size and composition of intracellular pools of nonesterified coenzyme A and coenzyme A thioesters in aerobic and facultatively anaerobic bacteria. Appl Environ Microbiol **63:**553-60.

46. **Chohnan, S., H. Izawa, H. Nishihara, and Y. Takamura.** 1998. Changes in size of intracellular pools of coenzyme A and its thioesters in *Escherichia coli* K-12 cells to various carbon sources and stresses. Biosci Biotechnol Biochem **62:**1122-8.

47. **Cleland, W. W.** 1979. Statistical Analysis of Enzyme Kinetic Data, p. 151-160. *In* D. S. Purich (ed.), Methods of Enzymology, vol. 62. Academic Press, New York.

48. **Conway, A., and D. E. Koshland, Jr.** 1968. Negative cooperativity in enzyme action. The binding of diphosphopyridine nucleotide to glyceraldehyde 3-phosphate dehydrogenase. Biochemistry **7:**4011-23.

49. **Cooper, R. A., K. Itiaba, and H. L. Kornberg.** 1965. The Utilization of Aconate and Itaconate by *Micrococcus* Sp. Biochem J **94:**25-31.

50. **Cooper, R. A., and H. L. Kornberg.** 1964. The utilization of itaconate by *Pseudomonas* sp. Biochem J **91:**82-91.

51. **Cornick, N. A., and M. J. Allison.** 1996. Anabolic incorporation of oxalate by *Oxalobacter formigenes*. Applied and Environmental Microbiology **62:**3011-3013.

52. **Cornick, N. A., and M. J. Allison.** 1996. Assimilation of oxalate, acetate, and CO_2 by *Oxalobacter formigenes*. Can J Microbiol **42:**1081-6.

53. **Coros, A. M., L. Swenson, W. T. Wolodko, and M. E. Fraser.** 2004. Structure of the CoA transferase from pig heart to 1.7 A resolution. Acta Crystallogr D Biol Crystallogr **60:**1717-25.

54. **Corthesy-Theulaz, I. E., G. E. Bergonzelli, H. Henry, D. Bachmann, D. F. Schorderet, A. L. Blum, and L. N. Ornston.** 1997. Cloning and characterization of *Helicobacter pylori* succinyl CoA:acetoacetate CoA-transferase, a novel prokaryotic member of the CoA-transferase family. J Biol Chem **272:**25659-67.

55. **Davis, J. T., R. N. Moore, B. Imperiali, A. J. Pratt, K. Kobayashi, S. Masamune, A. J. Sinskey, C. T. Walsh, T. Fukui, and K. Tomita.** 1987. Biosynthetic Thiolase from Zoogloea-Ramigera .1. Preliminary Characterization and Analysis of Proton-Transfer Reaction. Journal of Biological Chemistry **262:**82-89.

56. **Dawson, K. A., M. J. Allison, and P. A. Hartman.** 1980. Characteristics of anaerobic oxalate-degrading enrichment cultures from the rumen. Appl Environ Microbiol **40:**840-6.

57. **Dawson, K. A., M. J. Allison, and P. A. Hartman.** 1980. Isolation and some characteristics of anaerobic oxalate-degrading bacteria from the rumen. Appl Environ Microbiol **40:**833-9.

58. **Dehning, I., and B. Schink.** 1989. 2 New Species of Anaerobic Oxalate-Fermenting Bacteria, *Oxalobacter-vibrioformis* Sp-Nov and *Clostridium-oxalicum* Sp-Nov, from Sediment Samples. Archives of Microbiology **153:**79-84.

59. **DeLano, W. L.** 2002. PYMOL. DeLano Scientific LLC, Palo Alto, CA.

60. **Dickert, S., A. J. Pierik, D. Linder, and W. Buckel.** 2000. The involvement of coenzyme A esters in the dehydration of (R)-phenyllactate to (E)-cinnamate by Clostridium sporogenes. Eur J Biochem **267:**3874-84.

61. **Dimroth, P.** 1976. The prosthetic group of citrate-lyase acyl-carrier protein. Eur J Biochem **64:**269-81.

62. **Dimroth, P., W. Buckel, R. Loyal, and H. Eggerer.** 1977. Isolation and function of the subunits of citramalate lyase and formation of hybrids with the subunits of citrate lyase. Eur J Biochem **80:**469-77.

63. **Dimroth, P., and H. Eggerer.** 1975. Isolation of subunits of citrate lyase and characterization of their function in the enzyme complex. Proc Natl Acad Sci U S A **72:**3458-62.

64. **Dimroth, P., and H. Hilbi.** 1997. Enzymic and genetic basis for bacterial growth on malonate. Mol Microbiol **25:**3-10.

65. **Dimroth, P., R. Loyal, and H. Eggerer.** 1977. Characterization of the isolated transferase subunit of citrate lyase as a CoA-Transferase. Evidence against a covalent enzyme-substrate intermediate. Eur J Biochem **80:**479-88.

66. **Doane, L. T., M. Liebman, and D. R. Caldwell.** 1989. Microbial Oxalate Degradation - Effects on Oxalate and Calcium Balance in Humans. Nutrition Research **9:**957-964.

67. **Duggleby, R. G.** 2006. Domain relationships in thiamine diphosphate-dependent enzymes. Acc Chem Res **39:**550-7.

68. **Dunathan, H. C.** 1971. Stereochemical aspects of pyridoxal phosphate catalysis. Adv Enzymol Relat Areas Mol Biol **35:**79-134.

69. **Duncan, S. H., A. J. Richardson, P. Kaul, R. P. Holmes, M. J. Allison, and C. S. Stewart.** 2002. *Oxalobacter formigenes* and its potential role in human health. Appl Environ Microbiol **68:**3841-7.

70. **Edelhoch, H.** 1967. Spectroscopic determination of tryptophan and tyrosine in proteins. Biochemistry **6:**1948-54.

71. **Edwards, M. R., M. Singh, and P. K. Tubbs.** 1973. A simple purification of acetoacetate-succinate CoA-transferase using substrate elution chromatography. FEBS Lett **37:**155-8.

72. **Eisenmesser, E. Z., O. Millet, W. Labeikovsky, D. M. Korzhnev, M. Wolf-Watz, D. A. Bosco, J. J. Skalicky, L. E. Kay, and D. Kern.** 2005. Intrinsic dynamics of an enzyme underlies catalysis. Nature **438:**117-121.

73. **Elsden, S. R., and M. G. Hilton.** 1978. Volatile acid production from threonine, valine, leucine and isoleucine by clostridia. Arch Microbiol **117:**165-72.

74. **Elssner, T., C. Engemann, K. Baumgart, and H. P. Kleber.** 2001. Involvement of coenzyme A esters and two new enzymes, an enoyl-CoA hydratase and a CoA-transferase, in the hydration of crotonobetaine to L-carnitine by Escherichia coli. Biochemistry **40:**11140-8.

75. **Elssner, T., L. Hennig, H. Frauendorf, D. Haferburg, and H. P. Kleber.** 2000. Isolation, identification, and synthesis of gamma-butyrobetainyl-CoA and crotonobetainyl-CoA, compounds involved in carnitine metabolism of E. coli. Biochemistry **39:**10761-9.

76. **Emsley, P., and K. Cowtan.** 2004. Coot: model-building tools for molecular graphics. Acta Crystallogr D Biol Crystallogr **60:**2126-32.

77. **Engemann, C., T. Elssner, S. Pfeifer, C. Krumbholz, T. Maier, and H. P. Kleber.** 2005. Identification and functional characterisation of genes and corresponding enzymes involved in carnitine metabolism of *Proteus* sp. Arch Microbiol **183:**176-89.

78. **Engemann, C., T. Elssner, S. Pfeifer, C. Krumbholz, T. Maier, and H. P. Kleber.** 2005. Identification and functional characterisation of genes and corresponding enzymes involved in carnitine metabolism of *Proteus* sp. Archives of Microbiology **183:**176-189.

79. **Engemann, C., and H. P. Kleber.** 2001. Epigenetic regulation of carnitine metabolising enzymes in Proteus sp. under aerobic conditions. FEMS Microbiol Lett **196:**1-6.

80. **Feldberg, W., and T. Mann.** 1946. Properties and Distribution of the Enzyme System Which Synthesizes Acetylcholine in Nervous Tissue. Journal of Physiology-London **104:**411-425.

81. **Fersht, A.** 1999. Structure and Mechanism in Protein Science. A Guide to Enzyme Catalysis and Protein Folding, p. 44-51, 1 ed. Freeman, New York.

82. **Fiedler, E., S. Thorell, T. Sandalova, R. Golbik, S. Konig, and G. Schneider.** 2002. Snapshot of a key intermediate in enzymatic thiamin catalysis: crystal structure of the alpha-carbanion of (alpha,beta-dihydroxyethyl)-thiamin diphosphate in the active site of transketolase from *Saccharomyces cerevisiae*. Proc Natl Acad Sci U S A **99:**591-5.

83. **Fierke, C. A., and W. P. Jencks.** 1986. 2 Functional Domains of Coenzyme a Activate Catalysis by Coenzyme a Transferase - Pantetheine and Adenosine 3'-Phosphate 5'-Diphosphate. Journal of Biological Chemistry **261:**7603-7606.

84. **Foster, J. W.** 2004. *Escherichia coli* acid resistance: tales of an amateur acidophile. Nat Rev Microbiol **2:**898-907.

85. **Franceschi, V. R., and P. A. Nakata.** 2005. Calcium oxalate in plants: Formation and function. Annual Review of Plant Biology **56:**41-71.

86. **Frank, R. A., C. M. Titman, J. V. Pratap, B. F. Luisi, and R. N. Perham.** 2004. A molecular switch and proton wire synchronize the active sites in thiamine enzymes. Science **306:**872-6.

87. **Friedmann, S., A. Steindorf, B. E. Alber, and G. Fuchs.** 2006. Properties of succinyl-coenzyme A:L-malate coenzyme A transferase and its role in the autotrophic 3-hydroxypropionate cycle of *Chloroflexus aurantiacus*. J Bacteriol **188:**2646-55.

88. **Furey, W., P. Arjunan, A. Brunksill, K. Chandrasekhar, N. Nemeria, W. Wei, Y. Yan, Z. Zhang, and F. Jordan.** 2004. Structure and intersubunit information transfer in the *E. coli* pyruvate dehydrogenase multienzyme complex, p. 407-432. *In* F. Jordan and M. S. Patel (ed.), Thiamine: Catalytic Mechanisms in Normal and Disease States (Oxidative Stress and Disease). Marcel Dekker, New York.

89. **Gill, S. C., and P. H. von Hippel.** 1989. Calculation of protein extinction coefficients from amino acid sequence data. Anal Biochem **182:**319-26.

90. **Glasner, M. E., J. A. Gerlt, and P. C. Babbitt.** 2006. Evolution of enzyme superfamilies. Current Opinion in Chemical Biology **10:**492-497.

91. **Gobel, M., K. Kassel-Cati, E. Schmidt, and W. Reineke.** 2002. Degradation of aromatics and chloroaromatics by *Pseudomonas* sp. strain B13: cloning, characterization, and analysis of sequences encoding 3-oxoadipate:succinyl-coenzyme A (CoA) transferase and 3-oxoadipyl-CoA thiolase. J Bacteriol **184:**216-23.

92. **Gogos, A., J. Gorman, and L. Shapiro.** 2004. Structure of Escherichia coli YfdW, a type III CoA transferase. Acta Crystallogr D Biol Crystallogr **60:**507-11.

93. **Gokhale, R. S., S. Agarwalla, D. V. Santi, and P. Balaram.** 1996. Covalent reinforcement of a fragile region in the dimeric enzyme thymidylate synthase stabilizes the protein against chaotrope-induced unfolding. Biochemistry **35:**7150-8.

94. **Goto, S., T. Nishioka, and M. Kanehisa.** 2000. LIGAND: chemical database of enzyme reactions. Nucleic Acids Research **28:**380-382.

95. **Goto, S., Y. Okuno, M. Hattori, T. Nishioka, and M. Kanehisa.** 2002. LIGAND: database of chemical compounds and reactions in biological pathways. Nucleic Acids Research **30:**402-404.

96. **Goto, Y., and A. L. Fink.** 1989. Conformational states of beta-lactamase: molten-globule states at acidic and alkaline pH with high salt. Biochemistry **28:**945-52.

97. **Gruez, A., V. Roig-Zamboni, C. Valencia, V. Campanacci, and C. Cambillau.** 2003. The crystal structure of the Escherichia coli YfdW gene product reveals a new fold of two interlaced rings identifying a wide family of CoA transferases. J Biol Chem **278:**34582-6.

98. **Haas, E.** 2005. The study of protein folding and dynamics by determination of intramolecular distance distributions and their fluctuations using ensemble and single-molecule FRET measurements. Chemphyschem **6:**858-70.

99. **Hatch, M., J. Cornelius, M. Allison, H. Sidhu, A. Peck, and R. W. Freel.** 2006. *Oxalobacter* sp. reduces urinary oxalate excretion by promoting enteric oxalate secretion. Kidney Int **69:**691-8.

100. **Hayaishi, O.** 1955. Enzymatic decarboxylation of malonic acid. J Biol Chem **215:**125-36.

101. **Hayashi, T., K. Makino, M. Ohnishi, K. Kurokawa, K. Ishii, K. Yokoyama, C. G. Han, E. Ohtsubo, K. Nakayama, T. Murata, M. Tanaka, T. Tobe, T. Iida, H. Takami, T. Honda, C. Sasakawa, N. Ogasawara, T. Yasunaga, S. Kuhara, T. Shiba, M. Hattori, and H. Shinagawa.** 2001. Complete genome sequence of enterohemorrhagic *Escherichia coli* O157:H7 and genomic comparison with a laboratory strain K-12. DNA Res **8:**11-22.

102. **Heider, J.** 2001. A new family of CoA-transferases. FEBS Lett **509:**345-9.

103. **Heider, J., and G. Fuchs.** 1997. Microbial anaerobic aromatic metabolism. Anaerobe **3:**1-22.

104. **Heider, J., A. M. Spormann, H. R. Beller, and F. Widdel.** 1998. Anaerobic bacterial metabolism of hydrocarbons. Fems Microbiology Reviews **22:**459-473.

105. **Heilberg, I. P., and N. Schor.** 2006. Renal stone disease: Causes, evaluation and medical treatment. Arq Bras Endocrinol Metabol **50:**823-31.

106. **Hersh, L. B., and W. P. Jencks.** 1967. Coenzyme A Transferase. J Biol Chem **242:**3468-80.

107. **Hiltunen, J. K., and Y. Qin.** 2000. β-oxidation - strategies for the metabolism of a wide variety of acyl-CoA esters. Biochim Biophys Acta **1484:**117-28.

108. **Hirai, T., and S. Subramaniam.** 2004. Structure and transport mechanism of the bacterial oxalate transporter OxlT. Biophys J **87:**3600-7.

109. **Ho, S. N., H. D. Hunt, R. M. Horton, J. K. Pullen, and L. R. Pease.** 1989. Site-directed mutagenesis by overlap extension using the polymerase chain reaction. Gene **77:**51-9.

110. **Hodgkinson, A.** 1977. Oxalic acid in biology and medicine. Academic Press, London ; New York.

111. **Hokama, S., Y. Honma, C. Toma, and Y. Ogawa.** 2000. Oxalate-degrading *Enterococcus faecalis*. Microbiol Immunol **44:**235-40.

112. **Holmes, R. P., and D. G. Assimos.** 1998. Glyoxylate synthesis, and its modulation and influence on oxalate synthesis. J Urol **160:**1617-24.

113. **Hoppe, B., B. Beck, N. Gatter, G. von Unruh, A. Tischer, A. Hesse, N. Laube, P. Kaul, and H. Sidhu.** 2006. *Oxalobacter formigenes*: a potential tool for the treatment of primary hyperoxaluria type 1. Kidney International **70:**1305-1311.

114. **Hoppe, B., G. von Unruh, N. Laube, A. Hesse, and H. Sidhu.** 2005. Oxalate degrading bacteria: new treatment option for patients with primary and secondary hyperoxaluria? Urological Research **33:**372-375.

115. **Howard, J. B., L. Zieske, J. Clarkson, and L. Rathe.** 1986. Mechanism-based fragmentation of coenzyme A transferase. Comparison of alpha 2-macroglobulin and coenzyme A transferase thiol ester reactions. J Biol Chem **261:**60-5.

116. **Hubbell, W. L., D. S. Cafiso, and C. Altenbach.** 2000. Identifying conformational changes with site-directed spin labeling. Nat Struct Biol **7:**735-9.

117. **Ito, H., T. Kotake, and M. Masai.** 1996. In vitro degradation of oxalic acid by human feces. Int J Urol **3:**207-11.

118. **Jackowski, S., and C. O. Rock.** 1986. Consequences of reduced intracellular coenzyme A content in *Escherichia coli*. J Bacteriol **166:**866-71.

119. **Jacob, U., M. Mack, T. Clausen, R. Huber, W. Buckel, and A. Messerschmidt.** 1997. Glutaconate CoA-transferase from Acidaminococcus fermentans: the crystal structure reveals homology with other CoA-transferases. Structure **5:**415-26.

120. **James, L. F., J. C. Street, and J. E. Butcher.** 1967. In vitro degradation of oxalate and of cellulose by rumen ingesta from sheep fed *Halogeton glomeratus*. J Anim Sci **26:**1438-44.

121. **Johnson, E. F., W. Hinz, C. E. Atreya, F. Maley, and K. S. Anderson.** 2002. Mechanistic characterization of *Toxoplasma gondii* thymidylate synthase (TS-DHFR)-dihydrofolate reductase. Evidence for a TS intermediate and TS half-sites reactivity. J Biol Chem **277:**43126-36.

122. **Jones, D. T., and D. R. Woods.** 1986. Acetone-butanol fermentation revisited. Microbiol Rev **50:**484-524.

123. **Jonsson, S.** 2004. The mechanism of Formyl-Coenzyme A Transferase, A Family III CoA Transferase from *Oxalobacter formigenes*. PhD Dissertation. University of Florida, Gainesville.

124. **Jonsson, S., S. Ricagno, Y. Lindqvist, and N. G. Richards.** 2004. Kinetic and mechanistic characterization of the formyl-CoA transferase from *Oxalobacter formigenes*. J Biol Chem **279:**36003-12.

125. **Jordan, F., M. Liu, L. Serrano, Z. Zhang, A. Brunksill, P. Arjunan, and W. Furey.** 2004. Yeast pyruvate decarboxylase: new features of the structure and mechanism., p. 173-215. *In* F. Jordan and M. S. Patel (ed.), Thiamine: Catalytic Mechanisms in Normal and Disease States (Oxidative Stress and Disease). Marcel Dekker, New York.

126. **Jordan, F., and N. S. Nemeria.** 2005. Experimental observation of thiamin diphosphate-bound intermediates on enzymes and mechanistic information derived from these observations. Bioorg Chem **33:**190-215.

127. **Jordan, F., N. S. Nemeria, and E. Sergienko.** 2005. Multiple modes of active center communication in thiamin diphosphate-dependent enzymes. Acc Chem Res **38:**755-63.

128. **Jung, H., K. Jung, and H. P. Kleber.** 1990. L-carnitine metabolization and osmotic stress response in *Escherichia coli.* J Basic Microbiol **30:**409-13.

129. **Kannan, G., J. C. Wilks, D. M. Fitzgerald, B. D. Jones, S. S. Bondurant, and J. L. Slonczewski.** 2008. Rapid acid treatment of *Escherichia coli*: transcriptomic response and recovery. BMC Microbiol **8:**37.

130. **Kaplun, A., E. Binshtein, M. Vyazmensky, A. Steinmetz, Z. Barak, D. M. Chipman, K. Tittmann, and B. Shaanan.** 2008. Glyoxylate carboligase lacks the canonical active site glutamate of thiamine-dependent enzymes. Nat Chem Biol **4:**113-8.

131. **Kaschabek, S. R., B. Kuhn, D. Muller, E. Schmidt, and W. Reineke.** 2002. Degradation of aromatics and chloroaromatics by *Pseudomonas* sp. strain B13: purification and characterization of 3-oxoadipate:succinyl-coenzyme A (CoA) transferase and 3-oxoadipyl-CoA thiolase. J Bacteriol **184:**207-15.

132. **Katagiri, M., and O. Hayaishi.** 1957. Enzymatic degradation of beta-ketoadipic acid. J Biol Chem **226:**439-48.

133. **Kaur, J., and R. Sharma.** 2006. Directed evolution: An approach to engineer enzymes. Critical Reviews in Biotechnology **26:**165-199.

134. **Kern, D., G. Kern, H. Neef, K. Tittmann, M. Killenberg-Jabs, C. Wikner, G. Schneider, and G. Hubner.** 1997. How thiamine diphosphate is activated in enzymes. Science **275:**67-70.

135. **Kern, D., G. Kern, G. Scherer, G. Fischer, and T. Drakenberg.** 1995. Kinetic-Analysis of Cyclophilin-Catalyzed Prolyl Cis/Trans Isomerization by Dynamic Nmr-Spectroscopy. Biochemistry **34:**13594-13602.

136. **Kim, J., D. G. Beak, Y. T. Kim, J. D. Choi, and M. Y. Yoon.** 2004. Effects of deletions at the C-terminus of tobacco acetohydroxyacid synthase on the enzyme activity and cofactor binding. Biochemical Journal **384:**59-68.

137. **Kim, J., D. Darley, T. Selmer, and W. Buckel.** 2006. Characterization of (R)-2-hydroxyisocaproate dehydrogenase and a family III coenzyme A transferase involved in reduction of L-leucine to isocaproate by *Clostridium difficile*. Appl Environ Microbiol **72:**6062-9.

138. **Kleber, H. P.** 1997. Bacterial carnitine metabolism. FEMS Microbiol Lett **147:**1-9.

139. **Knoop, F.** 1904/05. Der Abbau aromatischer Fettsäuren im Tierkörper. Beitr. Chem. Physiol. Pathol. **6:**150-62.

140. **Kosaka, T., T. Uchiyama, S. Ishii, M. Enoki, H. Imachi, Y. Kamagata, A. Ohashi, H. Harada, H. Ikenaga, and K. Watanabe.** 2006. Reconstruction and regulation of the central catabolic pathway in the thermophilic propionate-oxidizing syntroph *Pelotomaculum thermopropionicum*. J Bacteriol **188:**202-10.

141. **Koshland, D. E., Jr.** 1996. The structural basis of negative cooperativity: receptors and enzymes. Curr Opin Struct Biol **6:**757-61.

142. **Kuhner, C. H., P. A. Hartman, and M. J. Allison.** 1996. Generation of a proton motive force by the anaerobic oxalate-degrading bacterium *Oxalobacter formigenes*. Appl Environ Microbiol **62:**2494-500.

143. **Laker, M. F., A. F. Hofmann, and B. J. Meeuse.** 1980. Spectrophotometric determination of urinary oxalate with oxalate oxidase prepared from moss. Clin Chem **26:**827-30.

144. **Laskowski, R. A., M. W. Macarthur, D. S. Moss, and J. M. Thornton.** 1993. Procheck - a Program to Check the Stereochemical Quality of Protein Structures. Journal of Applied Crystallography **26:**283-291.

145. **Leeper, F. J., D. Hawksley, S. Mann, C. P. Melero, and M. D. H. Wood.** 2005. Studies on thiamine diphosphate-dependent enzymes. Biochemical Society Transactions **33:**772-775.

146. **Leslie, A. G. W.** 1992. Jnt CCP4/ESF-EACBM Newsl. Protein Crystallogr. **26**.

147. **Leslie, A. G. W.** 1997. MOSFLM, version 5.40. MRC Laboratory of Molecular Biology, Cambridge, United Kingdom.

148. **Leuthner, B., and J. Heider.** 2000. Anaerobic toluene catabolism of *Thauera aromatica*: the *bbs* operon codes for enzymes of β oxidation of the intermediate benzylsuccinate. J Bacteriol **182:**272-7.

149. **Leutwein, C., and J. Heider.** 2001. Succinyl-CoA:(R)-benzylsuccinate CoA-transferase: an enzyme of the anaerobic toluene catabolic pathway in denitrifying bacteria. J Bacteriol **183:**4288-95.

150. **Liang, C. Z., and K. Mislow.** 1995. Topological Features of Protein Structures - Knots and Links. Journal of the American Chemical Society **117:**4201-4213.

151. **Lindqvist, Y., G. Schneider, U. Ermler, and M. Sundstrom.** 1992. Three-dimensional structure of transketolase, a thiamine diphosphate dependent enzyme, at 2.5 A resolution. Embo J **11:**2373-9.

152. **Lipmann, F.** 1945. Acetylation of Sulfanilamide by Liver Homogenates and Extracts. Journal of Biological Chemistry **160:**173-190.

153. **Lipmann, F., N. O. Kaplan, G. D. Novelli, and L. C. Tuttle.** 1950. Isolation of Coenzyme-A. Journal of Biological Chemistry **186:**235-243.

154. **Lipmann, F., N. O. Kaplan, G. D. Novelli, L. C. Tuttle, and B. M. Guirard.** 1947. Coenzyme for Acetylation, a Pantothenic Acid Derivative. Journal of Biological Chemistry **167:**869-870.

155. **Lipmann, F., N. O. Kaplan, and G. K. Novelli.** 1947. Chemistry and Distribution of the Coenzyme for Acetylation (Coenzyme-a). Federation Proceedings **6:**272-272.

156. **Lloyd, A. J., and P. M. Shoolingin-Jordan.** 2001. Dimeric pig heart succinate-coenzyme A transferase uses only one subunit to support catalysis. Biochemistry **40:**2455-67.

157. **Lohkamp, B., Emsley, P., and Cowtan, K.** 2005. CCP4 Newsletter **42:**Contribution 7.

158. **Lynen, F.** 1942. Zum biologischen Abbau der Essigsäure. I. Über die 'Induktionszeit' bei verarmter hefe. Liebig's Ann. **552:**270-306.

159. **Lynen, F., E. Reichert, and L. Rueff.** 1951. *Zum Biologischen Abbau Der Essigsaure .6. Aktivierte Essigsaure, Ihre Isolierung Aus Hefe Und Ihre Chemische Natur. Annalen Der Chemie-Justus Liebig **574:**1-32.

160. **Ma, Z., S. Gong, H. Richard, D. L. Tucker, T. Conway, and J. W. Foster.** 2003. GadE (YhiE) activates glutamate decarboxylase-dependent acid resistance in *Escherichia coli* K-12. Mol Microbiol **49:**1309-20.

161. **Machius, M., R. M. Wynn, J. L. Chuang, J. Li, R. Kluger, D. Yu, D. R. Tomchick, C. A. Brautigam, and D. T. Chuang.** 2006. A versatile conformational switch regulates reactivity in human branched-chain alpha-ketoacid dehydrogenase. Structure **14:**287-98.

162. **Mack, M., K. Bendrat, O. Zelder, E. Eckel, D. Linder, and W. Buckel.** 1994. Location of the two genes encoding glutaconate coenzyme A-transferase at the beginning of the hydroxyglutarate operon in *Acidaminococcus fermentans*. Eur J Biochem **226:**41-51.

163. **Mack, M., and W. Buckel.** 1997. Conversion of glutaconate CoA-transferase from *Acidaminococcus fermentans* into an acyl-CoA hydrolase by site-directed mutagenesis. Febs Letters **405:**209-212.

164. **Mack, M., and W. Buckel.** 1995. Identification of glutamate beta 54 as the covalent-catalytic residue in the active site of glutaconate CoA-transferase from *Acidaminococcus fermentans*. FEBS Lett **357:**145-8.

165. **Mallam, A. L., and S. E. Jackson.** 2005. Folding studies on a knotted protein. J Mol Biol **346:**1409-21.

166. **Mann, C. J., and C. R. Matthews.** 1993. Structure and stability of an early folding intermediate of *Escherichia coli* trp aporepressor measured by far-UV stopped-flow circular dichroism and 8-anilino-1-naphthalene sulfonate binding. Biochemistry **32:**5282-90.

167. **Mann, S., C. P. Melero, D. Hawksley, and F. J. Leeper.** 2004. Inhibition of thiamin diphosphate dependent enzymes by 3-deazathiamin diphosphate. Organic & Biomolecular Chemistry **2:**1732-1741.

168. **Masuda, N., and G. M. Church.** 2002. *Escherichia coli* gene expression responsive to levels of the response regulator EvgA. J Bacteriol **184:**6225-34.

169. **Masuda, N., and G. M. Church.** 2003. Regulatory network of acid resistance genes in *Escherichia coli*. Mol Microbiol **48:**699-712.

170. **Minkler, P. E., V. E. Anderson, N. C. Maiti, J. Kerner, and C. L. Hoppel.** 2004. Isolation and identification of two isomeric forms of malonyl-coenzyme A in commercial malonyl-coenzyme A. Anal Biochem **328:**203-9.

171. **Mishra, P. K., and D. G. Drueckhammer.** 2000. Coenzyme A Analogues and Derivatives: Synthesis and Applications as Mechanistic Probes of Coenzyme A Ester-Utilizing Enzymes. Chem Rev **100:**3283-3310.

172. **Mitchell, W. M.** 1968. Hydrolysis at arginylproline in polypeptides by clostridiopeptidase B. Science **162:**374-5.

173. **Mosbacher, T. G., A. Bechthold, and G. E. Schulz.** 2005. Structure and function of the antibiotic resistance-mediating methyltransferase AviRb from *Streptomyces viridochromogenes*. J Mol Biol **345:**535-45.

174. **Murshudov, G. N., A. A. Vagin, and E. J. Dodson.** 1997. Refinement of macromolecular structures by the maximum-likelihood method. Acta Crystallogr D Biol Crystallogr **53:**240-55.

175. **Murshudov, G. N., A. A. Vagin, and E. J. Dodson.** 1997. Refinement of macromolecular structures by the maximum-likelihood method. Acta Crystallographica Section D-Biological Crystallography **53:**240-255.

176. **Nachmansohn, D., and M. Berman.** 1946. Studies on Choline Acetylase .3. On the Preparation of the Coenzyme and Its Effect on the Enzyme. Journal of Biological Chemistry **165:**551-563.

177. **Nachmansohn, D., and A. L. Machado.** 1943. The formation of acetylcholine. A new enzyme 'choline acetylase'. J. Neurophysiol **6:**397-403.

178. **Nakai, T., N. Nakagawa, N. Maoka, R. Masui, S. Kuramitsu, and N. Kamiya.** 2004. Ligand-induced conformational changes and a reaction intermediate in branched-chain 2-oxo acid dehydrogenase (E1) from *Thermus thermophilus* HB8, as revealed by X-ray crystallography. J Mol Biol **337:**1011-33.

179. **Nureki, O., K. Watanabe, S. Fukai, R. Ishii, Y. Endo, H. Hori, and S. Yokoyama.** 2004. Deep knot structure for construction of active site and cofactor binding site of tRNA modification enzyme. Structure **12:**593-602.

180. **O'Brien, P. J., and D. Herschlag.** 1999. Catalytic promiscuity and the evolution of new enzymatic activities. Chemistry & Biology **6:**R91-R105.

181. **Pace, C. N., F. Vajdos, L. Fee, G. Grimsley, and T. Gray.** 1995. How to measure and predict the molar absorption coefficient of a protein. Protein Sci **4:**2411-23.

182. **Pao, S. S., I. T. Paulsen, and M. H. Saier, Jr.** 1998. Major facilitator superfamily. Microbiol Mol Biol Rev **62:**1-34.

183. **Parales, R. E., and C. S. Harwood.** 1992. Characterization of the genes encoding beta-ketoadipate: succinyl-coenzyme A transferase in *Pseudomonas putida.* J Bacteriol **174:**4657-66.

184. **Pauli, G., and P. Overath.** 1972. ato Operon: a highly inducible system for acetoacetate and butyrate degradation in *Escherichia coli.* Eur J Biochem **29:**553-62.

185. **Perkins, D. N., D. J. Pappin, D. M. Creasy, and J. S. Cottrell.** 1999. Probability-based protein identification by searching sequence databases using mass spectrometry data. Electrophoresis **20:**3551-67.

186. **Perna, N. T., G. Plunkett, 3rd, V. Burland, B. Mau, J. D. Glasner, D. J. Rose, G. F. Mayhew, P. S. Evans, J. Gregor, H. A. Kirkpatrick, G. Posfai, J. Hackett, S. Klink, A. Boutin, Y. Shao, L. Miller, E. J. Grotbeck, N. W. Davis, A. Lim, E. T. Dimalanta, K. D. Potamousis, J. Apodaca, T. S. Anantharaman, J. Lin, G. Yen, D. C. Schwartz, R. A. Welch, and F. R. Blattner.** 2001. Genome sequence of enterohaemorrhagic *Escherichia coli* O157:H7. Nature **409:**529-33.

187. **Pickart, C. M., and W. P. Jencks.** 1979. Formation of stable anhydrides from CoA transferase and hydroxamic acids. J Biol Chem **254:**9120-9.

188. **Pillai, A., and R. Nelson.** 2008. Probiotics for treatment of *Clostridium* difficile-associated colitis in adults. Cochrane Database Syst Rev**:**CD004611.

189. **Pleshe, E., J. Truesdell, and R. T. Batey.** 2005. Structure of a class II TrmH tRNA-modifying enzyme from *Aquifex aeolicus*. Acta Crystallograph Sect F Struct Biol Cryst Commun **61:**722-8.

190. **Preusser, A., U. Wagner, T. Elssner, and H. P. Kleber.** 1999. Crotonobetaine reductase from *Escherichia coli* consists of two proteins. Biochim Biophys Acta **1431:**166-78.

191. **Quayle, J. R.** 1963. Carbon assimilation by *Pseudomonas oxalaticus* (OX1). 6. Reactions of oxalyl-coenzyme A. Biochem J **87:**368-73.

192. **Quayle, J. R.** 1963. Carbon Assimilation by *Pseudomonas Oxalaticus* (Ox1). 7. Decarboxylation of Oxalyl-Coenzyme a to Formyl-Coenzyme A. Biochem J **89:**492-503.

193. **Quayle, J. R.** 1962. Chemical synthesis of oxalyl-coenzyme A and its enzymic reduction to glyoxylate. Biochim Biophys Acta **57:**398-400.

194. **Radika, K., and D. B. Northrop.** 1984. The kinetic mechanism of kanamycin acetyltransferase derived from the use of alternative antibiotics and coenzymes. J Biol Chem **259:**12543-6.

195. **Radika, K., and D. B. Northrop.** 1984. Purification of two forms of kanamycin acetyltransferase from *Escherichia coli*. Arch Biochem Biophys **233:**272-85.

196. **Rangarajan, E. S., Y. Li, P. Iannuzzi, M. Cygler, and A. Matte.** 2005. Crystal Structure of *Escherichia coli* Crotonobetainyl-CoA: Carnitine CoA-Transferase (CaiB) and Its Complexes with CoA and Carnitinyl-CoA. Biochemistry **44:**5728-5738.

197. **Ricagno, S., S. Jonsson, N. Richards, and Y. Lindqvist.** 2003. Formyl-CoA transferase encloses the CoA binding site at the interface of an interlocked dimer. Embo J **22:**3210-9.

198. **Richardson, K., and N. E. Tolbert.** 1961. Oxidation of Glyoxylic Acid to Oxalic Acid by Glycolic Acid Oxidase. Journal of Biological Chemistry **236:**1280-&.

199. **Ridlon, J. M., D. J. Kang, and P. B. Hylemon.** 2006. Bile salt biotransformations by human intestinal bacteria. J Lipid Res **47:**241-59.

200. **Robinson, J. B., Jr., M. Singh, and P. A. Srere.** 1976. Structure of the prosthetic group of *Klebsiella aerogenes* citrate (pro-3S)-lyase. Proc Natl Acad Sci U S A **73:**1872-6.

201. **Rochet, J. C., and W. A. Bridger.** 1994. Identification of glutamate 344 as the catalytic residue in the active site of pig heart CoA transferase. Protein Sci **3:**975-81.

202. **Rochet, J. C., E. R. Brownie, K. Oikawa, L. D. Hicks, M. E. Fraser, M. N. James, C. M. Kay, W. A. Bridger, and W. T. Wolodko.** 2000. Pig heart CoA transferase exists as two oligomeric forms separated by a large kinetic barrier. Biochemistry **39:**11291-302.

203. **Rost, B.** 2002. Enzyme function less conserved than anticipated. Journal of Molecular Biology **318:**595-608.

204. **Royer, C. A.** 2006. Probing protein folding and conformational transitions with fluorescence. Chem Rev **106:**1769-84.

205. **Ruan, Z. S., V. Anantharam, I. T. Crawford, S. V. Ambudkar, S. Y. Rhee, M. J. Allison, and P. C. Maloney.** 1992. Identification, purification, and reconstitution of OxlT, the oxalate: formate antiport protein of *Oxalobacter formigenes*. J Biol Chem **267:**10537-43.

206. **Russell, D. W.** 2003. The enzymes, regulation, and genetics of bile acid synthesis. Annu Rev Biochem **72:**137-74.

207. **Russell, J. J., and M. S. Patel.** 1982. Purification and properties of succinyl-CoA:3-oxo-acid CoA-transferase from rat brain. J Neurochem **38:**1446-52.

208. **Sambrook, J., E. F. Fritsch, and T. Maniatis.** 1989. Molecular cloning : a laboratory manual, 2nd ed. Cold Spring Harbor Laboratory, Cold Spring Harbor, N.Y.

209. **Sapan, C. V., R. L. Lundblad, and N. C. Price.** 1999. Colorimetric protein assay techniques. Biotechnol Appl Biochem **29 (Pt 2):**99-108.

210. **Savolainen, K., P. Bhaumik, W. Schmitz, T. J. Kotti, E. Conzelmann, R. K. Wierenga, and J. K. Hiltunen.** 2005. α-Methylacyl-CoA racemase from *Mycobacterium tuberculosis*. Mutational and structural characterization of the active site and the fold. J Biol Chem **280:**12611-20.

211. **Schink, B.** 1985. Mechanisms and Kinetics of Succinate and Propionate Degradation in Anoxic Fresh-Water Sediments and Sewage-Sludge. Journal of General Microbiology **131:**643-650.

212. **Schmitz, W., C. Albers, R. Fingerhut, and E. Conzelmann.** 1995. Purification and characterization of an α-methylacyl-CoA racemase from human liver. Eur J Biochem **231:**815-22.

213. **Schmitz, W., R. Fingerhut, and E. Conzelmann.** 1994. Purification and properties of an α-methylacyl-CoA racemase from rat liver. Eur J Biochem **222:**313-23.

214. **Schweiger, G., and W. Buckel.** 1984. On the dehydration of (R)-lactate in the fermentation of alanine to propionate by *Clostridium propionicum*. FEBS Lett **171:**79-84.

215. **Seal, S. N., and S. P. Sen.** 1970. Photosynthetic Production of Oxalic Acid in Oxalis-Corniculata. Plant and Cell Physiology **11:**119-&.

216. **Segel, I. H.** 1993. Enzyme Kinetics: Behavior and Analysis of Rapid Equilibrium and Steady-State Enzyme Systems, New ed. Wiley-Interscience.

217. **Selmer, T., and W. Buckel.** 1999. Oxygen exchange between acetate and the catalytic glutamate residue in glutaconate CoA-transferase from *Acidaminococcus fermentans* - Implications for the mechanism of CoA-ester hydrolysis. Journal of Biological Chemistry **274:**20772-20778.

218. **Selmer, T., A. Willanzheimer, and M. Hetzel.** 2002. Propionate CoA-transferase from *Clostridium propionicum*. Cloning of gene and identification of glutamate 324 at the active site. Eur J Biochem **269:**372-80.

219. **Selvin, P.** 1995. Fluorescence Resonance Energy Transfer, p. 300-34. *In* K. Sauer (ed.), Methods in Enzymology, vol. 246. Academic Press, Inc., San Diego.

220. **Seydoux, F., O. P. Malhotra, and S. A. Bernhard.** 1974. Half-site reactivity. CRC Crit Rev Biochem **2:**227-57.

221. **Sharp, J. A., and M. R. Edwards.** 1978. Purification and properties of succinyl-coenzyme A-3-oxo acid coenzyme A-transferase from sheep kidney. Biochem J **173:**759-65.

222. **Shaw, W. V., D. G. Brenner, and I. A. Murray.** 1985. Regulation of antibiotic resistance in bacteria: the chloramphenicol acetyltransferase system. Curr Top Cell Regul **26:**455-68.

223. **Shuster, L., and N. O. Kaplan.** 1953. A Specific B-Nucleotidase. Journal of Biological Chemistry **201:**535-546.

224. **Sidhu, H., B. Hoppe, A. Hesse, K. Tenbrock, S. Bromme, E. Rietschel, and A. B. Peck.** 1998. Absence of *Oxalobacter formigenes* in cystic fibrosis patients: a risk factor for hyperoxaluria. Lancet **352:**1026-9.

225. **Sidhu, H., S. D. Ogden, H. Y. Lung, B. G. Luttge, A. L. Baetz, and A. B. Peck.** 1997. DNA sequencing and expression of the formyl coenzyme A transferase gene, *frc*, from *Oxalobacter formigenes*. J Bacteriol **179:**3378-81.

226. **Singh, M., J. B. Robinson, and P. A. Srere.** 1977. Structure of Prosthetic Group of Citrate (Pro-3s)-Lyase. Journal of Biological Chemistry **252:**6061-6068.

227. **Sly, W. S., and E. R. Stadtman.** 1963. Formate Metabolism. I. Formyl Coenzyme a, an Intermediate in the Formate-Dependent Decomposition of Acetyl Phosphate in *Clostridium kluyveri*. J Biol Chem **238:**2632-8.

228. **Snell, E. E., G. M. Brown, V. J. Peters, J. A. Craig, E. L. Wittle, J. A. Moore, V. M. Mcglohon, and O. D. Bird.** 1950. Chemical Nature and Synthesis of the *Lactobacillus-bulgaricus* Factor. Journal of the American Chemical Society **72:**5349-5350.

229. **Solomon, F., and W. P. Jencks.** 1969. Identification of an enzyme-γ-glutamyl coenzyme A intermediate from coenzyme A transferase. J Biol Chem **244:**1079-81.

230. **Spencer, R. C.** 1998. Clinical impact and associated costs of *Clostridium difficile*-associated disease. J Antimicrob Chemother **41 Suppl C:**5-12.

231. **Sramek, S. J., and F. E. Frerman.** 1975. *Escherichia coli* Coenzyme A-transferase: kinetics, catalytic pathway and structure. Arch Biochem Biophys **171:**27-35.

232. **Sramek, S. J., and F. E. Frerman.** 1975. Purification and properties of *Escherichia coli* Coenzyme A-transferase. Arch Biochem Biophys **171:**14-26.

233. **Sramek, S. J., F. E. Frerman, D. J. McCormick, and G. R. Duncombe.** 1977. Substrate-induced conformational changes and half-the-sites reactivity in the *Escherichia coli* CoA transferase. Arch Biochem Biophys **181:**525-33.

234. **Stadtman, E. R.** 1953. The Coenzyme A transphorase system in *Clostridium kluyveri*. J Biol Chem **203:**501-12.

235. **Stenmark, P., D. Gurmu, and P. Nordlund.** 2004. Crystal structure of CaiB, a type-III CoA transferase in carnitine metabolism. Biochemistry **43:**13996-4003.

236. **Stern, J. R., M. J. Coon, A. Del Campillo, and M. C. Schneider.** 1956. Enzymes of fatty acid metabolism. IV. Preparation and properties of coenzyme A transferase. J Biol Chem **221:**15-31.

237. **Stewart, C. S., S. H. Duncan, and D. R. Cave.** 2004. *Oxalobacter formigenes* and its role in oxalate metabolism in the human gut. FEMS Microbiol Lett **230:**1-7.

238. **Stryer, L.** 1965. The interaction of a naphthalene dye with apomyoglobin and apohemoglobin. A fluorescent probe of non-polar binding sites. J Mol Biol **13:**482-95.

239. **Studier, F. W.** 2005. Protein production by auto-induction in high density shaking cultures. Protein Expr Purif **41:**207-34.

240. **Sulzenbacher, G., A. Gruez, V. Roig-Zamboni, S. Spinelli, C. Valencia, F. Pagot, R. Vincentelli, C. Bignon, A. Salomoni, S. Grisel, D. Maurin, C. Huyghe, K. Johansson, A. Grassick, A. Roussel, Y. Bourne, S. Perrier, L. Miallau, P. Cantau, E. Blanc, M. Genevois, A. Grossi, A. Zenatti, V. Campanacci, and C. Cambillau.** 2002. A medium-throughput crystallization approach. Acta Crystallogr D Biol Crystallogr **58:**2109-15.

241. **Svedruzic, D., S. Jonsson, C. G. Toyota, L. A. Reinhardt, S. Ricagno, Y. Lindqvist, and N. G. Richards.** 2005. The enzymes of oxalate metabolism: unexpected structures and mechanisms. Arch Biochem Biophys **433:**176-92.

242. **Takamura, Y., Y. Kitayama, A. Arakawa, S. Yamanaka, M. Tosaki, and Y. Ogawa.** 1985. Malonyl-CoA: acetyl-CoA cycling. A new micromethod for determination of acyl-CoAs with malonate decarboxylase. Biochim Biophys Acta **834:**1-7.

243. **Taylor, W. R.** 2000. A deeply knotted protein structure and how it might fold. Nature **406:**916-9.

244. **Thomas, P. D., H. Mi, and S. Lewis.** 2007. Ontology annotation: mapping genomic regions to biological function. Curr Opin Chem Biol **11:**4-11.

245. **Toyota, C. G., C. L. Berthold, A. Gruez, S. Jonsson, Y. Lindqvist, C. Cambillau, and N. G. Richards.** 2008. Differential substrate specificity and kinetic behavior of *Escherichia coli* YfdW and *Oxalobacter formigenes* formyl coenzyme A transferase. J Bacteriol **190:**2556-64.

246. **Turano, A., W. Furey, J. Pletcher, M. Sax, D. Pike, and R. Kluger.** 1982. Synthesis and Crystal-Structure of an Analog of 2-(Alpha-Lactyl)Thiamin, Racemic Methyl 2-Hydroxy-2-(2-Thiamin)Ethylphosphonate Chloride Trihydrate - a Conformation for a Least-Motion, Maximum-Overlap Mechanism for Thiamin Catalysis. Journal of the American Chemical Society **104:**3089-3095.

247. **Turroni, S., B. Vitali, C. Bendazzoli, M. Candela, R. Gotti, F. Federici, F. Pirovano, and P. Brigidi.** 2007. Oxalate consumption by lactobacilli: evaluation of oxalyl-CoA decarboxylase and formyl-CoA transferase activity in *Lactobacillus acidophilus*. J Appl Microbiol **103:**1600-9.

248. **Vagin, A., and A. Teplyakov.** 1997. MOLREP: an Automated Program for Molecular Replacement. J. Appl. Cryst. **30**.

249. **Vandamme, P., and T. Coenye.** 2004. Taxonomy of the genus *Cupriavidus*: a tale of lost and found. Int J Syst Evol Microbiol **54:**2285-9.

250. **Vanderwinkel, E., P. Furmanski, H. C. Reeves, and S. J. Ajl.** 1968. Growth of *Escherichia coli* on fatty acids: requirement for coenzyme A transferase activity. Biochem Biophys Res Commun **33:**902-8.

251. **Vincentelli, R., C. Bignon, A. Gruez, S. Canaan, G. Sulzenbacher, M. Tegoni, V. Campanacci, and C. Cambillau.** 2003. Medium-scale structural genomics: strategies for protein expression and crystallization. Acc Chem Res **36:**165-72.

252. **Voet, D., and J. Voet.** 1995. Biochemistry. J. Wiley & Sons, New York.

253. **Waggoner, A.** 1995. Covalent Labeling of Proteins and Nucleic Acids with Fluorophores, p. 362-73. *In* K. Sauer (ed.), Methods in Enzymology, vol. 246. Academic Press, Inc., San Diego.

254. **Wagner, J. R., J. S. Brunzelle, K. T. Forest, and R. D. Vierstra.** 2005. A light-sensing knot revealed by the structure of the chromophore-binding domain of phytochrome. Nature **438:**325-31.

255. **Wang, X. C., R. I. Sarker, and P. C. Maloney.** 2006. Analysis of substrate-binding elements in OxlT, the oxalate : formate antiporter of *Oxalobacter formigenes*. Biochemistry **45:**10344-10350.

256. **Welch, R. A., V. Burland, G. Plunkett, 3rd, P. Redford, P. Roesch, D. Rasko, E. L. Buckles, S. R. Liou, A. Boutin, J. Hackett, D. Stroud, G. F. Mayhew, D. J. Rose, S. Zhou, D. C. Schwartz, N. T. Perna, H. L. Mobley, M. S. Donnenberg, and F. R. Blattner.** 2002. Extensive mosaic structure revealed by the complete genome sequence of uropathogenic *Escherichia coli*. Proc Natl Acad Sci U S A **99:**17020-4.

257. **Westphal, A. H., A. Matorin, M. A. Hink, J. W. Borst, W. J. van Berkel, and A. J. Visser.** 2006. Real-time enzyme dynamics illustrated with fluorescence spectroscopy of *p*-hydroxybenzoate hydroxylase. J Biol Chem **281:**11074-81.

258. **White, W. B., J. P. Coleman, and P. B. Hylemon.** 1988. Molecular-Cloning of a Gene Encoding a 45,000-Dalton Polypeptide Associated with Bile-Acid 7-Dehydroxylation in *Eubacterium*-Sp Strain Vpi-12708. Journal of Bacteriology **170:**611-616.

259. **Whitty, A., C. A. Fierke, and W. P. Jencks.** 1995. Role of Binding-Energy with Coenzyme-a in Catalysis by 3-Oxoacid Coenzyme-a Transferase. Biochemistry **34:**11678-11689.

260. **Wider, G.** 2005. NMR techniques used with very large biological macromolecules in solution. Methods Enzymol **394:**382-98.

261. **Wiesenborn, D. P., F. B. Rudolph, and E. T. Papoutsakis.** 1989. Coenzyme A transferase from *Clostridium acetobutylicum* ATCC 824 and its role in the uptake of acids. Appl Environ Microbiol **55:**323-9.

262. **Wille, G., D. Meyer, A. Steinmetz, E. Hinze, R. Golbik, and K. Tittmann.** 2006. The catalytic cycle of a thiamin diphosphate enzyme examined by cryocrystallography. Nat Chem Biol **2:**324-8.

263. **Williams, R. J., D. M. Lyman, G. H. Goodyear, J. H. Truesdail, and J. Holaday.** 1933. "Pantothenic Acid," a growth determinant of universal biological occurrence. J Am Chem Soc **55:**2912-27.

264. **Williams, W. A.** 1990. University of Minnesota.

265. **Yang, Q., X. C. Wang, L. W. Ye, M. Mentrikoski, E. Mohammadi, Y. M. Kim, and P. C. Maloney.** 2005. Experimental tests of a homology model for OxlT, the oxalate transporter of *Oxalobacter formigenes*. Proceedings of the National Academy of Sciences of the United States of America **102:**8513-8518.

266. **Ye, H. Q., D. H. Mallonee, J. E. Wells, I. Bjorkhem, and P. B. Hylemon.** 1999. The bile acid-inducible baiF gene from *Eubacterium* sp. strain VPI 12708 encodes a bile acid-coenzyme A hydrolase. Journal of Lipid Research **40:**17-23.

267. **Ye, L., Z. Jia, T. Jung, and P. C. Maloney.** 2001. Topology of OxlT, the oxalate transporter of *Oxalobacter formigenes*, determined by site-directed fluorescence labeling. J Bacteriol **183:**2490-6.

268. **Yeh, W. K., and L. N. Ornston.** 1981. Evolutionarily homologous alpha 2 beta 2 oligomeric structures in beta-ketoadipate succinyl-CoA transferases from *Acinetobacter calcoaceticus* and *Pseudomonas putida*. J Biol Chem **256:**1565-9.

269. **Zhang, S., L. Zhou, N. Nemeria, Y. Yan, Z. Zhang, Y. Zou, and F. Jordan.** 2005. Evidence for dramatic acceleration of a C-H bond ionization rate in thiamin diphosphate enzymes by the protein environment. Biochemistry **44:**2237-43.

BIOGRAPHICAL SKETCH

Cory Glenn Toyota was born in 1970 in the Key City of the Kootenays, a small town at the foot of the Rockie Mountains called Cranbrook. He was studying Japanese language and illustration (Manga) in Osaka in the early 1990's, when he met Lori Lamb, his wife-to-be. After a wedding ceremony in the Mississippi June heat, Cory whisked his new bride back to Canada, where the young couple lived in a double-wide trailer for three years in Grand Forks, British Columbia; Cory sold furniture and Lori worked as a baker, travel agent, and cashier at the local supermarket. The next couple years saw them return to Cranbrook to help his father Ron with the family furniture and appliance business—Taks Home Furnishers. When his father closed the business, Cory took the opportunity to go back to college. The small family (now with a Springer Spaniel named Gumbo) travelled to Lori's hometown Jackson, MS. Upon graduation from Mississippi College with his Bachelor of Science degree in biochemistry, they pulled up stakes and moved to Gainesville, FL to attend graduate school in chemistry where, under the supervision of Nigel G. J. Richards, Cory began to study the metabolic enzymes of a bacterium called *Oxalobacter formigenes*. Despite a lengthy and monumental struggle with an ancient HPLC, Cory's time in Gainesville brought success in the form of papers published, awards, and fellowships. He and his wife celebrated by having their first son, Arwood Takeo, in January 2008. The family (now with a second dog named Weaver) plan to move back to Mississippi where Cory will take a postdoctoral fellowship at the University of Mississippi Medical Center in Jackson working with Michael Hebert.